POLYMORPHIC CRYSTALLIZATION PROCESS DEVELOPMENT

SATYANARAYANA THIRUNAHARI

(*M. Tech., Indian Institute of Technology Guwahati*)

A THESIS SUBMITTED

FOR THE DEGREE OF DOCTOR OF PHILOSOPHY

DEPARTMENT OF CHEMICAL AND BIOMOLECULAR ENGINEERING

NATIONAL UNIVERSITY OF SINGAPORE

2011

Acknowledgements

First and foremost, I would like to acknowledge National University of Singapore (NUS) for providing the financial support and Institute of Chemical and Engineering Sciences (ICES), one of the national research labs under the Agency for Science, Technology and Research (A*star) in Singapore, for funding this project and giving me the opportunity to avail the experimental resources to carry out this work.

I would like to express my deep and sincere gratitude to my advisor, A/Prof. Reginald Tan, for his invaluable guidance, patience and support throughout this work. He always believed in my abilities and gave enough freedom in pursuing this work. I am very grateful to my co-advisor, Dr. Pui Shan Chow of ICES, for her invaluable guidance, suggestions, critical comments and constant encouragement during this work. I sincerely appreciate her patience in teaching the basics of research at the preliminary stage of this work. Without their support and timely inputs, my progress was impossible. With the good associations of my advisors, I have not only improved my scientific knowledge but have also bettered my problem solving, writing and presentation skills.

I would like to specially thank Dr. Keith Carpenter (ICES) and Prof. Simon Black (Astrazeneca, UK) for insightful discussions and encouragement.

My gratefulness is extended to all the colleagues in ICES for technical assistance and useful advices during this work. I would like to specially thank Dr. Srini for helping me in solving and analyzing the single crystal structures. Being a chemist, he imparted me with chemistry aspects of crystallization. Dr. Zaiqun for helping with PAT experiments, Dr. Martin, for helping in VB.Net programming, Dr. Sendhil, for his useful

inputs and patient listening. My thanks are extended to Dr. Sudhakar, Dr. Venu, Dr. Balaji, Dr. Parijat, Dr. Srilakshmi and Mr. Prashant for their friendship and support during this work.

I would like to take this as an opportunity to thank all my professors who trained and inspired me to be what I am today. Special thanks to all my friends who have made the stay in Singapore a pleasant and a memorable one.

Finally, I am deeply indebted to my parents and beloved wife, Rani, for all the understanding, support and love they have given me during this long journey.

Satyanarayana Thirunahari

January, 2011

In memory of my beloved father

Table of Contents

Summary

One of the challenging issues in the development of crystallization processes for active pharmaceutical ingredients (APIs) is to obtain the desired polymorphic form of the product. Though chemically identical, polymorphs are structurally different crystalline solids. Consequently, they exhibit different physico-chemical properties which can impact both the processability and performance of the drug. Unfortunately, crystallization process may go out of control even with a small variation in the process conditions such as cooling rate, feed conditions etc. which can impact the polymorphic outcome. Given such a situation, a deeper understanding about the fundamental aspects of polymorphism and crystallization mechanisms governing the polymorph formation and transformation is necessary. Only then a robust process can be developed to isolate the desired crystal form. Having said this, the objective of this work is to understand the polymorphism and crystallization aspects of an anti-diabetic drug, Tolbutamide (TB), to develop a robust crystallization process for the isolation of the desired form for this drug.

In the first part, the structural and stability features of various TB polymorphs (Forms ($\mathbf{I^L}$, $\mathbf{I^H}$) and **II**–**IV**) were characterized using various analytical techniques. It has been found that the conformational flexibility of the TB molecule and strong hydrogen bonding ability of secondary amide via carbonyl and sulfonyl groups facilitate TB to crystallize into different polymorphic forms. The rich torsional freedom available for the terminal alkyl chain mainly assists TB molecule to adopt various conformers and crystalline packing arrangements. By elucidating the crystal structures of various polymorphic forms of TB, the present work resolves several discrepancies in the published data on structural features of the polymorphs of this API. The relative

thermodynamic relationships of TB polymorphic pairs were evaluated and the stability domains were elucidated in the form of a schematic energy-temperature diagram. Form **II** is found to be the thermodynamically stable polymorph from absolute zero to ~353 K and beyond which Form $\mathbf{I^H}$ is the stable polymorph. The discrepancies in the literature related to the relative stability of TB polymorphs at ambient conditions are highlighted and partially resolved.

In the second part, using Quality by Design (QbD) based strategy, a robust cooling crystallization process was developed to achieve the desired polymorph, Form ($\mathbf{I^L}$, $\mathbf{I^H}$), of TB. In applying QbD, crystallization process characterization studies were carried out using process analytical technology (PAT). A polymorphic transformation study of TB polymorphs Form $\mathbf{I^L}\rightarrow$ Form **II** suggests that the primary nucleation of the stable Form **II** is the controlling step for the transformation. Metastable zone width (MZW) measurements indicate that the cooling rate and solute concentration has a strong influence on the nucleation energy barrier and can be used as manipulators for achieving different TB polymorphs. Finally, using this information, a crystallization design space was derived in terms of metastability of Form ($\mathbf{I^L}$, $\mathbf{I^H}$) and a crystallization batch process was successfully operated within the design space to achieve the desired form.

This work also demonstrates the application of two PATs, ATR-FTIR combined with orthogonal partial least squares (OPLS), a robust chemometric method and Raman combined with a dynamic principal component analysis (PCA) based multivariate statistical process monitoring (MSPM) in crystallization process characterization and monitoring.

Nomenclature

ABBREVIATION

AFM	Atomic Force Microscopy
API	Active Pharmaceutical Ingredient
ATR	Attenuated Total Reflectance
CNT	Classical Nucleation Theory
CLD	Chord Length Distribution
COMPASS	Condensed-phase Optimized Molecular Potentials for Atomistic Simulation
CP	Cross Polarization
CSA	Chemical Shift Anisotropy
CSD	Cambridge Structural Database
CSP	Computational Crystal Structure Prediction
DSC	Differential Scanning Calorimetry
E-T	Energy-Temperature
EM	Electron Microscopy
FBRM	Focused Beam Reflectance Measurement
FDA	Food and Drug Administration
FTIR	Fourier Transform Infrared
HPLC	High Performance Liquid Chromatography
HSM	Hot Stage Microscopy
HT	High Throughput
IR	Infrared
LM	Light Microscopy
LOO	Leave One Out
LV	Latent Variable
MAS	Magic Angle Spinning
MC/SA	Monte Carlo/ Simulated Annealing
MS	Mass Spectroscopy
MSPM	Multivariate Statistical Process Monitoring

MZW	Metastable Zone Width
OC	Orthogonal Component
OPLS	Orthogonal Partial Least Squares
OSC	Orthogonal Signal Correction
PAT	Process Analytical Technology
PC	Principal Component
PCA	Principal Component Analysis
PCR	Principal Component Regression
PLS	Partial Least Squares
PRESS	Cumulative Predicted Residual Sum of Squares
PVM	Process Vision and Measurement
PXRD	Powder X-Ray Diffractometry
QbD	Quality by Design
QbT	Quality by Testing
RMSECV	Root Mean Square Error of Cross Validation
RT	Room Temperature
TG	Thermogravimetry
TB	Tolbutamide
ROY	Red Orange Yellow
SCXRD	Single Crystal X-Ray Diffractometry
SEM	Scanning Electron Microscopy
SEI	Secondary Electron Imaging
SMPT	Solvent Mediated Polymorphic Transformation
SS-NMR	Solid-State Nuclear Magnetic Resonance
VT-XRD	Variable Temperature X-Ray Diffractometry

GENERAL SYMBOLS

Z'	Number of molecules in asymmetric unit
Z	Number of molecules in unit cell
T	Temperature
T_t	Transition temperature

T_{fus}	Melting temperature
G	Free energy
H	Enthalpy
H_{LIQ}	Enthalpy of liquid
G_{LIQ}	Free energy of liquid
C_p	Molar heat capacity
S	Entropy
$\Delta_{fus}H$	Heat of fusion
$\Delta_{trs}H$	Heat of transition
G^0	Free energy of pure substance
G^{solid}	Free energy of solid
R	Gas constant
a_{solute}	Activity of solute
γ_{solute}	Activity coefficient of solute
C^{eq}	Solubility
σ	Supersaturation
γ	Interfacial energy
d	Distance between crystal planes
θ	X-ray diffraction angle
λ	Wavelength
R_{wp}	Weighted powder profile R-factor
R_p	Profile R-factor
Γ	Structural degree of freedom
μ^{ss}	Chemical potential of a molecule in a supersaturated solution
μ^{eq}	Chemical potential of a molecule in a saturated solution
C	Concentration
ΔG	Activation energy for nucleation
k	Boltzmann's constant
A_c	Surface area of cluster
n^*	Critical cluster size

J	Nucleation rate
ΔG^*	Critical activation energy for nucleation
A	Preexponential factor
N_o	Number of solute molecules in a unit volume of solution
v	Frequency of molecular transport at the nucleus-liquid interface
υ	Molecular volume
G_c	Crystal growth rate
g	Growth rate order
$\mathrm{F_a}$	Absolute Figure of Merit
$\mathrm{F_r}$	Relative Figure of Merit
d_p	Penetration depth of ATR-FTIR

MATHEMATICAL SYMBOLS

$\mathbf{X}$	Spectral data matrix
$\mathbf{X_{ortho}}$	Orthogonal spectral data matrix
$\mathbf{X_{filt}}$	Filtered spectral data matrix
$\mathbf{y}$	Solute concentration vector
n	Number of samples
m	Number of variables
K	Number of latent variables
$\mathbf{E}$	**X** Residual matrix
$\mathbf{E_{ortho\ (pca)}}$	Principal orthogonal **X** residual matrix
$\mathbf{f}$	**y** Residual vector
$\mathbf{T}$	**X** Scores matrix
$\mathbf{T_{ortho}}$	Orthogonal **X** scores matrix
$\mathbf{T_{ortho\ (pca)}}$	Principal orthogonal **X** scores matrix
$\mathbf{P}$	**X** Loadings matrix
$\mathbf{P_{ortho}}$	Orthogonal **X** loadings matrix
$\mathbf{P_{ortho\ (pca)}}$	Principal orthogonal **X** loadings matrix

$\mathbf{W}$	Weights matrix
$\mathbf{W_{ortho}}$	Orthogonal weights matrix
$\mathbf{q}$	**y** Loadings vector
$\mathbf{t}$	**X** Scores vector
$\mathbf{t_{ortho}}$	Orthogonal **X** scores vector
$\mathbf{t_{ortho\ (pca)}}$	Principal orthogonal **X** scores vector
$\mathbf{p}$	**X** Loadings vector
$\mathbf{p_{ortho}}$	Orthogonal **X** loadings vector
$\mathbf{p_{ortho\ (pca)}}$	Principal orthogonal **X** loadings vector
$\mathbf{w}$	Weights vector
$\mathbf{w_{ortho}}$	Orthogonal weights vector
λ_i	i^{th} Eigenvalue
x_j	Spectral value corresponding to j^{th} variable of a new sample
$\widehat{x_j}$	Predicted spectral value corresponding to j^{th} variable of a new sample
y_i	Measured value of i^{th} sample
$\hat{y}_i$	Model predicted value of i^{th} sample
R^2X	Correlation coefficient
Q^2	Cross validation coefficient
SS_{tot}	Sum of squares of measured data
SS_{res}	Sum of squares of model residuals
c_j	T^2 contribution of j^{th} variable

List of Tables

List of Figures

CHAPTER 1

Introduction

1.1. Background and Motivation

Solution crystallization is the most utilized technique in pharmaceutical industry for high purity separation (Variankaval et al., 2008). Being simple, flexible and energy efficient, it offers many advantages over other separation techniques. The main targets of crystallization are to produce crystals with high chemical purity and desired physical properties such as size, shape and crystal structure. However, despite the long history and widespread application, crystallization is not a well understood phenomena and suffers from poor control characteristics. It becomes more complex when multiple crystal forms (polymorphs) are produced. Therefore, crystallization process development and its control are regarded as challenging.

1.1.1. *Crystal Polymorphism and Its Importance*

Recently, there is a significant interest in crystal polymorphism in pharmaceutical industry (Henck et al., 1997; Rouhi, 2003). It is the ability of a molecule to crystallize in more than one crystal structure (also referred to as *form* or *polymorph*). It is a widespread phenomenon among drug molecules and more prevalent when the molecule has binding sites for solvent molecules in the crystal lattice leading to *pseudopolymorphs or solvates* (Bingham et al., 2001). Literature values suggest that 51% of the drug substances are truly polymorphic (Storey et al., 2004). If solvates are included this value goes up to 87%. In fact, according to McCrone (1965), polymorphism is not limited to a few but exists in every compound and the number of polymorphs known for a given compound is proportional to the amount of time and money spent in investigating the molecule. This is

well supported by many reports on the discovery of new polymorphs either serendipitously (Rubin-Preminger and Bernstein, 2005; Vishweshwar et al., 2005; Day et al., 2006; Rafilovich and Bernstein, 2006) or by expansive search e.g. high throughput screening (Almarsson et al., 2003; Morissette et al., 2003), using high pressure (Fabbiani et al., 2007), using supercritical fluids (Bettini et al., 2009) etc.

The practical importance of this phenomenon is based on the fact that the different solid forms may have different physical and chemical properties including chemical reactivity, solubility, stability, mechanical properties etc (Huang and Tong, 2004). The differences in surface and mechanical properties can influence the downstream processing of drug substances into drug products i.e. filtration, drying, handling in powder form, formulation activities etc. On the other hand, differences in thermodynamic properties like solubility may have profound effect on the *bioavailability*[1] of the drug by affecting its dissolution characteristics. This is critical particularly for low solubility compounds and any variations can lead to severe effects in patients. Another consideration is the physical stability of the drug substance which depends on the crystal form and unstable forms can spontaneously transform to more stable form over time during any stage of the drug manufacturing.

Hence, characterization of all possible polymorphs and identifying the desired form is a crucial step in drug development process. But, even after a thorough search for polymorphs, there are many instances where new polymorphs have been discovered later in development (Chemburkar et al., 2000; Desikan et al., 2005; Prashad et al., 2010). This can lead to serious manufacturing issues. Once new polymorphs appear, the previously

[1] is a measurement of the extent of a therapeutically active drug that reaches the systemic circulation and is available at the site of action

known polymorphs may disappear (Dunitz and Bernstein, 1995; Henck et al., 2001) or become irreproducible (Bauer et al., 2001). Besides this, the late discovery of new polymorphs can also lead to patent litigations (Bernstein, 2002). This unpredictable nature of polymorphism clearly demonstrates our lack of understanding in this phenomenon. Hence, from both the customers and regulatory agencies point of view, such as Food and Drug Administration (FDA), understanding polymorphism to improve the control over solid-state of drug substances remains a major theoretical, technological and economical issue.

1.1.2. *Crystallization Process Development for a Specific Polymorph*

When a desired polymorph is chosen for drug manufacturing, it is vital to have a robust crystallization process which consistently produces that form. To this aim, it is essential to understand the factors which govern the polymorph formation and its transformation. In crystallization, once the solution enters into the metastable state (non-equilibrium), the crystallization kinetic pathways will determine which form will crystallize and for how long it can survive (Bernstein, 2002). To achieve ultimate control over polymorphic crystallization, manipulation of these pathways to direct the process towards the desired polymorph is required. Over the last decade, many such strategies have been developed (Llinas and Goodman, 2008). Some important ones are *using tailor-made additives to stabilize the desired form* (Davey et al., 1997; He et al., 2001), *use of solvents to promote the nucleation of the desired polymorph* (Blagden and Davey, 2003; Weissbuch et al., 2005; Kitamura et al., 2006) and *control of nucleation using templates* (Mitchell et al., 2001; Dressler and Mastai, 2007). However, these methods are system specific and requires good understanding in molecular aspects of crystallization where

our knowledge is extremely poor and therefore limits the level of process control (Schuth, 2001; Towler and Taylor, 2007).

The other approach which has currently been practiced by industry is based on Quality by Design (QbD) which is motivated by the new recent initiatives from FDA to adopt modern technology to develop more science-based processes (McKenzie et al., 2006). The underlying premise of QbD is that the quality cannot be tested into products, instead it should be built by process design. Bohlin et al. (2009) have discussed the concept of QbD, its benefits and application to develop robust crystallization processes with several examples. Some potential benefits of developing processes in QbD approach are the regulatory flexibility i.e. manufacturers are allowed to make changes to process, greater robustness and easy trouble shooting.

Essentially, QbD involves experimental screening of input and process parameters to determine a design space[2] (operating region where the crystallization of the desired polymorph is guaranteed) and with appropriate controls installed to operate within the control space (upper and/or lower limits of operating parameters between which the process is controlled) to produce the desired form (Yu, 2008). To this aim, in situ analytical technologies, usually referred to as PATs (process analytical technologies), play a crucial role in process characterization, analysis and control (Yu et al., 2004; Variankaval et al., 2008). FDA also strongly recommends the liberal use of PAT to assist the implementation of QbD. Some of the potential benefits of PATs are: improved process understanding (Howard et al., 2009; Chen et al., 2009), faster and focused process development (Starbuck et al., 2002; Birch et al., 2005; Desikan et al., 2005;

[2] 'Design space' is also referred to as "crystallization space" or "occurrence domain" or "polymorphic window"

Saranteas et al., 2005; Muller et al., 2006; Zhou et al., 2009), online assessment of polymorphic quality (Ono et al., 2004; Scholl et al., 2006; Caillet et al., 2007; Borissova et al., 2009; Klimakow et al., 2010) and implementation of advanced control strategies (Abu Bakar et al., 2009; Kee et al., 2009a; Kee et al., 2009b).

However, recent reviews on applications of PATs in crystallization suggest that there still exists a significant gap between research and industrial PAT implementations (Yu et al., 2004; Fevotte, 2007; Wu et al., 2007; Yu et al., 2007). Technology, system reliability and the necessity for chemometric calibration exercise limiting its progression to industrial environments (Barrett et al., 2010). Therefore, developing and implementing PAT to improve the control over industrial crystallization processes is one of the most important research topics currently emerging in this area.

1.2. Research Objectives and Approach

The main objective of this work is to gain fundamental understanding about various aspects of crystal polymorphism and crystallization mechanisms governing the polymorph formation and transformation to develop a process to achieve the desired polymorph. Tolbutamide (TB), an anti-diabetic drug, was chosen as the model compound. The thesis work will comprise the following milestones:

- Determine the structural origin of polymorphism in TB by elucidating the internal arrangement of TB molecule in the crystal lattice of various polymorphs. To achieve this, X-ray diffraction experiments were conducted and crystal structures were solved. As a complementary technique, spectroscopic measurements were also performed.

- Establish the relative stabilities of TB polymorphs. To achieve this, thermal analysis, solubility measurements and slurry experiments were performed to understand the stability relationships between TB polymorphs. Finally, a schematic energy- temperature diagram was constructed to elucidate the stability domains.
- Design a robust crystallization process for the isolation of the desired polymorph in a QbD paradigm. To achieve this, two PATs, ATR-FTIR and Raman spectroscopy were employed. Solubility curves, metastable zone widths and polymorph transformation kinetics were characterized. Finally, a crystallization design space was derived and a crystallization batch process was successfully demonstrated while operating in the design space to achieve the desired polymorph.

1.3. Dissertation Outline

Chapter 2 introduces the fundamentals of crystal polymorphism, polymorph characterization techniques and crystallization aspects of polymorphs.

Chapter 3 introduces the model system (Tolbutamide) and its related previous work and describes the experimental techniques used for the characterization of crystal polymorphism of this system.

Chapter 4 reports the results on structural and thermodynamic features of TB polymorphs. Three new crystal structures of TB were solved and the thermodynamics were detailed in the form of an energy-temperature diagram. By reporting these results, several discrepancies in the published data on the structural and thermodynamic aspects

of polymorphs of this API have been resolved. It has also been highlighted the influence of anisotropic thermal motion of TB molecule on PXRD patterns of TB polymorphs.

Chapter 5 introduces PAT and QbD based crystallization process development and describes crystallization PATs used in the present work. Two novel chemometric methods which have been coupled with PATs were also introduced. The experimental setup, instrumentation and experimental methods used were outlined.

Chapter 6 reports the results on crystallization process development for the isolation of the desired polymorph of TB. Results obtained on crystallization characterization studies including solubility curves, transformation kinetics and metastable zone width were presented and discussed. Based on these results, a crystallization design space was derived and a crystallization batch was demonstrated while operating in the design space. This chapter also demonstrates the application of two PAT tools, ATR-FTIR combined with OPLS (PCA) and Raman combined with MSPM, in crystallization processes.

Chapter 7 gives a summary of the significant outcomes of this study together with the scope for future work.

CHAPTER 2

Crystallization and Polymorphism

2.1. Introduction

Crystallization is a molecular assembly process by which a group of random molecules in a fluid come together to form an ordered structure which we call a crystal. As an esteemed purification technique, crystallization relies on the stringent structural requirement of the growing crystal which only accommodate similar molecular segments to exclude impurities. However, the internal structure adopted by the crystal is an important property which must be carefully controlled to achieve a desired product quality. A holistic understanding of crystallization mechanisms, influence of operating conditions and their relation with structural outcome is, therefore, a prerequisite for the design and development of a robust crystallization process for the consistent production of the desired crystal form. This chapter mainly aims at introducing fundamentals of crystal polymorphism, polymorph characterization and crystallization aspects of polymorphic compounds.

2.2. Structural Aspects of Polymorphism

Polymorphism (Greek: *poly* = many, *morph* = form) is the ability of a substance to exist as two or more crystalline phases that have different arrangements and/or conformations of the molecules in the crystal lattice (Grant, 1999). Mitscherlich (1820) is the first to discover this phenomenon in relation to inorganic materials. Wohler and Liebig (1832) discovered the first example of polymorphism in organic material, benzamide. Subsequently, Ostwald (1897) concluded that almost every substance could exist in two or more solid phases provided the experimental conditions are suitable. The

development of solid state chemistry during the twentieth century has confirmed and exemplified this statement and a large number of polymorphic compounds have been noted and catalogued (Kuhnert-Brandstatter, 1971; Borka and Haleblian, 1990; Borka, 1991).

2.2.1. *Crystalline State: Fundamentals*

A crystal is a highly ordered solid constructed by identical structural units, termed unit cells, each of which contains all the structural features and symmetry elements and is repeated regularly in three-dimensional space. The dimensions of the unit cell are characterized by six quantities; three axial lengths (a, b, c) and three interaxial angles (α, β, γ). Each unit cell can be classified by one of the seven three-dimensional coordinate systems, which are the seven primitive crystal systems.

The internal symmetry of the unit cell (lattice) is expressed by crystallographers as a *space group* which is a combination of symmetry operations (14 Bravais lattices and 32 point groups) that enables a complete crystal structure to be generated from a single (or group of) molecule(s) called asymmetric unit (Z'). There are 230 space groups which describe all the possible ways in which identical objects can be packed in an infinite lattice. However, only certain space groups are seen frequently, whereas others have never been found in crystals. According to cambridge structural database (CSD), ~76% of all organic and organometallic compounds crystallize in only five space groups – $P2_1/c$, $P2_12_12_1$, $P\bar{1}$, $P2_1$, and $C2/c$.

2.2.2. *Structural Origin of Polymorphism*

As polymorphs are the different crystal structures adopted by a given molecule, they possess different unit cell dimensions, lattice parameters, molecular conformation

etc. However, these differences can vary from subtle to huge depending upon the structural origin of polymorphism. Structural differences between the polymorphs originate through two mechanisms, namely, *packing polymorphism* and *conformational polymorphism*. Packing polymorphism is a mechanism by which molecules that are conformationally relatively rigid can be packed into different three-dimensional structures, e.g. *p*-nitrophenol (Kulkarni et al., 1998) and sulfathiazole (Blagden et al., 1998). Conformational polymorphism is a mechanism by which conformationally flexible molecules can fold into different shapes that can pack into different crystal structures, e.g. anti-viral agent virazole (Prusiner and Sundaralingam, 1976).

In general, the differences in packing arrangements invariably affect the molecular geometry and, conversely, the differences in molecular geometry cause the molecules to pack differently. As a result, most examples of polymorphism in organic crystals have a mixed origin and exhibit differences in both the conformation and packing arrangement of the constituent molecules, e.g. ROY (Yu et al., 2000), ritonavir (Bauer et al., 2001).

2.3. Thermodynamics of Polymorphs

In crystalline solids, because of the long range order, the molecules sit together more tightly and pack more efficiently thereby greatly reduce their intermolecular distances and occupy the lowest energy level on the potential energy curve (Grant, 1999). Thermodynamically, polymorphs can be described as energetically closely spaced minima on the potential energy curve. The differences in energy between the polymorphs arise from the variations in non-covalent interactions between the constituent molecules in the crystal lattice, such as hydrogen bonds, van der Waals forces, electrostatic

interactions etc. The polymorph with the lowest energy is the thermodynamically most stable form and polymorph with the higher energy will sooner or later convert to the most stable form. Kinetically, however, the conversion rate is variable and depends on many factors such as activation energy, impurities etc (Giron, 2005; Cui, 2007).

2.3.1. *Polymorphic Transformations*

Based on the structural criteria, Buerger (1951) has classified the phase transformations in solids into two types. If the two structures involved in the transformation are largely different, the transition may proceed via a *reconstructive mechanism*, i.e. disintegration of the unstable form and reconstruction of the new stable form. This type of transformation requires higher activation energy and therefore would proceed in a sluggish fashion. Presence of solvent (solvent mediated transformation) or melt (melt mediated transformation) can facilitate the transformation by acting as a catalyst (Sato, 1993).

On the other hand, if the two structures are similar, the transition may proceed via a *displacive mechanism,* i.e. molecules of the unstable structure are displaced to yield the new structure in such a way that the nearest neighbor interactions are preserved and only the second neighbors will change. Such transitions require low activation energy and therefore would proceed very rapidly as equivalent as the transmission of heat (Dunitz, 1995).

2.3.2. *Thermodynamic Relationships*

Application of Gibbs phase rule to a polymorphic system derives that at constant pressure, two polymorphic forms can coexist in equilibrium only at one temperature, termed *transition temperature* (T_t). In other words, the free energy (G) of the two

polymorphs becomes equal at this temperature. Consequently, polymorphic systems can be divided into two categories – *monotropic* and *enantiotropic*. These relationships are illustrated in Fig. 2.1, where two polymorphs, Forms **I** and **II** are exemplified.

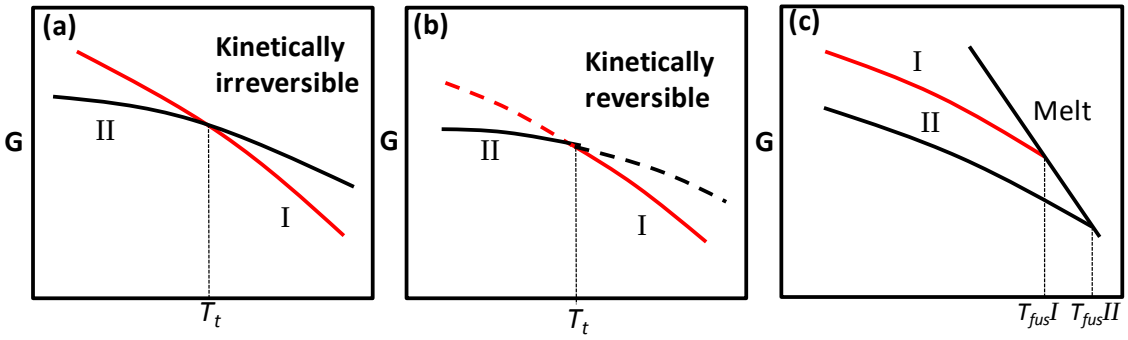

Figure 2.1 Gibbs energy profiles of dimorphic systems (**a**) and (**b**) enantiotropic, and (**c**) monotropic. ($T_{fus}I$ and $T_{fus}II$ are the melting temperatures of Forms **I** and **II** respectively).

Fig. 2.1(a) and (b) show the enantiotropic case in which T_t lies below the melting point of the lower melting polymorph. Therefore, the stability order reverses below and above T_t. However, this does not necessarily mean that the phase transformation to a more stable form is also reversible at T_t. As a result, enantiotropic systems are further divided into two types – *kinetically irreversible* and *kinetically reversible*. In kinetically irreversible systems, the transformation (reconstructive type) is kinetically hindered until it gains sufficient thermal energy to cross the energy barrier. The temperature at which transformation occurs is normally referred to as the experimental or kinetic transition temperature. In such case, both forms are experimentally accessible below and above T_t. On the other hand, in kinetically reversible systems, a reversible solid phase transformation (displacive type) occurs at T_t and both forms are mutually exclusive. As a result, only the more stable forms are experimentally accessible at all the temperatures. In

Fig. 2.1b, the dotted line represents the virtual states of Forms **I** and **II** that cannot be obtained experimentally.

In monotropic systems (Fig. 2.1c), T_t lies above the melting points of the polymorphs and no change in the stability order with respect to temperature i.e. $G_{II} < G_I$ at all temperatures. However, a phase transformation still may occur from the less stable to the more stable polymorph at any temperature.

2.3.3. *Energy-Temperature Diagrams*

Energy-temperature (E-T) diagrams were first introduced in crystallography by Buerger (1951) and subsequently, Burger and Ramberger (1979) and Grunenberg et al. (1996) further developed these diagrams to extend the applications to polymorphic systems. They are often used to present the relative stabilities of polymorphs and phase transformations in a compact form and provide a graphical solution to derive thermodynamic relationships. Threlfall (2009) has recently provided a comprehensive guide on experimental work and methodology involved in constructing these diagrams.

Typical E-T diagrams for a dimorphic system, Forms **I** and **II**, are shown in Fig. 2.2, for both enantiotropic and monotropic systems. They are semi schematic diagrams showing the relative positions and points of intersection of enthalpy (H) and free energy (G) curves of polymorphs at constant pressure, against temperature (T) ranging from absolute zero to melting temperature (T_{fus}). Two additional isobars, the H_{LIQ} and G_{LIQ} curves are also shown to represent the enthalpy and free energy of liquid. The theoretical foundation for the construction of these diagrams is based on three important observations related to a crystalline solid:

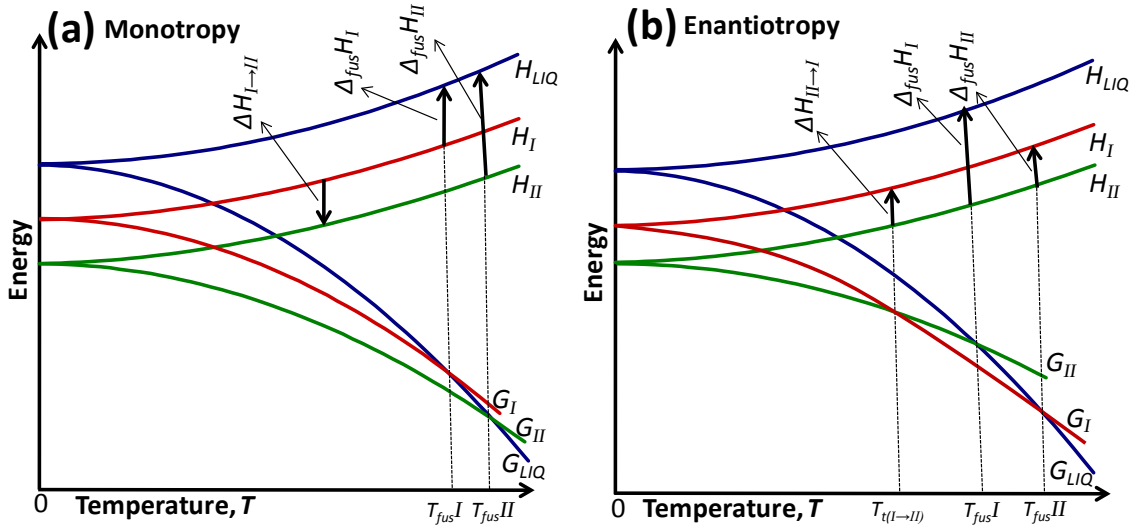

Figure 2.2 Schematic Energy-Temperature diagrams for a dimorphic system Forms **I** and **II** (**a**) monotropy and (**b**) enantiotropy. T_{fus} : Melting temperature, T_t : Transition temperature, H : Enthalpy, G : Free energy, $\Delta_{fus}H$: Enthalpy of fusion, ΔH : Enthalpy of transition, *LIQ* : Liquid.

- The molar heat capacity (C_p) increases with increase in temperature and defines a positive slope for the H isobar.
- Based on third law of thermodynamics, entropy (S) is shown as increasing with temperature starting from zero at absolute zero. This fixes as $G = H$ at absolute zero.
- As a result of first and second laws of thermodynamics, the G isobar is shown as decreasing with increasing temperature.

To predict the thermodynamic relations between the polymorphs, several empirical rules have been developed and popularly known as Burger and Ramberger's rules (Burger and Ramberger, 1979). Three important rules which proved useful are:

Heat of Transition Rule. This rule states that if the phase transformation observed at the kinetic transition temperature is endothermic, then the T_t lies below this temperature and

we can conclude that the two polymorphs are enantiotropically related. If it is exothermic, then there is no T_t below this temperature. This can occur either when the two polymorphs are monotropically related or when the two polymorphs are enantiotropically related with T_t lying above the kinetic transition temperature. This rule makes correct predictions in 99% of cases (Lohani and Grant, 2006).

Heat of Fusion Rule. This rule states that if the higher melting polymorph has the lower heat of fusion, then the two polymorphs are enantiotropic, otherwise they are monotropic. Often, phase transformations are too slow to be observed before melting and in such cases, heat of fusion rule may be applied. This rule is based on the assumption that the heat of transition can be approximated by the difference between the heats of fusion of the polymorphs (Hess's law of heat summation[3]). Exceptions to this rule may arise when the enthalpy curves of the two polymorphs diverge significantly, or when the difference between the melting points of the two polymorphs is larger than ~30 K (Giron, 1995).

Density Rule. This rule states that if a polymorph has highest density than others at room temperature, then it may be assumed that at absolute zero this form is the most stable. This rule assumes that most stable form has closest packing i.e. shorter intermolecular distances, thus lowest free energy. However, in some cases, directional hydrogen bonds dominate and stabilize the polymorph with lower density (Robertson and Ubbelohde, 1938; Haisa et al., 1974).

To construct the E-T diagrams for a compound which crystallizes in n polymorphs, $2n$ parameters are needed. These include the melting temperatures (T_{fus}) and heat of fusions ($\Delta_{fus}H$) of all the polymorphs. Melting temperatures fix the stability

[3] Hess's law of heat summation: the enthalpy change accompanying a transformation is the same whether the process occurs in one or many steps and total enthalpy change is the summation of all steps.

order of polymorphs at higher temperatures whereas the fusion data fix the stability order at absolute zero. The melting points and fusion data are usually measured calorimetrically (refer to section 2.5.3).

2.3.4. *Determination of Transition Temperature*

There are several methods currently available to experimentally determine or estimate the transition temperature (T_t) (Higuchi et al., 1963; Yu, 1995; Gu and Grant, 2001; Hu et al., 2007). The most commonly used method is the measurement of solubilities of the polymorphs (solubility extrapolation method). This method is based on the fundamental relationship between solubility and free energy of the polymorph.

Solubility expresses the maximum amount of material that can be dissolved in a known amount of solvent at a given temperature and pressure (Bennema et al., 2008). Thermodynamically, this corresponds to the balance of free energy (G) of solid phase against that of the solute in the solution phase. Therefore, at solid-liquid equilibrium,

$$G_{solid} = G_{solute} = G^0 + RTln\,(a_{solute}) \tag{2.2}$$

where G^0 is the free energy of pure substance, R the gas constant and a_{solute} the solute activity. With $a_{solute} = \gamma_{solute} C^{eq}$, with γ_{solute} being the activity coefficient of solute and C^{eq} the solubility, Eq. 2.2 can be rewritten as:

$$G_{solid} = G_{solute} = G^0 + RTln\,(\gamma_{solute} C^{eq}) \tag{2.3}$$

This important result shows that the free energy curve of solids can be followed by measuring the solubilities at different temperatures. Thus, transition temperature can be accurately located at which solubilities of two polymorphs crossover each other. For practical purposes, vant Hoff's plots i.e. $ln(C^{eq})$ versus $(1/T)$ are used. The solubility

curve is then linearized and can be interpolated and extrapolated (Beiny and Mullin, 1987).

2.4. Polymorph Screening - the Search for Polymorphs

The search for polymorphs of a given compound can be dealt with two different approaches; *experimental* and *computational* (Guillory, 1997; Hilfiker et al., 2006). Experimental approach mainly depends on the primary nucleation kinetics of the solid phase (Aaltonen et al., 2009; Mangin et al., 2009). Primary nucleation mainly depends on three parameters; solvent (which determines the interfacial energy γ between nucleus and solution), supersaturation (σ) and temperature (for more details, refer to section 2.7.2). Therefore, the strategy is to vary these parameters to cover a large range of experimental space to explore polymorphism.

The most commonly used experimental techniques are *crystallization from solution (cooling, evaporation, anti-solvent and slurry conversion)* and *crystallization from neat compound (melt crystallization, sublimation and thermal treatment).* For solvent based methods, the selection of right set of solvents is important. Ideally, solvents as diverse as possible in properties including polarity, hydrogen bond acceptor/donor propensity, dielectric constant etc. should be selected. In this regard, some recent work on solvent diversity can greatly facilitate rational and rapid selection of solvents (Gu et al., 2004; Alleso et al., 2008). To accelerate the screening process, high-throughput (HT) methods which utilizes an automated robotic system capable of performing thousands of crystallizations has been developed (Morissette et al., 2004; Alvarez et al., 2009). Such new technologies not only accelerate screening but also provide more insights into the relationships between crystallization outputs and inputs (McCabe, 2010).

Computational approach is based on molecular modeling and global optimization techniques which energetically evaluate all possible packing arrangements of a given molecule in all reasonable space groups with all possible conformations (Lewis et al., 2003; Gavezzotti, 2005; Young and Ando, 2007). The resulting crystal structures of low lattice energy are regarded as the potential polymorphs. This approach has been able to generate the previously known polymorphs of molecules such as progesterone (Payne et al., 1999). However, computational methods generally overestimate the propensity of polymorphism and outputs too many structures in which many are never observed (Davey, 2003; Price, 2008). Further reduction in predicted structures requires inclusion of kinetic effects as well as more accurate thermodynamic models (Price, 2004; Price, 2008). Nevertheless, analysis of predicted structures provides useful information such as common hydrogen bonding motifs etc. which can be used in designing experimental strategies to crystallize specific predicted packing motifs (Cross et al., 2003; Florence et al., 2006; Hulme et al., 2007).

2.5. Polymorph Characterization Techniques

Solid-state characterization is a crucial step in drug development to understand the solid-state properties to provide the drug in a solid form that has optimum performance in various stages of drug manufacturing. It also renders useful information in devising methods for analysis and control of the desired form (Byrn et al., 1994; Newman and Byrn, 2003). Several analytical techniques are commonly used for polymorph characterization. A brief discussion of some commonly used methods is presented here.

2.5.1. *X-ray Crystallography*

X-ray crystallographic techniques are concerned with the structural aspects of polymorphs and provide the clearest indication of the existence of polymorphism. These techniques are based on the remarkable discovery made by Laue (1912) that crystals can diffract X-rays. However, Bragg (1913) was the first to exploit this finding to deduce a simple relationship, now known as the Bragg's law— $n\lambda = 2d \sin\theta$ in which d is the distance between the crystal planes, θ is the angle of diffraction of the X-rays, λ is the wavelength of X-rays and n is an integer. When Bragg's law is satisfied at a crystal plane, X-rays are reflected from the plane and the intensity of the radiation is maximized. With a single crystal brought into all orientations with respect to the X-ray beam, a unique set of Bragg's reflections representing the internal structure can be obtained. Together with 2θ positions of diffraction maxima and their vector parameters (magnitude and phase) in the lattice space, the complete crystal structure which includes the unit cell, lattice parameters and positions of all the atoms in the crystal lattice can be determined (Glusker et al., 1994).

These techniques can be performed with either single crystal or crystalline powder. Single crystal X-ray diffractometry (SCXRD) gives the most precise structural information for polymorphs and provides greatest understanding related to molecular conformation, packing differences and hydrogen bonding pattern etc. However, the stringent requirement of high quality single crystals of suitable size (0.05–0.1mm) and longer data processing time (1–2 days) preclude it from being used on a routine basis for characterization (Datta and Grant, 2004). Special procedures are often required to prepare

satisfactory crystals such as slow cooling, solvent diffusion, vapor diffusion, seeding etc (Etter et al., 1986; Etter and Baures, 1988; Vandersluis and Kroon, 1989).

Powder X-ray diffractometry (PXRD) is the other and the most utilized technique for the study of polycrystalline materials. It is fast, flexible and well suited for the routine characterization of polymorphs. In principle, it captures the same information as obtained by SCXRD, but with three dimensional data compressed into one dimension, thus yielding a unique powder pattern for each polymorph (Brittain, 1999). Moreover, recent advances in this field have made possible, although challenging, complete structural solution from the powder pattern (refer to section 2.6).

One common problem with PXRD is the preferred orientation effects from crystals which are non-isometric such as plates, needles etc. These may result in inconsistent patterns which are difficult to interpret (Pecharsky and Zavalij, 2003). Grinding may significantly improve the results, but this is risky as applying energy may induce polymorphic transformation.

2.5.2. *Solid-State Spectroscopy*

Solid-state spectroscopy is another category of techniques complementary to diffraction techniques. Infrared (IR), Raman and solid-state nuclear magnetic resonance (SS-NMR) are the most prominent in this category. The basic principles and applications of spectroscopy in crystal polymorphism are summarized in a number of reviews (Threlfall, 1995; Brittain, 1997; Bugay, 2001). Typically, the purpose of spectroscopic investigation in polymorphic systems is to gather information about the underlying structural aspects that give rise to the observed crystallographic differences. This analysis

is particularly useful when crystallographic data is not available (Brittain et al., 1993; Raghavan et al., 1993; Raghavan et al., 1994).

IR and Raman Spectroscopy. IR and Raman are based on transitions between molecular vibrational states upon interaction with electromagnetic radiation (Chalmers and Dent, 2006). In IR spectroscopy, radiation passing through the sample is selectively absorbed by molecular vibrations of the same frequency as incident radiation to transit to a higher vibrational state. In Raman spectroscopy, a high energy monochromatic radiation (laser) is incident upon a sample to affect the electron cloud of a molecular bond and makes it to oscillate from its equilibrium position to an unstable excited state and back. For a small portion of incident light, inelastic relaxation occurs; the electron relaxes to a higher or lower level than what it started from, leading to *stokes* or *anti-stokes scattering* with energy displacements (Raman shift) corresponding to the molecular vibrational transition frequencies.

While in IR and Raman spectrum, the band position i.e. absorption frequency in IR and wavenumber shift (Δ cm^{-1}) in Raman depends on the molecular vibrational frequency, the intensity depends on how effectively the photon energy is transferred to the molecule (Colthup et al., 1990). The mechanism by which photon energy transfers differs in both techniques; in IR, it is associated with a change in *dipole moment* where as in Raman, it is associated with a change in *polarizability*. As a result, these two techniques complement one another and IR inactive vibrations can be strong in Raman spectra and *vice versa*.

When applied to polymorphic systems, Raman has some important advantages over IR (Findlay and Bugay, 1998; Vankeirsbilck et al., 2002). (1) Raman spectra are

collected readily in the 40–400 cm^{-1} spectral region (typically unavailable on an IR spectrometer) where crystal lattice vibrations occur (Carteret et al., 2009). (2) No sample preparation is required (3) Glass is transparent to excitation and emitted radiation and gives no interfering bands therefore, spectra can be obtained without removing the sample from the specimen tube (Threlfall, 1995). (3) Insensitive to moisture effects owing to the weak scattering nature of water and hence much easier to study aqueous based systems.

However, a major problem with Raman measurements is the fluorescence (intrinsic or caused by impurities) of the sample which masks the Raman bands. However, in most cases, this can be avoided by increasing the laser wavelength at the expense of loss in signal intensity (Romero-Torres et al., 2009).

SS-NMR spectroscopy. SS-NMR is based on the differences in energy absorption by the observed nuclei in a magnetic field (Bugay, 1993). Most SS-NMR spectra of pharmaceutical solids are acquired using cross polarization with magic-angle spinning (CP-MAS), most often with ^{13}C nuclei detections (Tishmack et al., 2003; Geppi et al., 2008). CP-MAS is a double resonance technique with cross polarization (CP) facilitating magnetization transfer from abundant nuclei (usually ^{1}H) to dilute nuclei (e.g. ^{13}C, ^{15}N). ^{1}H to ^{13}C CP results in a four-fold increase in the sensitivity of ^{13}C nuclei and reduction in relaxation delay between successive pulse sequences (Brittain, 1997). Magic-angle spinning (MAS) serves to reduce or eliminate the inhomogeneous broadening effects of chemical shift anisotropy (CSA), such that only the isotropic chemical shift is observed. These two techniques, coupled with high power ^{1}H decoupling can enable acquisition of SS-NMR spectra that approach the resolution attainable in solution NMR experiments.

SS-NMR is well-suited for the study of polymorphism because small changes in conformation and/or local electronic structure can cause analogous nuclei to resonate at different frequencies and observable differences in chemical shift (Apperley et al., 1999; Harris, 2006). When compared to IR and Raman, it can provide some 'extra' information on crystallographic aspects such as number of molecules in the asymmetric unit in a unit cell (Doherty and York, 1988; Harris et al., 1997), molecular dynamics and short-range order (Gao, 1998; Masuda et al., 2006). In fact, NMR-crystallography is a growing subject area which focuses on the complete crystal structure solution from SS-NMR data alone (Harris, 2004; Brouwer et al., 2005).

2.5.3. *Thermal Techniques*

Thermal techniques are those in which a property of the analyte is determined as a function of an externally applied temperature. In the context of polymorphism, they play a crucial role in elucidating the energetic aspects of polymorphs including thermodynamic relationships, E-T diagrams etc. Applications of thermal techniques in solid-state characterization are extensively reviewed in the literature (Barnes et al., 1993; Giron, 1995; Giron, 2002; Giron et al., 2004; Craig, 2006).

Under this category, the most widely used technique is differential scanning calorimetry (DSC). Conceptually, DSC measures the change in enthalpy of the analyte (the heat differential between the sample and a reference) as a function of temperature. Intrinsically, the measured quantity is the heat capacity ($^{dH}/_{dT}$) and as the analyte undergoes any thermal event, the total heat capacity of the system changes due to the latent heat associated with it. The commonly observed thermal events in a DSC thermogram are melting (endotherm), crystallization (exotherm), phase transition

(endotherm or exotherm) and glass transition (change of heat capacity without either absorption or emission of heat) etc. The area under the curve for a thermal event will be proportional to the energy involved in the process; hence, by suitable calibration with standards, properties like heat of fusion and heat of transition can be quantitatively determined (Clas et al., 1999).

In addition to DSC, there are a few other thermal methods which have been proven useful for the study of polymorphism. Thermogravimetry (TG) measures the change in mass of the analyte upon heating a sample is useful in the study of pseudopolymorphs (Giron, 1995). Solution calorimetry which measures the heat of solution as the solid dissolves in an excess of solvent is an elegant method for detecting and characterizing polymorphic transitions (Canotilho et al., 1997; Royall and Gaisford, 2005). High-speed DSC which gives the flexibility of using high heating rates was proven useful in studying metastable forms (McGregor and Bines, 2008).

Thermal methods are often combined with X-ray diffraction or spectroscopic techniques to get deeper insight into the physical and chemical processes which occur upon heating. Variable temperature X-ray diffractometry (VT-XRD) is the commonly used technique in which controlled environment allows the study of polymorphic transformations as a function of temperature (Asnani et al., 2009). TG-mass spectroscopy (TG-MS) and TG-IR are the two combined techniques also proved useful in the study of pseudopolymorphs to identify the volatile compound (Materazzi and Curini, 2001; Materazzi and Curini, 2001).

2.5.4. *Microscopy*

Microscopic techniques are preliminary tools which can be used to identify crystal forms based on the differences in morphological and optical properties (birefringence, indices of refraction, dispersion colour etc.). They are divided into two types; *light microscopy* (LM) that probe features on the order of a micron or larger and *electron microscopy* (EM) that study materials at sub-micron level.

LM combined with fusion methods (hot stage microscopy (HSM)) is a powerful technique in which a sample is heated or cooled to observe any physical or chemical change e.g. melting, crystallization, polymorphic transformation, desolvation etc. Kuhnert-Brandstatter and his co-authors used HSM alone in his extensive search for new polymorphs/solvates of pharmaceutical compounds and to determine their stability relationships (Kuhnert-Brandstatter, 1971). LM can also be interfaced with spectroscopy, for example, hot stage IR microscopy, has been used to characterize polymorphic purity and conversions (Giron, 2002).

Under EM, two important techniques are scanning electron microscopy (SEM) and atomic force microscopy (AFM). In polymorphism research, SEM is commonly used to obtain high resolution images of crystals to characterize the habit and surface features etc (Borka, 1991). AFM has been used mainly to study the crystal growth mechanisms (Bauer et al., 2001).

2.6. Crystal Structure Solution from Powder X-ray Diffraction Data

The *ab initio* crystal structure determination of molecular materials from PXRD data is a rapidly expanding field, and has grown substantially in the last ten years (Harris

et al., 2002). This section highlights some of the difficulties associated with structure solution method and recent advances in this field to overcome them.

2.6.1. *Why are Powders more difficult than Single Crystals?*

As mentioned before, in the case of powders, the diffraction data is compressed into one dimension. As a consequence, the Bragg's reflections from different crystal planes are averaged over directions and there is a considerable overlap of peaks in PXRD pattern. This obscures the information on intensities of individual diffraction maxima which are required for the construction of the underlying crystal structure (Harris et al., 2001). Moreover, space group determination using powders is more ambiguous because the regions in the pattern, which should be free of peaks because of systematic absences, are often overlaid with peaks of other reflections (Datta and Grant, 2004). In addition to these, a more general problem is the preferred orientation of crystals which can affect the relative intensities of peaks and hinders the correct solution of the pattern.

2.6.2. *Powder Indexing – the Crucial Step*

Two key steps in structure solution from diffraction data are *indexing* and *structure solution*. Indexing involves the determination of unit cell parameters and space group by analyzing the peak positions in the powder pattern. Structure solution focuses on the determination of atomic co-ordinates from the peak intensities. Clearly, if the correct unit cell is found at the indexing stage, it is possible to proceed further to solve the structure. The three indexing programs most commonly in use are *ITO* (Visser, 1969), *TREOR* (Werner et al., 1985) and *DICVOL* (Boultif and Louer, 1991) which typically require the first 20–25 well resolved peaks. Using this input, a number of possible solutions are generated and ranked according to their *figure of merit* (Jenkins and

Gilfrich, 1992). However, the existing algorithms frequently fail due to the occurrence of peak overlap and the correct unit cell is difficult to distinguish from the large number of incorrect solutions with similar figures of merit.

2.6.3. *Recent Advances*

Despite these difficulties, significant progress has been made in this area mainly due to the advances in diffraction instrumentation and computational power. On the instrumental side, improvements in resolution, particularly with *synchrotron* X-ray sources, have lead to dramatic reductions in peak overlap and allowed highly accurate measurements of peak positions and intensities (Hastings et al., 1984; Cheetham and Wilkinson, 1991). This has given the opportunity to use single crystal structure solution techniques (e.g. direct methods or Patterson methods) to powder diffraction data (Altomare et al., 2004) and much success has been reported. However, these techniques which are referred to as *traditional* methods have certain intrinsic limitations. The extraction of accurate intensities from PXRD pattern, which is a crucial requirement for success of this approach, is not always possible and limits the complexity of structures that can be solved by traditional methods (Knudsen et al., 1998).

Because of the above limitation, much recent interest has focused on the development of new methods for solving crystal structures from PXRD data. *Direct space* approach is such a method which is based on global optimization methods (Harris et al., 1994). In this approach, instead of extracting the intensity data from PXRD pattern, the molecular fragments within the unit cell are directly manipulated to vary the position, orientation and conformation to generate trial structures independent of the experimental PXRD data. The suitability of each trial structure is assessed by direct comparison

between the PXRD pattern calculated for the trial structure and the experimental PXRD pattern. This comparison is quantified via a least-squares fit parameter R_{wp}, known as weighted powder profile R-factor. This process is equivalent to exploring a hyper surface $R_{wp}(\Gamma)$ to find the global minimum, where Γ represents the set of variables that define the structure (structural degrees of freedom). A number of different optimization algorithms have been applied as part of direct space strategy including Monte Carlo simulated annealing (MC/SA), genetic algorithm techniques etc.

On the other hand, with the emergence of direct space strategies and scoring high success in obtaining crystal structures from PXRD pattern, powder indexing has emerged as a new important bottleneck. Improved versions of the existing algorithms such as X-cell (Neumann, 2003), N-TREOR (Altomare et al., 2000) were developed to address various issues typically encountered in indexing such as contamination, strong peak overlap, zero-point shift etc. Kariuki et al. (1999) described a new approach aiming at indexing PXRD data by using a whole profile fitting technique and a global optimization method based on genetic algorithm.

Recently, Harris and Cheung (2004) have provided a tutorial review on methodology for structure determination from PXRD pattern using direct space strategies with many examples ranging from simple to complex molecules. Stephenson (2000) has examined the application of this method to solve structures of true/pseudo polymorphs of pharmaceutical molecules and highlighted the role of complementary spectroscopic techniques in assessing the correct solution.

2.7. Crystallization Fundamentals

Essentially, crystallization is a kinetic process occurs in a boundary fixed by thermodynamics. In crystallization of polymorphs, each crystal form is associated with a different kinetic path and a thermodynamic boundary. To achieve ultimate control over polymorphic crystallization, it is essential to understand the factors which govern the kinetics and thermodynamics of polymorphs.

Supersaturation. Supersaturation (σ), a dimensionless parameter, is commonly used to quantify the thermodynamic driving force for crystallization. The generic definition of supersaturation is, the difference of chemical potential of a molecule in its supersaturated state (μ^{ss}), and in its equilibrium state (μ^{eq}). In terms of measurable quantities, supersaturation can be defined using solute activity (a_{solute}) or concentration (C) as (Davey and Garside, 2000):

$$\ln \sigma = {(\mu^{ss} - \mu^{eq})}/{kT} = ln\left(\frac{a_{solute}^{ss}}{a_{solute}^{eq}}\right) \approx ln\left(\frac{C^{ss}}{C^{eq}}\right) \tag{2.2}$$

If $\sigma < 1$, the solution is *undersaturated* and the existing crystals will dissolve; if $\sigma > 1$, the solution is *supersaturated* and crystals can nucleate and grow; and if $\sigma = 1$, the solution is at *equilibrium*. Supersaturation can be achieved in several ways – for example cooling a solution, or by solvent evaporation, or by addition of an anti-solvent etc.

Nucleation. The formation of crystals in a supersaturated solution begins with 'nucleation' which is a kinetic process of molecular aggregation and formation of nanoscopically small molecular clusters of the new crystalline phase (Kashchiev and van Rosmalen, 2003). Nucleation can be either *primary*, which occurs in the absence of crystalline surfaces, or *secondary*, which requires the presence of a crystal surface for

further generation of crystal nuclei. Primary nucleation can be divided into two types; primary homogeneous which occurs in the pure bulk solution and primary heterogeneous which is catalyzed by surface or interface of different composition than the crystallizing solute. These mechanisms are thoroughly discussed by Mullin (1993) and Zettlemoyer (1969).

The general behavior of supersaturated solutions is well described by *classical nucleation theory* (CNT) based on the work of Gibbs (1948) and Volmer (1939). This theory assumes that the formation of nuclei arises from a sequence of bimolecular reactions of solute molecules. The thermodynamic description of this process defines the free energy change (ΔG) for formation of a nucleus of size n, as the balance between the energy gained by formation of bulk phase ($-nkTln\,\sigma$) and the energy required to form new surface area (γA_c). The equation can be written as:

$$G_{solution} - G_{cluster} = \Delta G = -nkTln\,\sigma + \gamma A_c \tag{2.3}$$

where γ is the interfacial tension of the cluster-solution interface, k is the Boltzmann's constant, and A_c is the surface area of the cluster. Therefore, as the cluster size increases ΔG goes through a maximum at a critical size n^*, above which the ΔG decreases continuously and growth becomes energetically favorable, resulting in the formation of crystal nuclei. Assuming spherical clusters, the homogeneous *nucleation rate J*, the number of supernuclei ($n > n^*$) generated in the solution of constant supersaturation per unit time per unit volume, can be written in an Arrhenius-type expression:

$$J = A\exp\left(\frac{-\Delta G^*}{kT}\right) = N_o v\ \exp\left(\frac{-16\pi\upsilon^2\gamma^3}{3(kT)^3(ln\,\sigma)^2}\right) \tag{2.4}$$

where ΔG^* is the critical free energy change, A is the preexponential factor, N_o is the number of solute molecules in a unit volume of solution, ν is the frequency of atomic or molecular transport at the nucleus-liquid interface, and υ is the molecular volume.

One of the key outcomes of this theory is the concept of kinetic barrier for nucleation. Thus, even though $\sigma > 1$ nucleation does not occur unless σ exceeds certain threshold value which is called the *metastable zone width* (MZW) (the maximum allowable supersaturation before solid phase separation occurs). Eq. 2.4 also suggests that the nucleation kinetics and the kinetic barrier depend not only on supersaturation σ but also on kinetic parameters such as molecular transport (hidden in preexponential factor A) and solid-liquid interfacial tension etc.

Crystal Growth. Once the nuclei are formed and exceed the critical size, they become crystals which grow around the nuclei as the solute molecules deposit from the supersaturated solution. The rate of crystal growth G_c, the incremental mass of solute deposited per unit surface area per unit time is generally expressed as the following empirical equation (Garside et al., 2002):

$$G_c = k_g \sigma^g \tag{2.5}$$

where σ is the supersaturation, k_g is an empirical coefficient depending on temperature and agitation, g is a numerical known as growth rate order.

Crystal growth involves two consecutive and independent processes: transport of the solute molecules from the bulk of the solution to the surface of the crystal and incorporation of the incoming molecules into the crystal lattice. Therefore, crystal growth kinetics depends on both external factors (supersaturation, temperature, solvent, impurities, and hydrodynamics) and internal factors (structure, crystal defects). The rate

limiting step may be one or the other depending on the growth conditions. The crystal growth and rate controlling mechanisms are discussed in detail by Nyvlt et al. (1985) and Mullin (1993).

2.8. Polymorphic Crystallization

Let us consider a monotropically related dimorphic system of Forms **I** and **II**. Fig. 2.3, is a schematic representation of the solubility curves of the two solid phases with Form **II** being less soluble i.e. more stable phase. Let us suppose we prepare a saturated solution with respect to Form **II** which corresponds to point A in Fig. 2.3. When it is cooled to point B, the solution becomes supersaturated with respect to both Forms **I** and **II**, however, crystals will not nucleate because the activation energy for nucleation (ΔG) is too high. As the process cools further, the supersaturation level increases and ΔG decreases and finally reaches the MZW where spontaneous nucleation of crystals occur (point C). However, the interesting question here is which polymorph will nucleate at point C.

Ostwald (1897) who systematically studied many polymorphic systems observed that a chemical system does not directly tend towards equilibrium but rather towards the closest metastable state. Therefore, according to his rule, the metastable Form **I** is always expected to nucleate prior to the more stable Form **II**. Though there are many examples that support this rule, there are also many exceptions. Later, Etter (1991) based on CNT proposed that, in a polymorphic system, there may exist several types of aggregates or clusters in solution resembling the structure of matured crystal forms which can compete for molecules. The polymorph which favored to crystallize is the one that nucleates the

fastest. Using this hypothesis and Eq. 2.3, three possibilities can be expected at point C in Fig. 2.3.

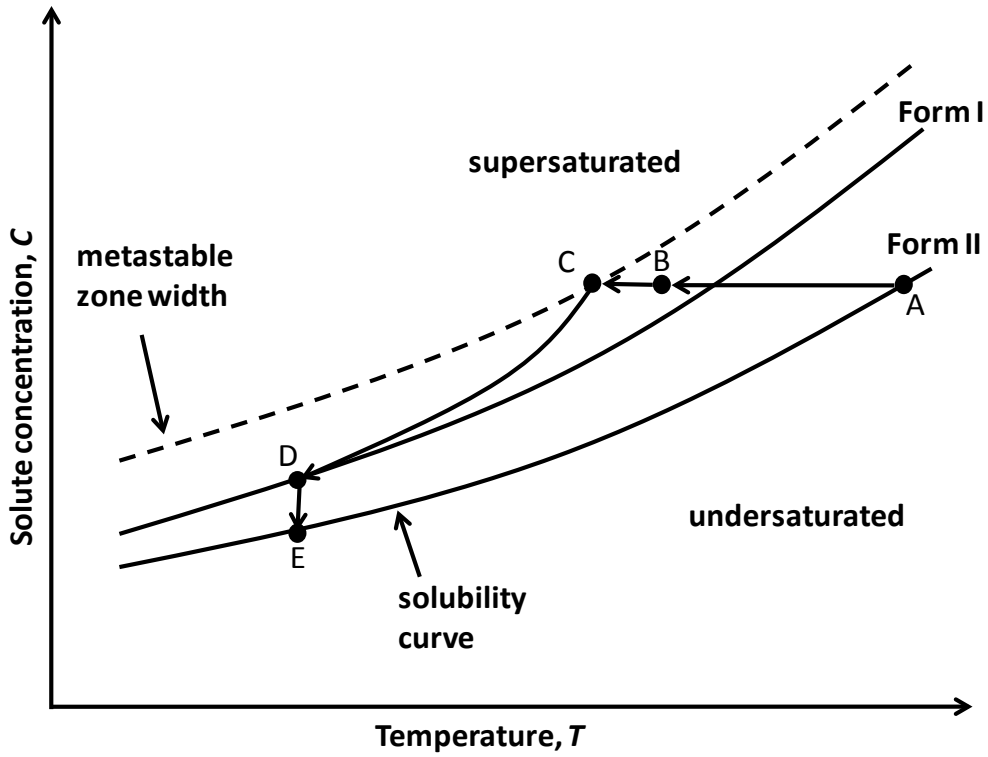

Figure 2.3 Schematic solubility-temperature diagram for a cooling crystallization process for a dimorphic system Forms **I** and **II**. **A**: Saturated solution with respect to Form **II**, **B**: Metastable solution supersaturated with respect to both Forms **I** and **II**, **C**: Metastable zone width, **D**: Solubility of Form **I**, **E**: Solubility of Form **II**.

1. If all the kinetic parameters are similar for both Forms **I** and **II**, nucleation rate will increase by increasing the supersaturation. This favors the condition ($J_{II} > J_I$) leads to nucleation of more stable Form **II**.
2. At constant supersaturation, increase in molecular transport favors the condition ($J_I > J_{II}$). Because, metastable forms have higher solubility, thus $A_I > A_{II}$ is expected.

3. At constant supersaturation, decrease in interfacial energy (γ) favors the condition ($J_I > J_{II}$). Because, it has been proven that γ decreases with decreasing heat of dissolution and increasing value of solubility, both generally favor the metastable forms (Sangwal, 1989).

Though CNT successfully predicts the general behavior of nucleation, its applications in polymorphism are very limited because of its implicit assumptions (Oxtoby, 1998). Moreover, it does not capture the contribution from structural factors such as solute-solvent interactions, therefore, it cannot provide any information on the structure of aggregates and the pathways leading the solution to solid crystal (Schuth, 2001). If the structure of aggregates could be identified and related to structure in the final solid form, then a greater amount of control over the structural outcome of the crystallization might be achieved. A much recent work on nucleation both from simulations and experiments reveal that crystals obtained from solution are often not formed via the much simplified classical pathways but by much more complex routes in which specific intermolecular interactions play an important role (Anwar and Boateng, 1998; Vekilov, 2004; Davey et al., 2006). These studies suggest that our understanding on nucleation is very limited and prediction of polymorphic outcome is only possible if we fully understand the structural aspects of nucleation.

However, in Fig. 2.3, at point C, if we suppose that experimental conditions favored the nucleation of metastable Form **I**. Then, crystallization continues further by the growth of Form **I** crystals. During this, solution concentration drops as solute molecules transfer from the liquid phase to the growing crystals until equilibrium is reached at point D, which is the solubility of Form **I**. However, at this point, the solution

is still supersaturated with respect to Form **II** and ultimately, Form **I** will have to transform to Form **II** by a process which is described below.

2.9. Solvent Mediated Polymorphic Transformations (SMPT)

In crystallization, a metastable form can transform to the more stable form via solvent mediated polymorphic transformation (SMPT) in which the solvent molecules facilitate the molecular rearrangement and crystal growth. The basic phenomenon involved in SMPT is well understood and expressed as a three step process (Cardew and Davey, 1985).

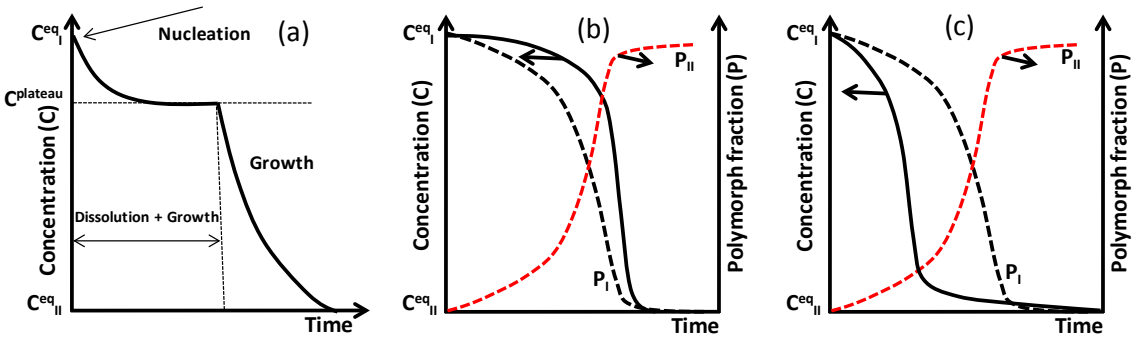

Figure 2.4 Solute concentration (C) and polymorph fraction (P) Vs time profiles during a polymorphic transformation in solution, $\mathbf{C^{eq}_I}$ and $\mathbf{C^{eq}_{II}}$ are the solubilities of Forms **I** and **II**, **(a)** General solute concentration profile and **(b)** Transformation is controlled by growth of the stable Form **II (c)** Transformation is controlled by dissolution of the metastable Form **I (**Cardew and Davey, 1985; Mangin et al., 2009).

1. *Primary nucleation of the stable phase.* This is the trigger for the transformation process and it can be homogeneous or heterogeneous (Croker and Hodnett, 2010).
2. *Dissolution of the metastable phase.* As the nuclei of the stable phase grow, the solution concentration drops below the solubility of metastable phase. The metastable crystals thus dissolve producing supersaturation for the continued growth of stable phase.

3. *Growth of the stable phase.* This step simultaneously occurs with the step 2 and dissolution-growth process continues until all of the metastable crystals disappear. The growth of stable form continues further and finally transformation ends when solubility of stable form is reached.

Depending on both the properties of solute and solvent, (1) or (2) or (3) can be the slowest step. When step (1) is rate controlling, any factor that affects nucleation kinetics (see Eq. 2.4) will determine the overall kinetics. When step (2) or (3) is controlling, the factors which can influence the solute mass transfer such as particle size, agitation etc. will determine the overall kinetics.

Experimentally, transformation kinetics can be characterized by a combination of measurements of solid phase composition and solute concentration with respect to time (Davey et al., 1986). Fig. 2.4a shows the general behavior of solute concentration during a transformation process. It indicates that there exists a plateau concentration between the solubility of two forms as a result of the balance between kinetics of dissolution and growth. Based on the position of the plateau, two extreme cases are possible. (1) The consumption of solute by growth is slower than the production of solute by dissolution, and the plateau is located in a "high" position, in the vicinity of the solubility of the metastable polymorph (see Fig. 2.4b). Therefore, the nucleation and growth mechanism of the stable polymorph limits the transformation and thus is the rate-controlling step. There are many examples in the literature for this type of transformation: *L-glutamic acid* **α→β** in water (Kitamura, 1989), *glycine* **α→γ** in water (Yang et al., 2008), *irbesartan* Form **A** → Form **B** in water (Garcia et al., 2002), *taltireline* **α→β** transformation in water (Maruyama et al., 1999), c*arbamazepine* anhydrate → hydrate transformation in

ethanol/water solution (Qu et al., 2006), *citric acid* anhydrate → monohydrate transformation in water (Caillet et al., 2006), *sulfamerazine* Form **I** → Form **II** in various solvents (Gu et al., 2001). (2) The concentration plateau is just above the solubility of the stable polymorph (see Fig. 2.4c). The dissolution mechanism of the metastable phase limits the transformation and is thus the rate-controlling step. To our knowledge, only one example available in the literature: *glycine* **β→α** in ethanol/water solution (Ferrari et al., 2003).

2.10. Closing Remarks

Crystal structure is an important property which needs to be carefully controlled during crystallization to achieve the desired product quality. A thorough understanding of fundamentals of crystal polymorphism and the crystallization mechanisms which govern the polymorph formation and transformation is a prerequisite for the design and control of a robust crystallization process for the isolation of desired polymorph.

CHAPTER 3

Experimental – Materials, Methods and Analytics

In this chapter, experimental methods used for polymorph characterization of the model compound are presented. In addition, the computational procedure for the structure determination from PXRD pattern is also described.

3.1. Model System - Tolbutamide

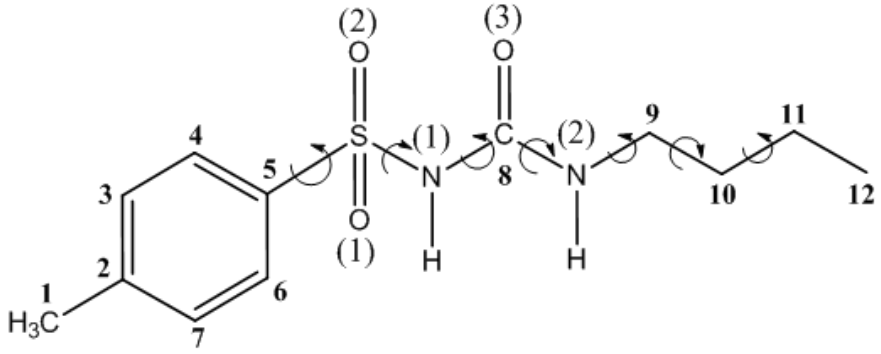

Figure 3.1 Chemical diagram of Tolbutamide (TB) with several rotational degrees of freedom (τ = torsional angle).

Sulfonylurea compounds are considered as an important class of therapeutical agents in medicinal chemistry for their hypoglycemic activity (Patlak, 2002). Tolbutamide *(1-Butyl-3-(4-methylphenylsulfonyl) urea, TB)* is a first generation oral anti-diabetic drug that belongs to this class. It is used in the treatment of non-insulin dependent (type II) diabetes as an adjunct to diet control. It controls the blood glucose levels by stimulating the pancreas for secretion of insulin. TB tablets are marketed under the brand name *Orinase*®. The chemical structure of TB (Fig. 3.1) shows that apart from the rigid benzene ring, it has seven bonds that can rotate freely along the alkyl chain. Due

to this flexibility, one can expect this molecule to crystallize into different polymorphic structures.

3.1.1. *Previous Work*

The first study on polymorphism of TB was reported in the extensive study carried out by Kuhnert-Brandstatter and Wunsch (1969) on polymorphism and drugs using hot stage microscopy. The existence of three polymorphic forms with melting points of 127 °C, 117 °C and 106 °C were reported. Subsequently, the system was studied by Simmons et al. (1972) who reported two polymorphic forms which were prepared by crystallization experiments and named them as Forms **A** and **B**. Later, Burger (1975) further investigated the polymorphism of this drug and was able to prepare four polymorphic forms (Forms **I**–**IV**). He claimed that Forms **I** and **III** were identical with Simmon's Forms **A** and **B**. The stability order was estimated to be Form **I** > Form **III** > Form **II** > Form **IV** with Form **I** being the most stable form at ambient conditions. Later, Rowe and Anderson (1984) further examined the stability order of Forms **I** and **III** and observed that Form **I** readily transforms to Form **III** in solution at ambient conditions. Hence, they claimed that Form **I** is less stable than Form **III**.

In CSD, two crystal structures of TB, reference codes ZZZPUS01 (Nirmala and Gowda, 1981) and ZZZPUS02 (Donaldson et al., 1981), are indexed and both correspond to Form **I**. Form **I** crystallizes in the orthorhombic, $Pna2_1$ space group (Z = 4; a = 20.23 Å, b = 7.83 Å, c = 9.09 Å). The unit cell data for Form **III** has been reported but without atomic co-ordinates (Leary et al., 1981). Form **III** crystallizes in the monoclinic, $P2_1$ space group (Z = 2; a = 8.11 Å, b = 8.96 Å, c = 10.19 Å, β = 101°). More recently, Kimura et al. (1999) further characterized Burger's Forms **II** and **IV** using various

physical methods. The unit cell data of Form **II** was determined and deposited in CSD (refcode: ZZZPUS03) without atomic co-ordinates. This form crystallizes in the monoclinic, $P2_1/n$ space group (Z = 4, a = 11.81 Å, b = 9.06 Å, c = 13.98 Å, β = 104.5°).

From the previous studies, it is evident that TB can crystallize in at least four polymorphic forms which have been well characterized by various techniques. However, there is some confusion about the stability order of TB polymorphs at ambient conditions. Except for Form **I**, the crystal structures of other polymorphic forms (Forms **II**–**IV**) have not been reported to date. Since the unit cell data of Forms **II** and **III** were already reported, it can be assumed that the crystal structures have been determined but not reported in the literature. In the case of Form **II**, the comparison of calculated X-ray powder pattern from its crystal structure with the experimental powder pattern was reported (Kimura et al., 1999).

While this work is underway, Hasegawa et al. (2009) reported a detailed analysis on the thermal behavior of Form **I** and showed that this form undergoes a reversible structural transformation to a new crystal form upon heating beyond 38 °C. The newly transformed phase has been named as Form $\mathbf{I}^{\mathbf{H}}$ and the phase below 38 °C as Form $\mathbf{I}^{\mathbf{L}}$. We adopt this naming convention for our discussion in this work. Recently, in an attempt to co-crystallize TB resulted in a novel polymorph Form **V** whose structure is also reported (Nath and Nangia, 2011).

3.2. Characterization Techniques

3.2.1. *Light Microscopy*

The crystal habit was examined using an optical polarized light microscope (Olympus, BX51) connected to a CCD camera. The image was collected using a Soft Imaging System's *Analysis* image capture software.

3.2.2. *Differential Scanning Calorimetry (DSC)*

DSC analysis was carried out using a Perkin-Elmer Diamond DSC (Perkin-Elmer, Beaconsfield, UK). The samples (2–5 mg) were hermetically sealed in aluminum pans and heated from 25 to 150 °C at a scanning rate of 10 °C min^{-1} under nitrogen purge at a flow rate of 20 mL min^{-1}. Prior to analysis, the heat of fusion was calibrated with indium (purity, 99.999%; melting point, 156.4 °C; heat of fusion, 28.47 mJ mg^{-1}; heating rate; 10 °C min^{-1}).

3.2.3. *Hot Stage Microscopy (HSM)*

Thermomicroscopic investigations were performed with an optical polarizing microscope (Olympus, BX51) equipped with a Linkam hot stage THMS 600 connected to a TMS 94 temperature controller (Linkam Scientific Instruments Ltd., Tadworth, Surrey, UK). The microscopic images were recorded with a CCD camera attached to the Olympus BX-51 microscope (Olympus Optical GmbH, Vienna) at every 10 s time interval using Soft Imaging System's Analysis image capture software. Samples were heated over the temperature range of 25 to 150 °C at a constant heating rate of 5 °C min^{-1}.

3.2.4. *Powder X-Ray Diffraction (PXRD)*

PXRD experiments were conducted in Bragg-Brentano geometry with a Bruker D8 Advance (Bruker AXS GmbH, Germany) X-ray powder diffractometer equipped

with Cu-Kα source (λ = 1.5406 Å), a Nickel-filter, 0.3° divergence slit, a linear position sensitive detector (Vantec-1) and an Anton Paar Model HTK 1200 high temperature chamber. Data were collected at room temperature (RT) over a 2θ range of 5–50° with an equivalent step size of 2θ = 0.018° at a scan rate of 0.02° sec^{-1}. For Form **IV**, data were collected over the same 2θ range and with same step size, but at a reduced scanning rate of 0.01° sec^{-1}. All samples were rotated to improve the counting statistics. To collect the PXRD pattern of Form $\mathbf{I^H}$, Form $\mathbf{I^L}$ was heated to 50 °C at a heating rate of 0.4 °C/sec and delayed for 10 minutes for stabilization. Then, the data were collected with the same scanning parameters as used before for Form $\mathbf{I^L}$. Due to the crystal habit of Forms **II** and **III**, their experimental peak intensities were strongly affected by preferred orientation resulting in severe differences in relative intensities of observed and computed PXRD patterns. Hence, their samples were hand ground to a fine powder before collecting the powder pattern.

3.2.5. *Scanning Electron Microscopy (SEM)*

Morphology of the TB polymorphs was examined using a high resolution SEM (JSM-6700F, JEOL Ltd, Tokyo, Japan) operating at 5 keV under secondary electron imaging (SEI) mode. Each sample was mounted on an aluminum stub and platinum coated for 1 min by a sputter coater (Cressington 208HR, Cressington Scientific Instruments Inc, Watford, UK), prior to analysis.

3.2.6. *Fourier Transform-Infrared Spectroscopy (FTIR)*

A Perkin-Elmer 2000 FTIR spectrometer was used in KBr diffuse reflectance mode for collecting the IR spectra of the polymorphs. A total of 32 scans were collected over the range of 400–4000 cm^{-1}.

3.2.7. *Solid-State Nuclear Magnetic Resonance Spectroscopy (SS-NMR)*

Solid-state ^{13}C NMR spectra were collected at RT on a Bruker Avance 400 spectrometer with a CP-MAS pulse sequence operating at a frequency of 100.61 MHz (^{13}C frequency). The samples were packed in zirconium rotors, spun at typical speeds of around 6 kHz at the magic angle. A contact time of 2 ms and a relaxation delay of 15 sec were used between each scan. *Toss* program was used to suppress the spinning side bands. The chemical shift data was referenced to an external standard of Adamantane.

3.2.8. *Single Crystal X-Ray Diffraction (SCXRD)*

X-ray reflections were collected on a Rigaku Saturn CCD area detector with graphite monochromated Mo-Kα radiation (λ = 0.71073 Å). Data were collected and processed using *CrystalClear* (Rigaku) software. For data collection at different temperatures, the crystal was allowed to equilibrate at the desired temperature for 15 min in a stream of cold nitrogen supplied by Rigaku Cryostat. The structure was solved by direct methods and expanded using Fourier techniques. The non-hydrogen atoms were refined anisotropically. All hydrogen atoms were fixed at idealized positions except for N-H protons which were located from the difference Fourier map and allowed to ride on their parent atoms in the refinement cycles.

3.3. *Computational Procedure for Structure Solution of Form IV*

To solve the crystal structure of Form **IV**, *Reflex Plus* module in Materials Studio molecular modeling (Accelrys Software Inc. Version 4.3.) has been used. Reflex Plus is a complete package for structure determination from PXRD data, including indexing, Pawley refinement, structure solution and Rietveld refinement. The successive dichotomy indexing program *X-cell* (Neumann, 2003) was used to index the first 23 reflections ($2\theta <$

25°) which were shown along with the tabulated values in Fig 3.2. The proposed unit cell and the function profile parameters (background coefficients, zero-point shift and peak width parameters) were refined over a 2θ range of 5–50° by the *Modified Pawley* method. Pseudo-Voigt function was used for approximating the peak shape profile. The background was determined by linear interpolation using 20 terms. Asymmetric corrections were applied in the range of $2\theta < 45°$ using Berar-Baldinozzi correction. After Pawley refinement, the R_{wp} value was found to be 4.13%.

2θ (degree)
8.938
10.58
11.269
13.219
14.445
14.944
16.481
17.889
18.323
18.770
19.246
19.613
19.931
20.319
20.820
21.209
21.956
22.316
22.750
23.638
24.024
24.471
24.767

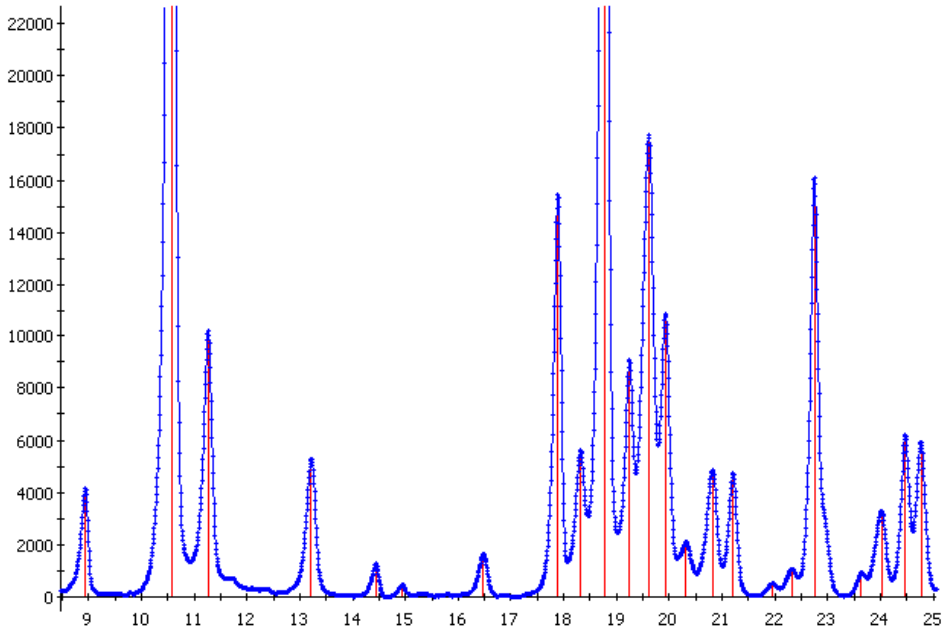

Figure 3.2 The first 23 observed 2θ values used for powder indexing in the structure determination of Form **IV** from powder X-ray diffraction.

The subsequent structure solution was performed by Monte Carlo/parallel tempering method using PowderSolve (Engel et al., 1999). The initial molecular model of TB was taken from Form **II** crystal structure and placed in the refined unit cell. A total of

13 degrees of freedom (position of the molecule defined by three co-ordinates, orientation of the molecule defined by three rotation angles and seven torsional angles as shown in Fig. 3.1) were assigned inside an asymmetric unit and the structure solution was executed. Hydrogen atoms were not used during the structure solution. March-Dollase method (Dollase, 1986) was used to model the preferred orientation effects in the powder pattern because this crystal form grows into thin needles.

For final Rietveld refinement, hydrogen atoms were included and refined by using the same degrees of freedom as used for the structure solution. Global isotropic temperature factors were applied for modeling the temperature effects on atoms. The final R_{wp} value was converged at 5.38%. The feasibility of hydrogen bonding and close contacts were verified before accepting the final solution.

3.4. Solubility Measurements

The solubilities of TB were measured at different temperatures starting from 15 to 60 °C using a UV-Vis spectrophotometer (Varian Cary 50 Conc) which was calibrated at 229 nm in ethanol solvent. Using a 20 ml crystallization vessel, an excess of TB was placed in 10 ml of ethanol, which was maintained at the desired temperature (± 0.1 °C) by circulating water in the outer jacket using a Julabo circulator. Immediately after addition, 400 rpm agitation was applied by means of a magnetic stirrer. Samples were taken at different intervals and measured until constant concentration was achieved. For all samples, the equilibration time was approximately 2–3 hours. During sampling, the agitation was stopped and solution was allowed to settle for 1 hour. Approximately, 1 ml of the supernatant was then filtered through a millipore (0.2 µm) syringe filter. After sufficient dilution, the concentration of the filtered supernatant was determined by

measuring the absorbance at 229 nm. PXRD was used to confirm that no polymorphic transformation had occurred at the end of the solubility measurement. The solubility of each sample is measured in duplicate.

CHAPTER 4

Structural and Stability Features of Tolbutamide Polymorphs

Central to the understanding of the origin and control of polymorphism is the ability to describe and interpret the similarities and differences in intermolecular interactions in the possible polymorphic structures. In this chapter, crystal structures of four polymorphic forms of TB (Forms **I^L**, **II–IV**) were presented and analyzed to understand the structural origin of polymorphism in TB. Spectroscopy has been used as a complementary technique to further understand the structural features of TB. Furthermore, influence of TB molecular dynamics on PXRD patterns is also highlighted.

4.1. Preparation of Polymorphs

Form **I^L** of TB was prepared by dissolving TB (3 g) in 6 ml of acetonitrile at 60 °C and naturally cooled to RT. Form **II** was prepared by dissolving 1.2 g of TB in 10 g of acetonitrile in a 20 ml vial followed by slow addition of 5 ml of water using a pipette into the unagitated solution. After one week, crystals were harvested and dried in vacuum at 40 °C.

For preparing Form **III**, the method used by Simmons et al. (1972) was employed but this resulted in a mixture of Forms **I^L** and **III** in our experiments. The microscopic observations revealed that these two polymorphs nucleate simultaneously under these conditions and it is one of the cases of dimorphic concomitant crystallization (Bernstein et al., 1999). To obtain this form, a slightly modified procedure was designed in which a saturated solution of TB in ethanol was prepared and then, water was slowly added into the unagitated solution using a pipette till spontaneous nucleation of Form **III** crystals

occurred. The crystals were allowed to grow for one day before they were harvested and dried in vacuum at 40 °C. The crystals obtained for Forms **I^L**, **II** and **III** were pure and of suitable size for SCXRD experiments.

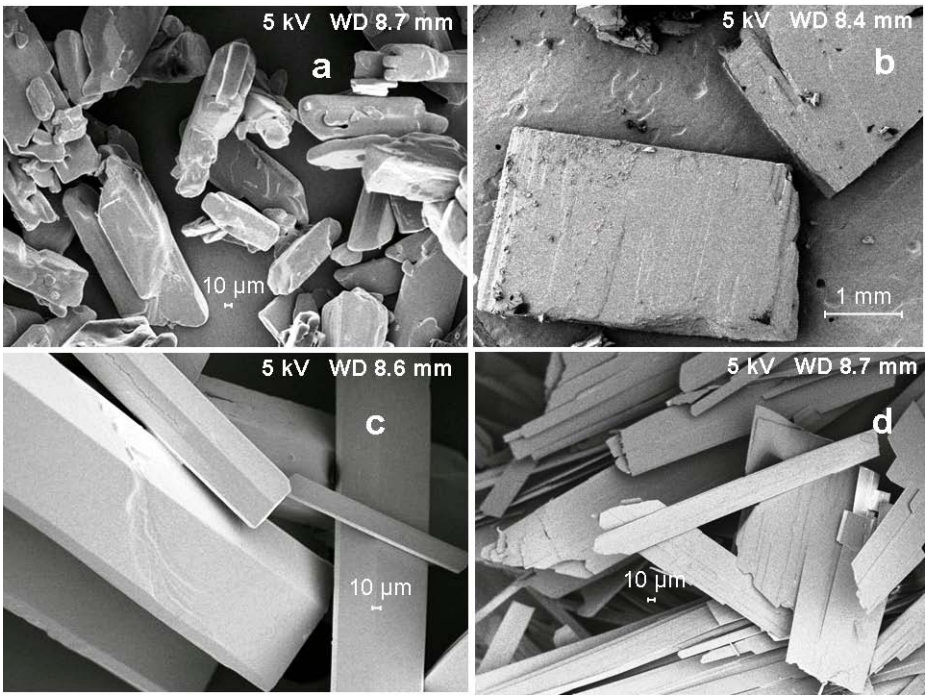

Figure 4.1 Scanning electron microscope images of TB polymorphs (**a**) Form **I^L** (**b**) Form **II** (**c**) Form **III** (**d**) Form **IV**.

To prepare Form **IV,** a slow evaporation method was used which was otherwise prepared only by either spray drying (Kimura et al., 1999) or from melt crystallization (Burger, 1975). TB (0.5 g) was dissolved in 10 ml of acetonitrile, filtered and then transferred to a 20 ml conical flask. The mouth of the flask was covered with aluminum foil (a few holes were made in the foil) and left at ambient temperature for slow evaporation of the solvent. The crystals of Form **IV** obtained by this method were not of suitable size for SCXRD experiment. Fig. 4.1 shows the SEM images of TB polymorphs.

Form $\mathbf{I^L}$ is of prismatic shape and Form **II** grows into thin plates. Form **III** consists of long bladed needles whereas Form **IV** grows like very thin needles.

4.2. Structural Features of TB Polymorphs

The crystal structures of TB polymorphs Forms $\mathbf{I^L}$ and II–IV were determined and the corresponding crystallographic data was given in Table 4.1. The comparison between the unit cell parameters determined in this work and those reported in the literature reveals some interesting observations. (1) The unit cell data reported for Form **III** (Leary et al., 1981) does not match with any of our crystal data; and (2) The unit cell data reported for Form **II** (Kimura et al., 1999) is found to be different from that of ours, but, matches with our Form **III**. A careful examination of the calculated PXRD pattern of Form **II** reported in Kimura et al. (1999) and of the unit cell given for Form **II** by the same authors (CSD refcode ZZZPUS03), reveals a clear discrepancy - the calculated 2θ positions of ZZZPUS03 do not match with the 2θ positions reported in their publication. It may be possible that they presented the PXRD pattern of Form **II** but gave the unit cell data of Form **III**.

4.2.1. *TB Conformers and Packing Schemes*

In all the polymorphic forms, TB molecule adopts different conformations hence it is another representative case of conformational polymorphism. The conformers found in the crystal structures can be divided into two types (U and chair, Fig. 4.2) based on the phenyl and alkyl tail orientation with respect to S-N1-C8-N2-C9 plane (refer to Fig. 3.1 for atom numbering). In the U-type conformation, both the phenyl ring and alkyl tail are on the same side of the S-N1-C8-N2-C9 plane, whereas, in chair-type, these are oriented in the opposite side of the plane.

Table 4.1 Summary of crystallographic data of TB polymorphs.

Crystal data	Form $\mathbf{I^L}$	Form **II**	Form **III**	Form **IV**
Empirical formula	$C_{12}H_{18}N_2O_3S$	$C_{12}H_{18}N_2O_3S$	$C_{12}H_{18}N_2O_3S$	$C_{12}H_{18}N_2O_3S$
Formula weight	270.34	270.34	270.34	270.34
Crystal habit	Prism	Plate	Needle	Needle
Sample type	Single crystal	Single crystal	Single crystal	Powder
Crystal system	Orthorhombic	Monoclinic	Monoclinic	Monoclinic
Temperature (K)	153	153	153	298
Color	Colorless	Colorless	Colorless	White
Space group	$Pna2_1$	Pc	$P2_1/n$	$P2_1/c$
a/Å	19.626(9)	9.087(8)	11.735(2)	10.091
b/Å	7.803(4)	17.228(3)	9.042(8)	15.646
c/Å	9.058(4)	17.951(4)	13.732(3)	9.261
α/°	90	90	90	90
β/°	90	95.01(3)	103.57(3)	100.49
γ/°	90	90	90	90
V/Å^3	1387.3(11)	2799.8(10)	1416.4(5)	1438.9
Z	4	8	4	4
d_{calc}/g cm^{-3}	1.294	1.283	1.268	1.248
μ (mm^{-1})	0.236	0.234	0.231	0.227 (calculated)
Reflections collected	6197	14332	11123	--
Unique reflections	2118	8617	3514	--
Observed reflections	2002	8016	2669	--
$R_1[I > 2\sigma(I)]$	0.0572	0.0555	0.0976	R_p = 3.96 %
wR_2 [all]	0.1559	0.1434	0.2742	R_{wp} = 5.38 %
Goodness-of-Fit	1.115	1.070	1.159	--
Diffractometer	Rigaku Saturn CCD area detector	Rigaku Saturn CCD area detector	Rigaku Saturn CCD area detector	Bruker AXS

Based on this classification, the molecular packing arrangements in Forms $\mathbf{I^L}$ and **II**–**IV** can be classified into four schemes (A–D) as shown in Fig. 4.2. These schemes were derived based on the orientation of phenyl ring and alkyl tail of adjacent molecules in a hydrogen bonding network. For example, in scheme A, the two adjacent molecules are arranged in such a way that the phenyl ring and alkyl tail of TB molecule are laid on the opposite side of the S-N1-C8-N2-C9 plane, whereas in scheme B, they are on the same side of the plane.

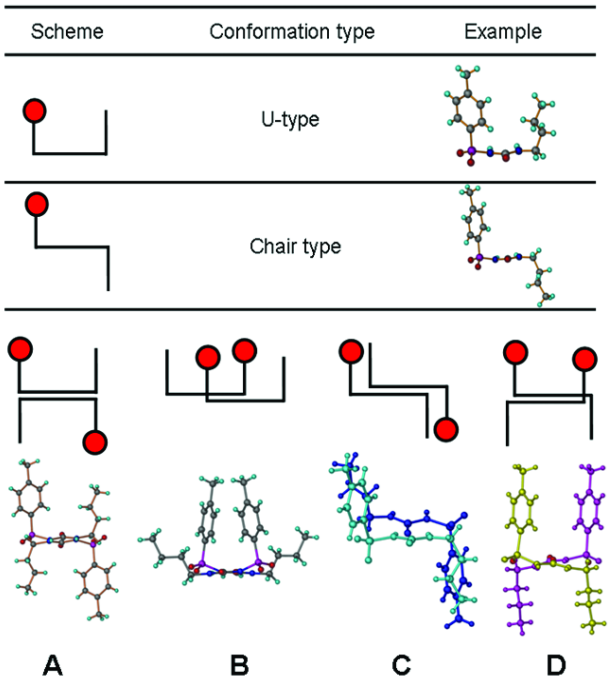

Figure 4.2 Types of conformers and packing schemes observed in TB polymorphs Forms $\mathbf{I}^{\mathbf{L}}$ and **II**–**IV**.

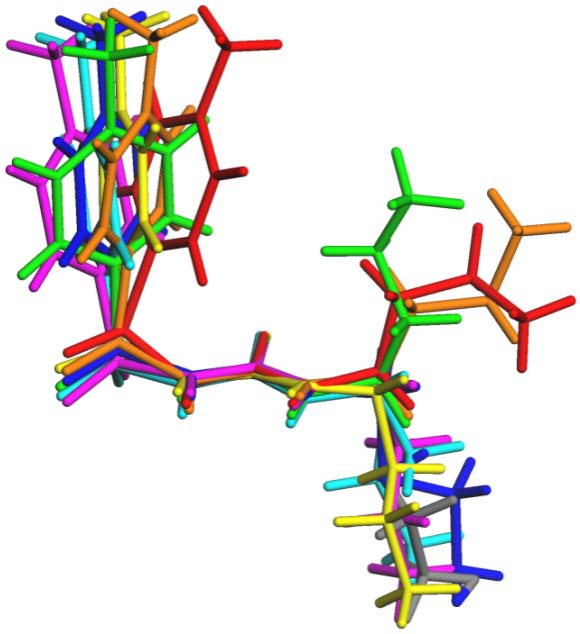

Figure 4.3 Overlay of conformers observed in TB polymorphs Forms $\mathbf{I}^{\mathbf{L}}$ and **II**–**IV** (Red-U1 (Form $\mathbf{I}^{\mathbf{L}}$); Green-U2 (Form **III**); Brown-U3 (Form **IV**); Pink-Ch1, Yellow-Ch2, Light blue-Ch3, Thick blue and Grey-Ch4 (Form **II**).

Table 4.2 The calculated torsional angles (τ_1 to τ_7) of conformers observed in TB polymorphs (U: U-type and Ch: chair type); Occupancy factors for Ch4, [a] 0.34, [b]0.66, [c]0.5.

Torsion angle (°)	Form **I**^{L} (U1)	Form **III** (U2)	Form **II**					Form **IV**
			Ch1	Ch2	Ch3	Ch4		U3
τ_1(C6–C5–S–N1)	141.9	57.7	81.5	141.4	137.2	87.5		94.3
τ_2(C5–S–N1–C8)	-50.8	-73.6	-84.7	-67.8	-73.7	-75.6		63.2
τ_3(S–N1–C8–N2)	147.6	163.3	-176.6	164.8	-173.3	176.0		-154.3
τ_4(N1–C8–N2–C9)	-174.3	-176.6	174.5	172.7	-177.5	172.3		-174.4
τ_5(C8–N2–C9–C10)	81.5	100.4	-77.8	-83.9	-105.1	-90.8		-85.7
τ_6(N2–C9–C10–C11)	-178.8	-67.3	-60.4	-66.0	61.7	-102.4[a]	-172.3[b]	-179.3
τ_7(C9–C10–C11–C12)	-69.3	-176.9	175.5	-175.4	-178.9	-159.7[c]	-179.9[c]	162.6

Table 4.3 Hydrogen bond distances and angle parameters with neutron normalized N–H (1.009 Å) distances in TB polymorphs.

Crystal structure	D–H···A[a]	H···A [Å]	D···A [Å]	D–H···A [°]
Form **I**^{L}	N1–H2···O3	1.77	2.739(5)	161
	N2–H2A···O3	2.03	2.939(5)	148
	N2–H2A···O1	2.35	3.070(5)	127
Form **III**	N1–H1···O3	1.83	2.771(5)	154
	N2–H2A···O3	2.24	3.141(5)	143
	N2–H2A···O2	2.16	2.903(5)	133
Form **II**	N1–H1···O3	2.05	2.949(6)	147
	N2–H2···O3	1.85	2.787(5)	154
	N1–H1···O1	2.43	3.131(6)	126
	N3–H3···O4	1.77	2.754(5)	164
	N4–H4···O4	2.23	3.115(5)	145
	N4–H4···O5	2.22	3.021(5)	135
	N8–H5···O12	1.78	2.722(5)	153
	N7–H6A···O12	2.11	2.972(5)	142
	N7–H6A···O10	2.25	3.045(5)	135
	N5–H7···O9	1.78	2.730(5)	155
	N6–H8···O9	2.13	3.012(5)	145
	N6–H8···O7	2.61	3.228(5)	120
Form **IV**	N1–H1···O1	1.96	2.756	151
	N2–H2···O1	2.40	3.132	152
	N1–H2···O2	2.35	3.017	119

For geometric description of hydrogen bond interactions, the following criteria has been used: H···A distance < r(A) + r(H) (A: acceptor, D: donor and r: van der Waals radius).

Despite forming various schemes, the usual "head-to-tail" packing mode, which is typically observed in the crystal structures of urea derivatives persists in all the TB polymorphs (Kim et al., 1999). The traditional urea tape motif, a chain of bifurcated N–H···O hydrogen bond between NH donors and the carbonyl oxygen acceptor is the dominant supramolecular synthon (key intermolecular interaction) in all the crystal structures (George et al., 2004). In addition to that, one of the sulfonyl oxygens engaged in hydrogen bonding with alkyl amide. The torsional angles for various TB conformers were tabulated in Table 4.2 and the extent of conformational diversity of TB molecule was highlighted with the overlay of conformers in Fig. 4.3. The geometrical features of hydrogen bonding were listed in Table 4.3.

4.2.2. *Crystal Structure Analysis*

Forms I^L and III. Form $\mathbf{I^L}$ crystallizes in the orthorhombic, $Pna2_1$ space group whereas Form **III** crystallizes in the monoclinic, $P2_1/n$ space group. Both polymorphs crystallize with one molecule of TB in the crystallographic asymmetric unit ($Z' = 1$) and adopt the U-type conformation. However, significant differences were observed in the orientation of the terminal alkyl chain of these two conformers. The torsional angles τ_6 and τ_7 are in *anti*- and *gauche*- conformation in Form $\mathbf{I^L}$, whereas they are in *gauche*- and *anti*- conformation in Form **III**, respectively (see Table 4.2).

The crystal packing diagrams of Forms $\mathbf{I^L}$ and **III** were shown in Fig. 4.4 and both forms adopt the packing scheme A. They are also similar in terms of hydrogen bonding and the other structure stabilizing interactions (see Table 4.3). The one-dimensional (1D) chains involving N–H···O hydrogen bonds run along [0 0 1] and [0 1 0] in Forms $\mathbf{I^L}$ and **III**, respectively. The concomitant nucleation of these two forms from

the crystallization batches could be because of their similarities in conformation, hydrogen bonding and crystal packing ability.

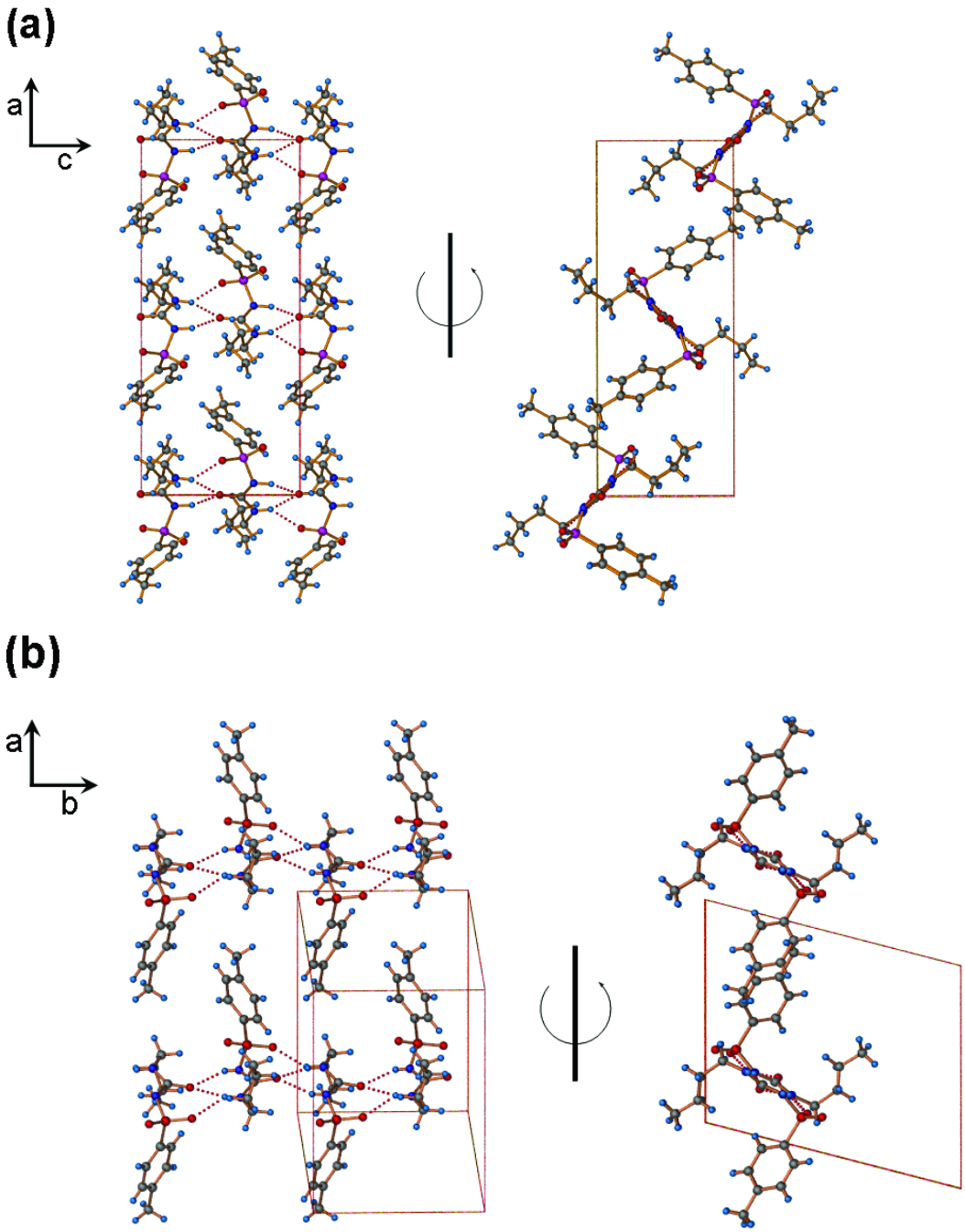

Figure 4.4 Crystal packing diagrams of TB polymorphs (**a**) Form $\mathbf{I}^{L}$ (**b**) Form **III**.

***Form II*.** Form **II** crystallizes in the monoclinic, *Pc* space group with four molecules of TB in the crystallographic asymmetric unit ($Z' = 4$). Unlike the conformers in Forms $\mathbf{I}^{\mathbf{L}}$ and **III**, the TB molecule adopts the chair type conformation in this polymorph. It is interesting to note that all symmetry independent molecules (Ch1, Ch2, Ch3 and Ch4) are conformationally different (i.e., conformational isomorphism) (Nangia, 2008).

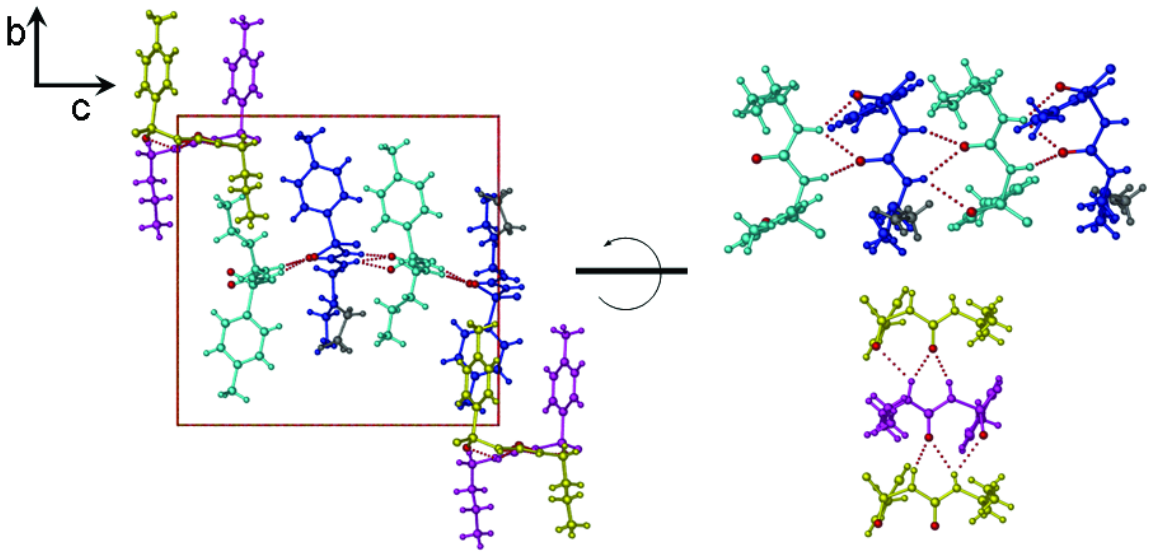

Figure 4.5 Crystal packing diagram of Form **II** (Pink-Ch1; Yellow-Ch2; Light blue-Ch3; Thick blue and Grey-Ch4).

The major differences were observed in τ_1 and τ_6 torsion angles. In Ch1 and Ch4, the torsion around τ_1 is in *gauche-* conformation, whereas in Ch2 and Ch3 it is in *anti-* conformation. The torsion around τ_6 is in *gauche-* conformation except for Ch4 which is found to be in *anti-* conformation. In Ch4, the two terminal carbon atoms (C55 and C57) were found to be disordered. The disorder at C55 was modeled over two sites with an occupancy ratio of 66:34, whereas C57 was modeled with an occupancy ratio of 50:50. For clarity, these disordered atoms were shown in two different colors (thick blue and grey) for Ch4 molecule in the overlay (Fig. 4.3) and packing diagrams (Fig. 4.5).

As shown in Fig. 4.5, the crystal structure of Form **II** reveals two types of packing schemes (C and D). Conformers Ch1 (pink molecule) and Ch2 (yellow molecule) follow scheme D i.e. phenyl rings and alkyl tails on opposite side of the plane. They form 1D chains along [1 0 0] direction involving N–H···O hydrogen bonds. Conformers Ch3 (thick blue) and Ch4 (light blue) form another 1D network which runs perpendicular to the 1D tape motif formed by Ch1 and Ch2 molecules. There are some significant differences in the orientation of molecules in the formation of these networks. When Ch1 and Ch2 are involved, the asymmetric molecules were related by a mere translation followed by a 2-fold rotation whereas in the other network with Ch3 and Ch4, they are related by a glide plane followed by a 2-fold rotation. Because of these differences, a single packing scheme (D) was observed between Ch1 and Ch2 while two types of packing schemes (C and D) were observed between Ch3 and Ch4. The structure is further stabilized by various C–H···π and C–H···O (2.86 – 3.96 Å and 100 –164°) interactions.

***Form IV*.** Despite several attempts to obtain the single crystals suitable for X-ray data collection, Form **IV** resulted only in crystalline powder. An alternative is the structure solution from the PXRD pattern. In this work, the direct space approach with the Monte Carlo method followed by Rietveld refinement has been used and the structure solution was implemented in Materials studio environment. The powder indexing unambiguously found a monoclinic unit cell with $P2_1/c$ space group with one molecule in the asymmetric unit ($Z' = 1$). The high values of absolute figure of merit (F_a) of 1999 (0.0055, 35)) and relative figure of merit (F_r) of 3.45 strongly suggest that the converged solution is the correct one (Neumann, 2003). From the calculated unit cell volume, four molecules (Z =

4) were expected in the unit cell. Fig. 4.6 shows the difference plot of Rietveld simulated profile and experimental profile.

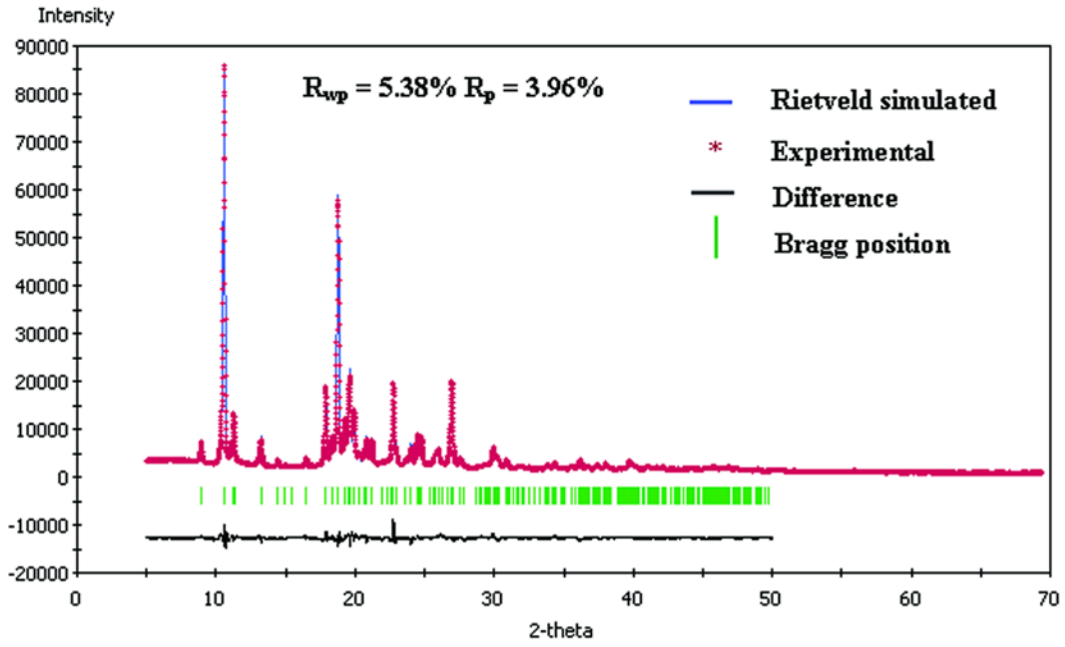

Figure 4.6 The difference plot of Rietveld simulated and experimental powder patterns of Form **IV**.

The unit cell (*a* = 10.09 Å, *b* = 15.64 Å, *c* = 9.27 Å, *β* = 100.5°, V = 1440 Å^3) was found to be closely related with that of Form $\mathbf{I^L}$. The *a*-axis is halved and *b*-axis is doubled in the case of Form **IV** when compared to Form $\mathbf{I^L}$. The TB molecule adopts the U-type conformation. When compared to other U-type conformers, major differences were observed in the alkyl tail orientation. The torsion angles τ_6 and τ_7 are both found to be in *anti* conformation. The crystal packing diagram was shown in Fig. 4.7. The adjacent molecules were related by a mere translation followed by a 2-fold relation. This leads to a unique packing scheme, scheme B, however, the 1D hydrogen bond urea tape motif persists in the crystal structure involving N–H···O hydrogen bonds which runs along [0 0 1] direction.

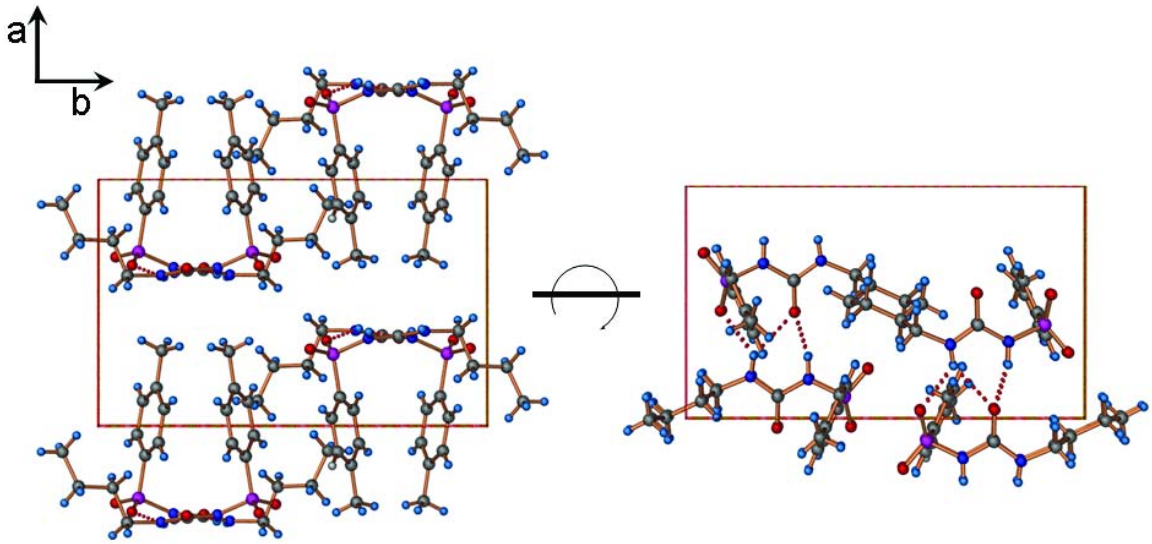

Figure 4.7 Crystal packing diagram of Form **IV**.

4.3. IR Spectroscopy

Comparison of FTIR spectra of TB polymorphs was shown in Fig. 4.8. The carbonyl stretching was observed at 1662, 1659, 1666 and 1665 cm^{-1} for Forms $\mathbf{I^L}$ and **II**–**IV**, respectively. This suggests that carbonyl group is involved in a similar hydrogen bonding in all the polymorphs. This is consistent with the hydrogen bonding patterns observed in the crystal structures. The symmetric and asymmetric stretching frequencies of sulfonyl group are observed at 1336, 1156 cm^{-1} for Form $\mathbf{I^L}$, 1347 and 1164 cm^{-1} for Form **II**, 1342, 1166 cm^{-1} for Form **III** and 1349, 1166 cm^{-1} for Form **IV**. This suggests that sulfonyl group was involved in a stronger hydrogen bonding in Form $\mathbf{I^L}$ compared to other forms.

In all the crystal structures, the sulfonyl group involves in hydrogen bonding with alkyl amide and in other intermolecular C–H···O interactions. The N–H···O distances are 3.07 Å, 3.106 Å, 2.903 Å and 3.01 Å for Forms $\mathbf{I^L}$, **II**, **III** and **IV**, respectively. This comparison suggests that sulfonyl group in Form **III** has a stronger hydrogen bonding

with alkyl amide among others. This is inconsistent with IR absorption data and the lower IR absorption frequency for Form **I**^{L} can be attributed to other strong intermolecular interactions around sulfonyl oxygens. The IR absorption for the sulfonyl amide stretching is observed at 3328, 3338, 3331 and 3338 cm^{-1} for Forms **I**^{L} and **II**–**IV**, respectively. This is consistent with the hydrogen bonding involving sulfonyl amide and carbonyl group.

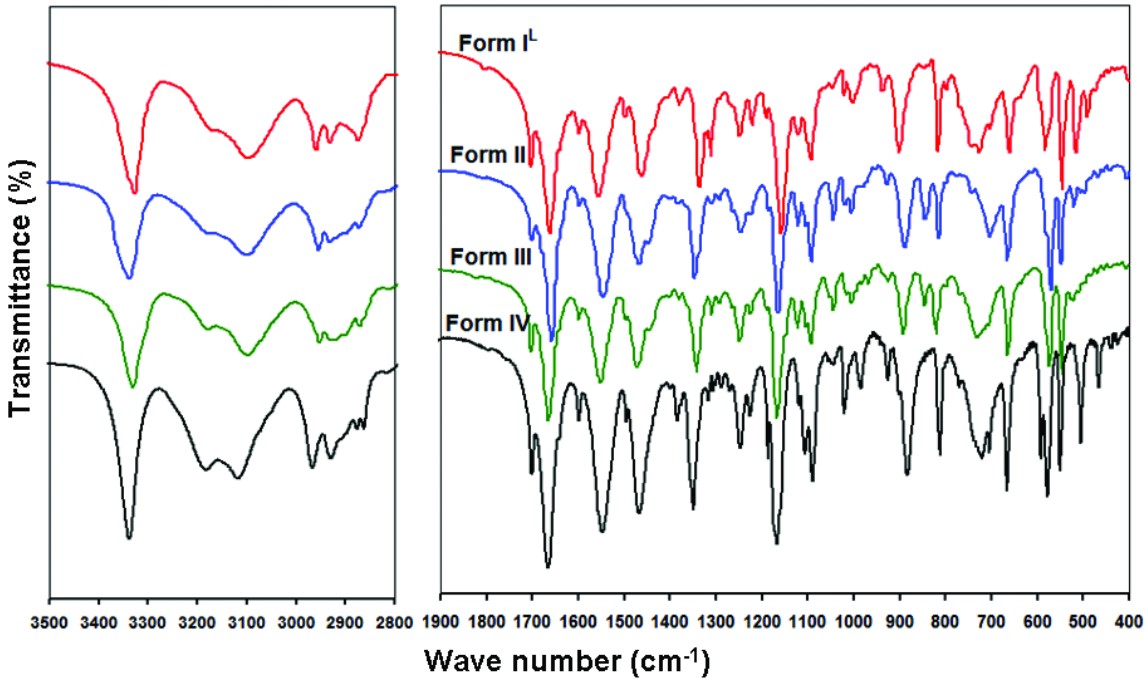

Figure 4.8 FTIR spectra of TB polymorphs.

The alkyl amide N–H stretch is observed at 3172, 3179, 3178 and 3182 cm^{-1} for Forms **I**^{L} and **II**–**IV**, respectively. This group involves in hydrogen bonding with both carbonyl and sulfonyl groups in all the polymorphs and these interactions are strongest in Form **I**^{L} and weakest in Form **IV** and in accordance with IR absorption. Apart from hydrogen bonding features, another difference in IR spectra was observed in the aliphatic C-H stretching region (2800–3000 cm^{-1}). The respective methyl group (one at the end of the tail and another connected to aromatic group) stretching frequencies were observed at

2960, 2931 cm^{-1} for Form $\mathbf{I^L}$, 2955, 2932 cm^{-1} for Form **II**, 2952, 2922 cm^{-1} for Form **III** and 2966, 2929 cm^{-1} for Form **IV**. This represents the conformational variations observed in the orientations of alkyl tail and aromatic ring in various polymorphs.

4.4. Solid-State NMR Spectroscopy

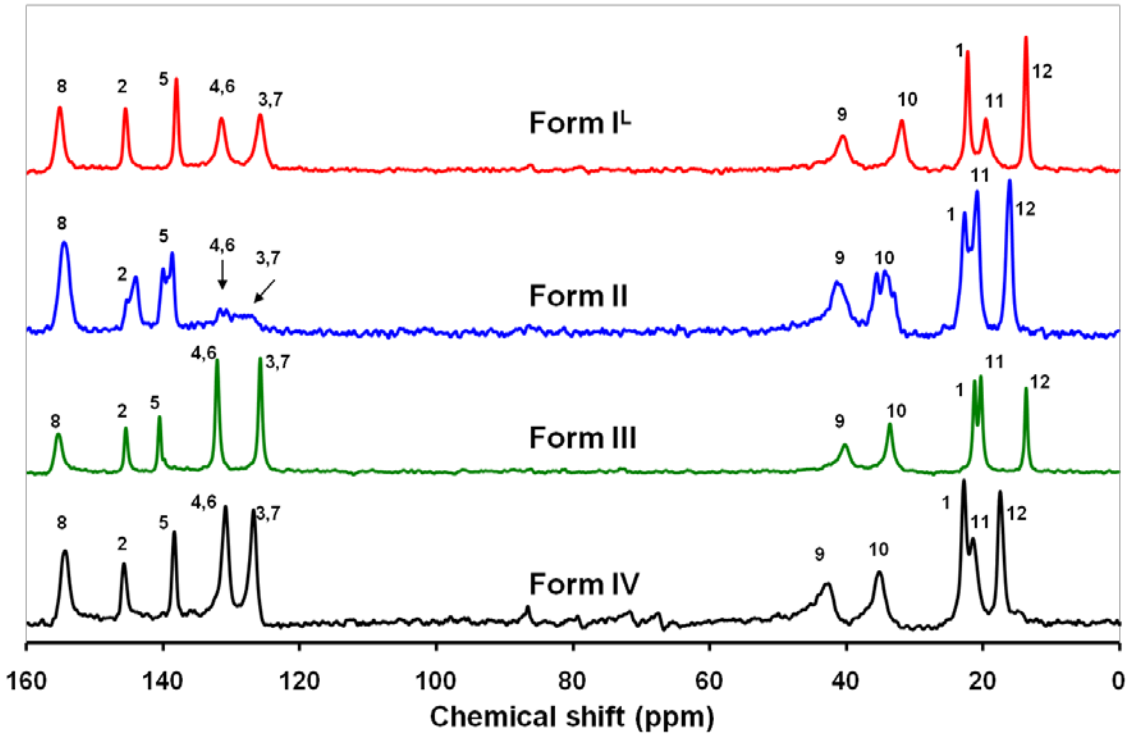

Figure 4.9 SS-NMR spectra of TB polymorphs.

CPMAS ^{13}C spectra of Forms $\mathbf{I^L}$ and **II**–**IV** were shown in Fig. 4.9. The ^{13}C resonances were assigned according to Kimura et al. (1999). NMR chemical shifts are indicative of molecular arrangement in the crystal lattice and for NMR principle and its data interpretation refer to section 2.5.2. In the case of Forms $\mathbf{I^L}$ and **III**, the number of resonances is equal to the number of carbon atoms in the molecule, so it can be concluded that the asymmetric unit consists of one molecule. This is consistent with our crystal data. Between these two forms, the major differences in the chemical shifts were

observed around C5 and C10 (131.8, 31.8 for Form $\mathbf{I^L}$ and 140.6, 33.6 for Form **III** for C5 and C10, respectively). These differences can be attributed to the torsional differences observed around C5–S (phenyl ring orientation) bond and C10–C11 bond (alkyl tail orientation) in the conformers found in these two forms. Apart from these differences, the spectra look quite similar. This can be easily recognized from the fact that they adopt the same type of packing scheme and form similar hydrogen bonding networks. In the case of Form **II**, there are three resonances for each of the carbon atoms of TB molecule indicating that at least three crystallographically nonequivalent molecules are present in the unit cell. This is in accordance with the crystal structure of Form **II** as it has four molecules in the asymmetric unit.

The NMR spectrum of Form **IV** is highly consistent with the determined crystal structure from powder diffraction in that all carbons were crystallographically equivalent resulted in single resolved peaks indicating that this polymorph has a single molecule in the asymmetric unit. Though this form adopts the U-type conformation like Forms $\mathbf{I^L}$ and **III**, major differences in carbon resonances were observed at alkyl tail carbons (C9–C12) due to the different packing scheme adopted by this polymorph. In all the TB polymorphs, the chemical shift for C8 observed in a narrow range (154.5–155.3), presumably because in all the cases it is participating in hydrogen bonding as an acceptor.

4.5. Powder X-Ray Diffraction Analysis

To verify the differences between Forms $\mathbf{I^L}$ and $\mathbf{I^H}$, we have collected the PXRD pattern of Form $\mathbf{I^H}$ and compared with that of Form $\mathbf{I^L}$ as shown in Fig. 4.10. The differences were mainly evident in the 2θ region of 19–21°. The similarity in the low

angle region (5° < 2θ < 19°) highlights the isomorphous characteristic of these two forms with minor conformational changes (Hasegawa et al., 2009).

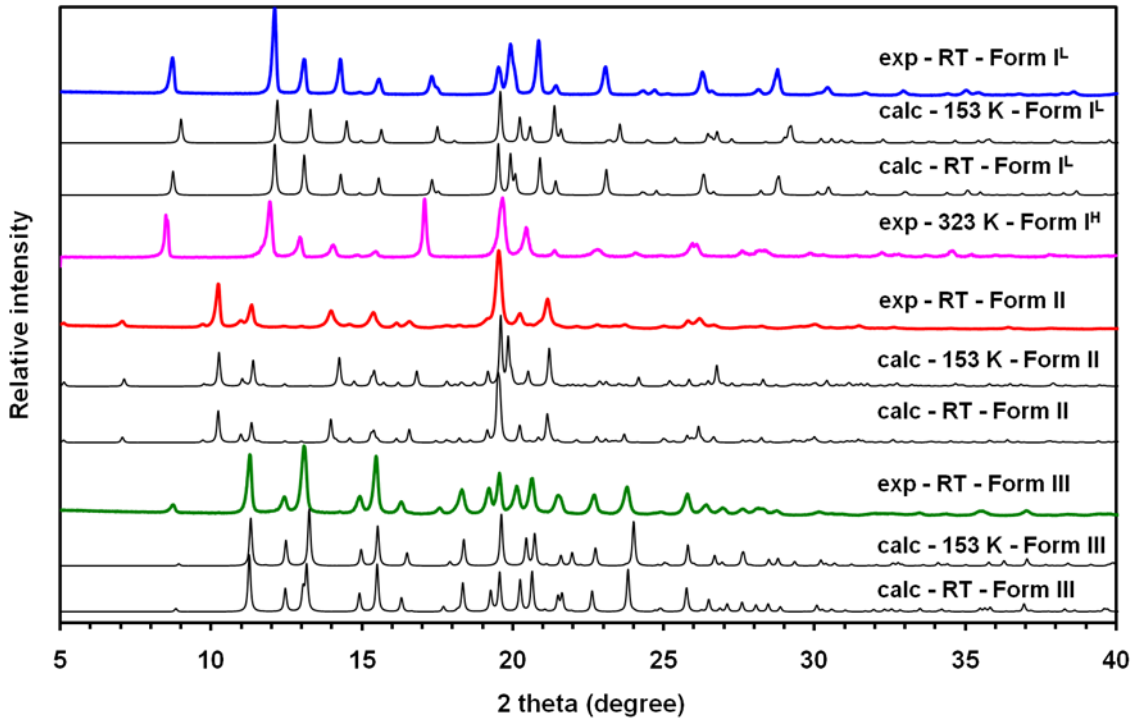

Figure 4.10 Comparison of experimental (RT) and calculated (153 K and RT) PXRD patterns of TB polymorphs.

Fig. 4.10 also shows the comparison of experimental PXRD patterns of TB polymorphs with the calculated patterns from their respective crystal structures determined at RT and 153 K. To our surprise, when compared with 153 K structures, significant differences were observed particularly in the 2θ region of 19–25°. Typically, deviation in peak positions in powder patterns is expected due to thermal contraction of the lattice at low temperature (Stephenson, 2006). If the unit cell contraction is isotropic, these differences reflect in shifting of peak positions to higher angles. If it is anisotropic, some peaks may shift to lower angles and some to higher angles. Rarely, severe

differences in intensities may also occur which can be attributed to molecular motion in the solid state (Cruickshank, 1956).

In the case of TB polymorphs, the differences in the PXRD patterns are manifested not only in peak shifting to both higher and lower 2θ values but also in peak splitting. These differences are so severe that it is difficult to identify the polymorphic phase. Hence, the crystal structures were redetermined at RT and the calculated PXRD patterns were compared with the experimental patterns as shown in Fig. 4.10. Now, the powder patterns are in good agreement and this implies that the differences observed in low temperature powder patterns were due to thermal effects.

To verify the lattice contraction and its effect on crystal structures, we have compared the unit cell data and the molecular conformations of the three polymorphs at RT and 153 K. In the case of Form **II**, we have determined the crystal structures at different temperatures between RT and 153 K to track the changes occurring in its crystal structure. In the case of Form $\mathbf{I^L}$, the anisotropy of lattice contraction is $\Delta a/a \times 100 =$ 2.95 %, $\Delta b/b \times 100 = 0.35\%$ and $\Delta c/c \times 100 = 0.35\%$. The contraction along the *b*- and *c*-axis is similar but the contraction along the a-axis is nearly 10 times more. In the case of Form **III**, the anisotropy is $\Delta a/a \times 100 = 0.85\%$, $\Delta b/b \times 100 = 0.33\%$, $\Delta c/c \times 100 =$ 2%. In the case of Form **II**, it is $\Delta a/a \times 100 = 0.73\%$, $\Delta b/b \times 100 = 0.24\%$, $\Delta c/c \times 100 =$ 1.63%. The overall anisotropy and contraction in the cases of Forms **II** and **III** are relatively less compared to Form $\mathbf{I^L}$. This explains the greater deviation observed in peak positions for Form $\mathbf{I^L}$ compared to other forms. These differences are much more severe at higher 2θ values.

Table 4.4 Torsional changes calculated in the alkyl tail of TB conformers observed in Forms $\mathbf{I^L}$, **II** and **III** at different temperatures (Ch4 is not shown because of disorder in the alkyl tail). RT-Room Temperature; LT-Low Temperature (153K); $|\Delta\tau|$ - Absolute torsional change.

Conformer	τ_5	$\lvert\Delta\tau_5\rvert$	τ_6	$\lvert\Delta\tau_6\rvert$	τ_7	$\lvert\Delta\tau_7\rvert$
U1(LT)	81.5		-178.8		-69.3	
U1(RT)	79.9	1.6	-176.2	2.6	-75.9	6.6
U2(LT)	-100.3		67.2		176.8	
U2(RT)	-99	1.3	61.4	5.8	174.2	2.6
Ch1(LT)	77.8		60.4		-175.5	
Ch1(RT)	88.7	10.8	-4.68	65.08	-179.5	4
Ch2(LT)	-83.9		-66.0		-175.4	
Ch2(RT)	-93.9	10	-22.9	43.1	-175.6	0.2
Ch3(LT	105.1		-61.7		178.9	
Ch3(RT)	97.6	7.5	-52.2	9.5	178.6	0.3

Table 4.4 lists the torsional variation observed in TB conformers found in the structures determined at RT and 153 K. The major changes were observed in the alkyl tail of the TB molecule (τ_5, τ_6 and τ_7). According to Threlfall, upon decreasing the temperature, the molecule releases the extra thermal energy by weakening of shortest intermolecular interactions followed by unwinding the structure with intermolecular torsional changes around the hydrogen bonds (Threlfall, 2003). In the case of TB, we could rationalize that, as the temperature decreases, the strongest interactions such as N–H···O hydrogen bonds loosen up to allow conformational changes in the alkyl tail (probably this part of the molecule has the lowest energy barrier). This would have forced the cell axes to contract anisotropically to accommodate these conformational changes.

Fig. 4.11 shows the calculated PXRD patterns of Form **II** at different temperatures ranging from RT to 153 K. As the temperature decreases, the peak at 19.6° corresponding to (2 0 0) plane was observed to split into two peaks. The new peak appeared

corresponded to (0 0 4) plane for which the intensity increased as the temperature dropped further. These changes can be attributed to the variation in the unit cell parameters and molecular conformational changes. The fact that the nature of this variation is continuous indicates that the differences in PXRD patterns are not due to phase transformation.

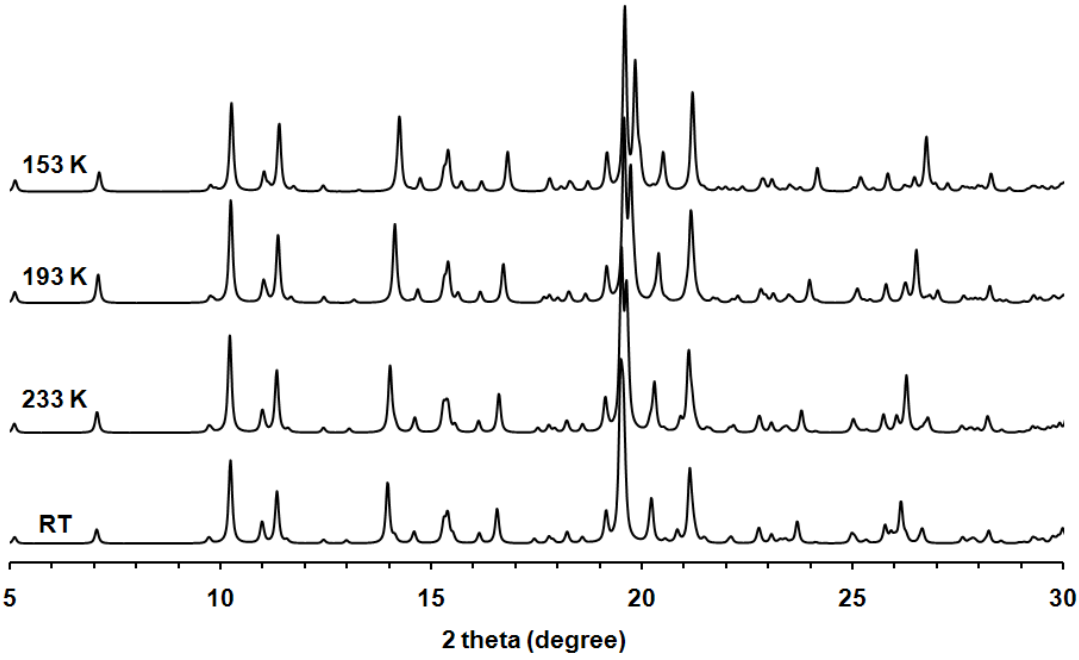

Figure 4.11 Comparison of calculated PXRD patterns of Form **II** at different temperatures.

4.6. Thermal Analysis

DSC thermograms of the TB polymorphs were shown in Fig. 4.12 and the corresponding data was summarized in Table 4.5. The calculated enthalpy values were the averages of three independent experiments. Hess's law of heat summation ($\Delta_{fus}H + \Delta_{trs}H$) was used to estimate the heat of fusion as no direct melting was observed except Form $\mathbf{I^H}$. The thermogram of Form $\mathbf{I^L}$ shows two peaks; a small endotherm at 40 °C followed by another endotherm at 128 °C. The first peak was ascribed to a kinetically

reversible polymorphic transition to Form **I**$^{\mathbf{H}}$ (Kawakami, 2007; Hasegawa et al., 2009) and the second peak was ascribed to melting of Form **I**$^{\mathbf{H}}$.

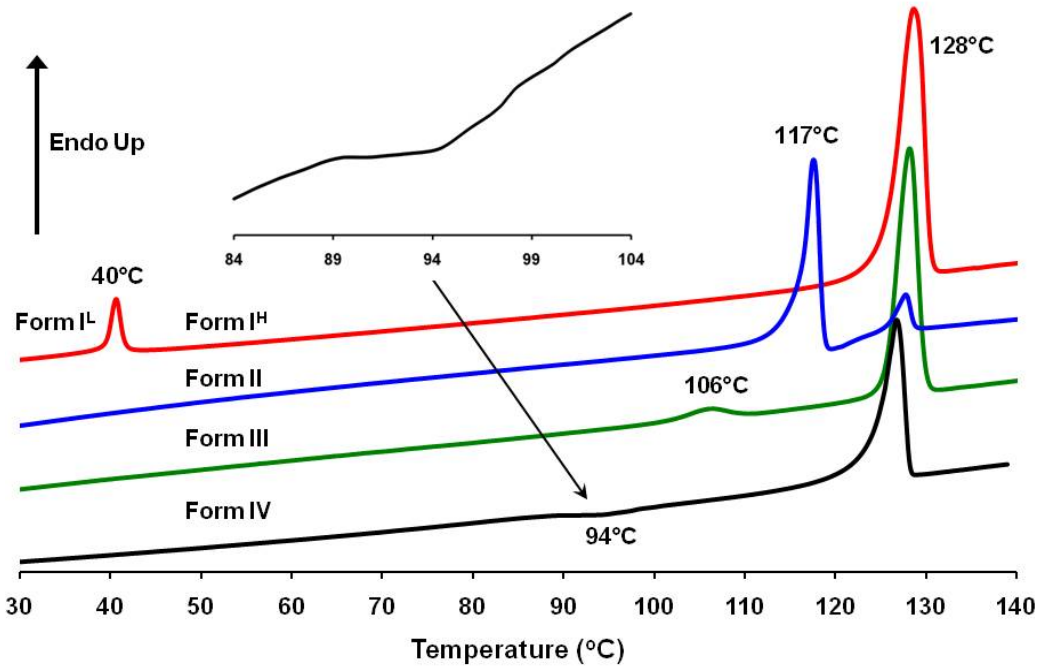

Figure 4.12 DSC thermograms of TB polymorphs at a heating rate of 10 °C min^{-1}.

Table 4.5 DSC data of TB polymorphs.

TB Polymorph	Melting temperature (°C)	Transition temperature (°C)	$^{a}\Delta_{trs}H$ (KJ mol^{-1})	$^{b}\Delta_{fus}H$ (KJ mol^{-1})
Form **I**$^{\mathbf{H}}$	128	--	--	23.8
Form **I**$^{\mathbf{L}}$	--	40	+1.9 (**I**$^{\mathbf{L}}$→**I**$^{\mathbf{H}}$)	25.7
Form **II**	117	--	+2.2 (**II**→**I**$^{\mathbf{H}}$)	26
Form **III**	--	106	+1.72 (**III**→**I**$^{\mathbf{H}}$)	25.6
Form **IV**	--	94	-1.3 (**IV**→**I**$^{\mathbf{H}}$)	19.8

^{a}heat of transition ^{b}heat of fusion (calculated by Hess's law of heat summation)

In the case of Form **II**, a sharp endothermic melting peak at 117 °C was observed followed by an exotherm due to recrystallization of Form **I**$^{\mathbf{H}}$ from the melt of Form **II**. An endotherm at 128 °C due to the melting of Form **I**$^{\mathbf{H}}$ was subsequently observed. This behavior was visually observed under hot stage microscope (HSM) and shown in Fig.

4.13. When Form **II** crystals were heated on the hot stage, in a temperature range of 120–123 °C, a series of events like melting, nucleation and growth of new crystals from the melt were observed simultaneously. The prismatic shape and melting point (128 °C) of the newly formed crystals revealed that they belong to Form $\mathbf{I^H}$.

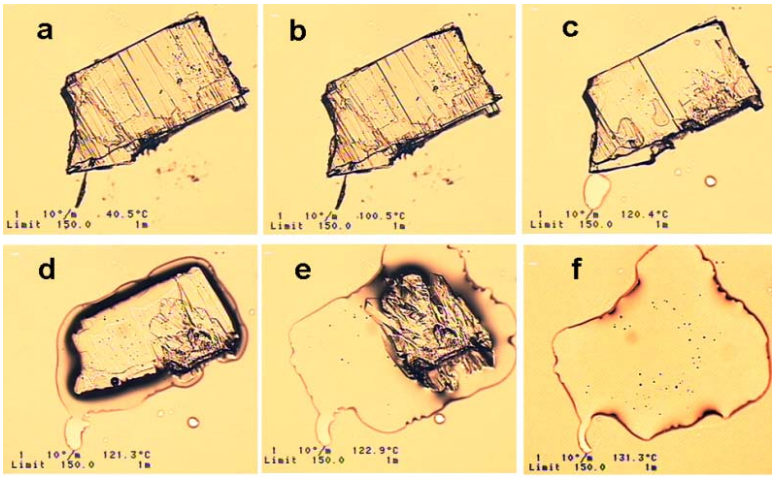

Figure 4.13 Hot stage microscope images of Form **II** (a) plated crystal of Form **II** at 40 °C (b) plated crystal of Form **II** at 100 °C (no change observed) (c) melting of Form **II** at 120 °C (d) and (e) prism like crystals characteristic of Form $\mathbf{I^H}$ growing from the melt of Form **II** (f) melting of Form $\mathbf{I^H}$ at 130 °C.

On the other hand, Forms **III** and **IV** undergo an endothermic transition at 106 °C and an exothermic transition at 94 °C to Form $\mathbf{I^H}$, respectively. The thermal behavior of Forms **I–IV** is consistent with Burger's forms (Burger, 1975). However, some differences in the thermal behavior of Forms **II** and **III** were observed when compared to Kimura's forms (Kimura et al., 1999). The DSC thermograms of Forms **II** and **III** in the current work closely matches with those of Forms **III** and **II** in Kimura's work, respectively.

4.7. Energy-Temperature Diagram of TB Polymorphs

Based on the DSC data listed in Table 4.5, the relative thermodynamic relationships among TB polymorphs are estimated and a schematic energy-temperature

diagram (E-T diagram, Fig. 4.14) was constructed. For more details on constructing E-T diagrams, refer to section 2.3.3. In the case of Forms $\mathbf{I^L}$ and $\mathbf{I^H}$, the nature of transition is reversible and only one of the two forms is experimentally accessible. So for clarity, the virtual states of these two forms were shown as dotted lines in the E-T diagram.

From the DSC analysis, it is clear that all the TB polymorphs undergo transition to a high temperature stable Form $\mathbf{I^H}$. According to the heat of transition rule, the polymorphic pairs **III**/$\mathbf{I^H}$ and **IV**/$\mathbf{I^H}$ should be enantiotropically and monotropically related respectively. On the other hand, Form **II** shows a melting transition to Form $\mathbf{I^H}$ and according to the heat of fusion rule, these two polymorphs should be enantiotropically related. The stability relationships between other polymorphic pairs cannot be derived from DSC data because the melting points of Forms $\mathbf{I^L}$, **III** and **IV** are not known. However, the constructed E-T diagram allowed us to derive these relationships.

In the case of Form **IV**, the course of its G isobar clearly suggests that it should be monotropically related to all the other forms. It is also clear from E-T diagram that G isobars of Forms **III** and $\mathbf{I^L}$ should intersect below the transition temperature of Forms $\mathbf{I^L}$ and $\mathbf{I^H}$ (~ 40 °C) to make this pair enantiotropic. This suggests that Form **III** is less stable than Form $\mathbf{I^L}$ below their transition temperature after which Form **III** becomes more stable. Our previous experiments suggest that Forms **III** and $\mathbf{I^L}$ concomitantly crystallize at RT and finally only Form $\mathbf{I^L}$ survives. This implies that the transition temperature between these two forms should be between RT and 40 °C. The only thermodynamic relationship that is not clear is that between **II**/**III** pair. It is difficult to conclude from E-T diagram because the melting point of Form **III** is not available.

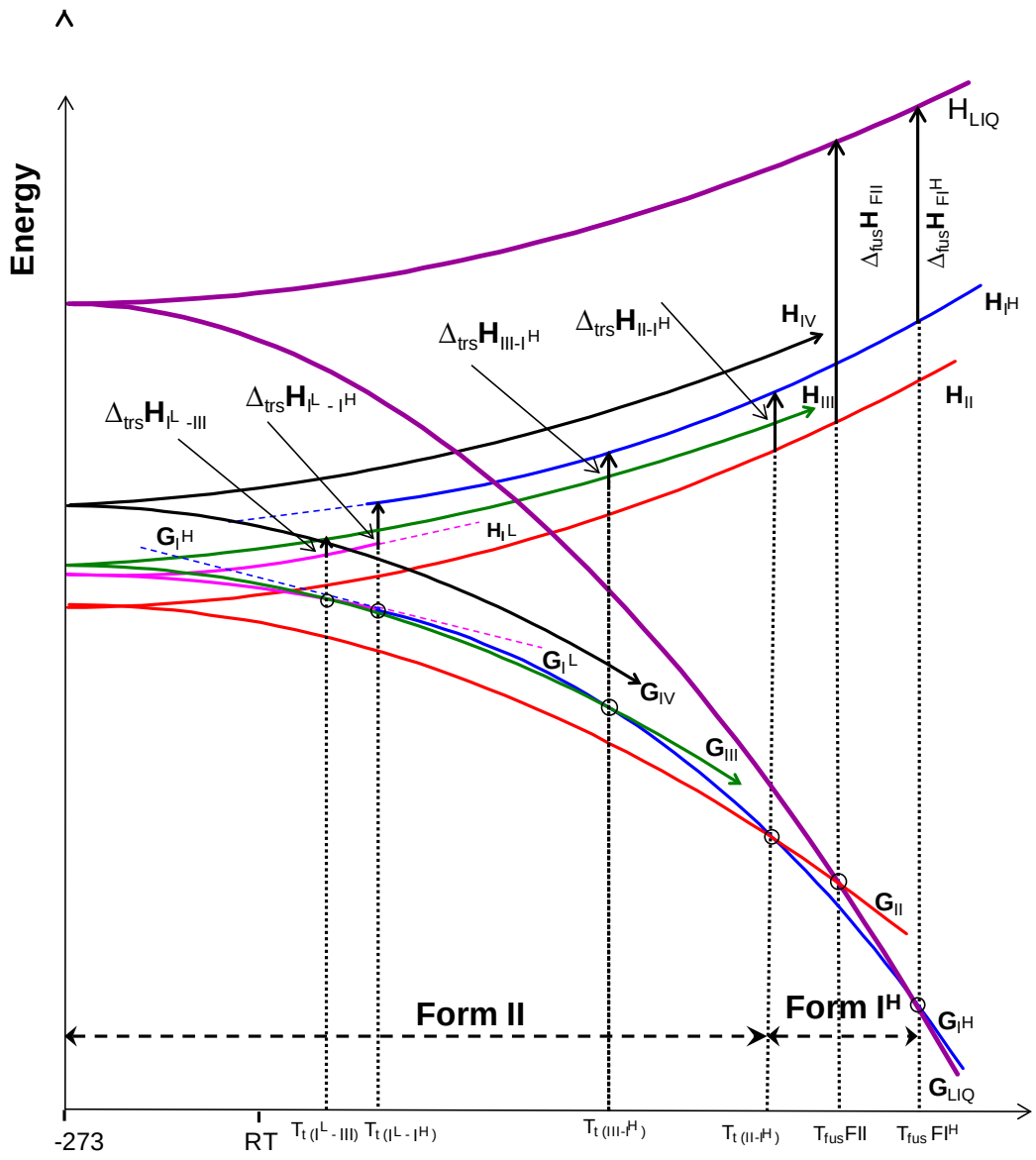

Figure 4.14 Schematic energy-temperature diagram of TB polymorphs. T_{fus}: Melting temperature, T_t: Transition temperature, $\Delta_{trs}H$: Enthalpy of transition, $\Delta_{fus}H$: Enthalpy of fusion, G: Gibbs free energy, H: Enthalpy, LIQ: Liquid phase (melt). The horizontal double headed arrows mark temperature ranges where either Form **II** or **I**$^{\mathbf{H}}$ is the thermodynamically stable form.

The E-T diagram suggests that the stability order of TB polymorphs at ambient conditions should be Form **II** > Form **I**$^{\mathbf{L}}$ > Form **III** > Form **IV** with Form **II** being the most stable form. To confirm the stable form at RT and also to establish the transition

temperature of Forms $\mathbf{I^H}$ and **II**, we have measured the solubilities of Forms $\mathbf{I^H}$, $\mathbf{I^L}$ and **II** in the temperature range from 15 to 60 °C in ethanol. Fig. 4.15 shows the Van't Hoff's plot. We have not measured the solubilities of Form $\mathbf{I^L}$ between 30–40 °C because the transformation from Form $\mathbf{I^L}$ to $\mathbf{I^H}$ is highly probable in this range. These measurements suggest that Form **II** is less soluble than Form $\mathbf{I^L}$ and hence it should be the thermodynamically stable form at RT. The Van't Hoff's plot of Form **II** intersects that of Form $\mathbf{I^H}$ at ~80 °C. This suggests that these two forms are enantiotropically related and Form $\mathbf{I^H}$ is the stable form above ~80 °C.

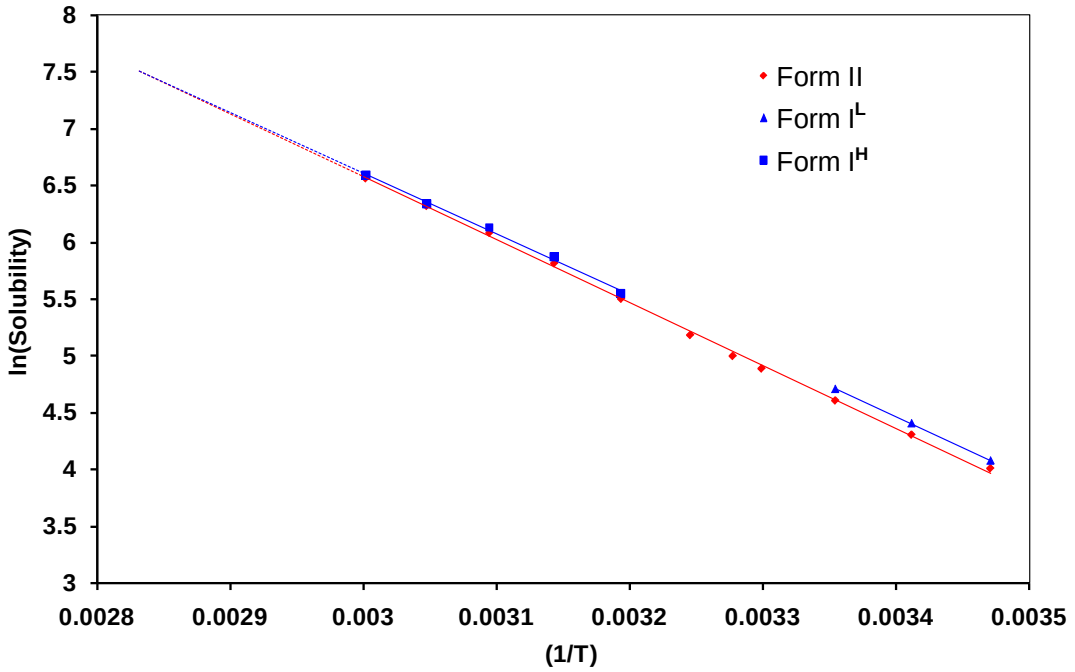

Figure 4.15 Van't Hoff's plot of TB polymorphs in ethanol (The lines are extrapolated to the intersection point to estimate the transition temperature showed as dotted line), T: temperature in Kelvin, Solubility: g of TB per g of ethanol.

4.8. Further Verifications

These measurements were further verified by solution mediated transformation experiments. Fig. 4.16 (a) shows the microscope image showing the transformation of

Form $\mathbf{I^L}$ to the more stable Form **II** in a saturated solution of ethanol at RT. The high temperature transition from Form **II** to $\mathbf{I^H}$ was verified using the HSM. Form **II** crystals were suspended in paraffin oil in a hot stage crucible and heated to 100 °C. During the heating, the crucible was rotated to dissolve the crystals. Then, the crucible was kept at 100 °C for a few minutes and cooled down to 95 °C at a rate of 1 °C min^{-1}. The growth of prismatic crystals typical of Form $\mathbf{I^H}$ was observed (see Fig. 4.16 (b)). This suggests that the transition temperature from Form **II** to $\mathbf{I^H}$ exists between RT and 95 °C.

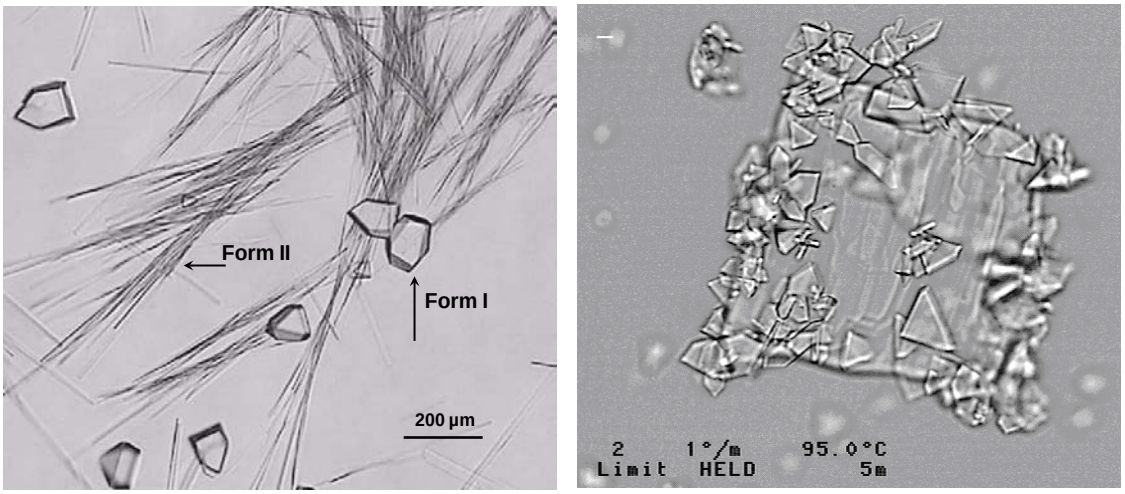

Figure 4.16 (a) Polymorphic transformation of Form $\mathbf{I^L} \rightarrow$ **II** in ethanol solution at RT **(b)** Polymorphic transformation of Form **II** $\rightarrow \mathbf{I^H}$ in paraffin oil at 95 °C.

The calculated densities from the crystal structures at RT are: 1.246, 1.252, 1.233 g/cm^3 for Forms $\mathbf{I^L}$, **II** and **III,** respectively. The density rule (refer to section 2.3.3) suggests that the stability order should be Form **II** > Form $\mathbf{I^L}$ > Form **III** at absolute zero, and this is consistent with our previous results. But, the calculated densities of low temperature crystal structures are: 1.294, 1.283 and 1.268 g/cm^3. In this case, density rule is still valid for $\mathbf{I^L}$/**III** and **II**/**III** pairs but fails to predict the stability order of $\mathbf{I^L}$/**II** pair.

This is not surprising because these two forms show different thermal contraction properties and Z' parameter, and density rule often fails in such cases (Sun, 2007).

The crystal lattice energies were calculated using COMPASS with force field assigned parameters in Materials Studio (Accelrys Software Inc. Version 4.3.). These values at 153 K are: -50.6, -46.9, and -46.2 kcal/mol and at RT are: -49.1, -45.9 and -44.8 kcal/mol for Forms $\mathbf{I^L}$, **II** and **III**, respectively. Again, the energy order at both temperatures is consistent with $\mathbf{I^L}$/**III** and **II**/**III** pairs, but fails with respect to $\mathbf{I^L}$/**II** pair. This can be attributed to the disorder found in the alkyl chain of TB molecule in Form **II** structure which leads to a higher R-factor. The calculated density and lattice energy values of Form **IV** are 1.248 g/cm^3 and -43.3 kcal/mol. We cannot compare these values with other forms because this structure is determined from the PXRD data. But, the higher lattice energy and lower density (compared to low temperature structures) indicates that it is the least stable among the others.

4.9. Further Discussion

Although we could identify the TB polymorphic forms prepared in this work with Burger's Forms **I**–**IV**, discrepancies were observed in their relative stability. Results from different studies variously suggest that the thermodynamically stable polymorph at ambient conditions should be Form **I** (Burger's work); Form **III** (Rowe's work); and Form **II** (present work). Hence, we have decided to scrutinize their results to find the reasons for these discrepancies. In Rowe's work, it is difficult to identify the stable polymorph because no characteristic data was provided. But, the morphological description indicates that it crystallizes with a very fine needle shaped morphology which tends to form a highly flocculated structure. Interestingly, this morphology closely

matches with Form **II** obtained from our slurry experiments (refer to Fig. 4.16 (a)). Hence, we suspect that they might have misinterpreted the more stable phase as Form **III** which was actually Form **II**.

In Burger's case, the discrepancy is mainly observed in the stability of Form **II**. Burger reported that Form **II** is a metastable polymorph, but the present work suggests that it is the stable polymorph. Kimura et al. who further investigated Burger's forms and studied the transition behavior of Form **IV** under different humidity conditions suggested that Form **IV** transforms to Form **II** which then converts to Form **I** at 75% RH in the temperature range of 35–70 °C. This is consistent with Burger's stability order but contradicts our observation that Form **II** is the thermodynamically stable polymorph in this temperature range. When we tested our Form **II** at 75% RH and 45 °C for several months, no such transformation was observed. This raises the question of whether our Form **II** is the same as Burger's reported Form **II** (or Kimura et al.'s Form **II**). Further structural investigations may be needed to fully answer this question. To clarify the nomenclature amongst the various publications referring to TB, a table summarizing the known reports on TB polymorphs and inconsistencies in nomenclature was provided (Table 4.6). The discrepancies found in their relative stability and structural data and clarifications provided by current work were also shown.

4.10. Summary

The conformational flexibility of the TB molecule and strong hydrogen bonding ability of secondary amide via carbonyl and sulfonyl groups facilitate this drug to crystallize into different polymorphic forms (Forms ($\mathbf{I^L}$, $\mathbf{I^H}$) and **II**–**IV**). All the polymorphs show similar hydrogen bonding motif (urea tape motif and hydrogen

bonding to sulfonyl group) with different orders of magnitude. The major differences were observed due to the rich torsional freedom available for the terminal alkyl chain of TB molecule. Forms $\mathbf{I^L}$, **III** and **IV** adopt different U-type conformations, whereas Form **II** adopts four different chair type conformations (Ch1–Ch4). These molecular features clearly suggest that this system is a representative case of conformational polymorphism. Due to conformational differences, the molecular orientations in hydrogen bonding networks are considerably different and result in different packing arrangements in each polymorph.

By reporting the crystal structures of various polymorphic forms of TB, the present work resolves several discrepancies in the published data on the structural information of the polymorphs of this API. This study also highlights the influence of anisotropic thermal motion of molecules on PXRD patterns of solids.

Based on the DSC data, the relative thermodynamic relationships of TB polymorphic pairs were evaluated and graphically visualized in a schematic energy-temperature diagram. Form **II** is found to be the thermodynamically stable polymorph from absolute zero to ~353 K and beyond which Form $\mathbf{I^H}$ is the stable polymorph. These observations were further verified by solution mediated transformation experiments. The discrepancies in the literature related to the relative stability of TB polymorphs at ambient conditions are highlighted and discussed.

Table 4.6 Comparison of current work with previous work reported in the literature on TB polymorphs.

Author and Publication Year	Polymorphs Reported	Characterization and Relative Stability	Forms Equivalent in Present Work and Comments on Relative Stability and Structure
Kuhnert-Brandstätter and Wunsch (1969)	Forms **I**, **II** and **III**	Hot stage microscopy	Forms (**I^L**, **I^H**)[a], **II** and **IV**
Simmons et al. (1972)	Forms **A** and **B**	DSC, FTIR and PXRD	Forms (**I^L**, **I^H**) and **III**
Burger (1975)	Forms **I**, **II**, **III** and **IV**	DSC, FTIR and Hot-stage microscopy Stability order (ambient): Form **I** > Form **III** > Form **II** > Form **IV** Stability relationship with Form **I**: Form **II**: enantiotropic, T_t < 37°C Form **III**: enantiotropic, T_t < 37°C Form **IV**: monotropic	Forms (**I^L**, **I^H**), **II, III** and **IV** Stability order (ambient): Form **II** > Form **I^L** > Form **III** > Form **IV** Stability relationship with Form (**I^L**, **I^H**): Form **II**: enantiotropic T_t[b] (**II** →**I^H**) (~ 80 °C) Form **III**: enantiotropic 25 °C < T_t (**I^L** →**III**) < 40 °C 40 °C < T_t (**I^H** →**III**) < 106°C Form **IV**: monotropic
Nirmala et al. (1981) & Donaldson et al. (1981)	Form **A**	Single crystal XRD Orthorhombic, $Pna2_1$, Z = 4 a = 20.23 Å, b = 7.83 Å, c = 9.09 Å	Form **I^L** Crystal structure agrees with present work.
Leary et al. (1981)	Forms **A** and **B**	DSC and Single crystal XRD Form **B**: monoclinic, $P2_1$, Z = 2, a = 8.11 Å, b = 8.96 Å, c = 10.19 Å, $\beta = 101^o$	Forms (**I^L**, I^H) and **III** Unit cell data does not match with any form.
Rowe and Anderson (1984)	Forms **I** and **III**	Form **III** is more stable than Form **I** below 75°C (using solubility measurements).	Forms (**I^L**, **I^H**) and **II** Stability order and transition temperature agree with current work.
Kimura et al. (1999)	Forms **I**, **II**, **III** and **IV**	DSC, PXRD, FTIR, SS-NMR and Single-Crystal XRD Form **II**: monoclinic, $P2_1/n$, Z = 4, a = 11.81 Å, b = 9.06 Å, c = 13.98 Å, $\beta = 104.5^o$ Stability order (ambient): Form **I** > Form **III** > Form **II** > Form **IV**	Forms (**I^L**, **I^H**), **II**, **III** and **IV** DSC thermograms of Forms **II** and **III** probably correspond to those of Forms **III** and **II** in the current work, respectively. Unit cell data reported for Form **II** was actually that of Form **III**. Stability order (ambient) : Form **II** > Form **I^L** > Form **III** > Form **IV**

[a] Form **I^L**: Form **I** below 38°C; Form **I^H**: Form **I** above 38°C [b] T_t : Thermodynamic transition temperature

CHAPTER 5

PAT AND EXPERIMENTAL SETUP

5.1. FDA's PAT Initiative

Pharmaceutical production has historically involved the manufacture of the finished product via fixed batch recipes, followed by laboratory testing to ensure its quality. Such a Quality by Testing (QbT) approach may satisfy the customer needs, but sometimes at the expense of cost and loss of profit to the company e.g. longer cycle times, product variability, failed batches etc. To address this issue, FDA has changed its regulatory approach from focusing on end product to process and released a new guidance to the industry. The desired goal is to design and develop well understood processes that will consistently ensure a predefined quality at the end of the process. This new approach is referred to as Quality by Design (QbD).

PAT is the critical element in QbD approach which includes process analyzers, chemometrics (e.g. data based modeling techniques) and process monitoring and control techniques (multivariate supervision and diagnosis strategies). Process analyzers are in situ sensors which collect the data related to process variables and product quality attributes. Chemometrics are necessary to extract the 'relevant information' from the highly correlated data generated by process analyzers to develop quantitative models. Process monitoring and control techniques facilitate detecting faults and diagnosing in real time to ensure process control.

5.2. QbD based Crystallization Process Development for the Desired Polymorph

QbD based strategies for the design of robust crystallization of the specific polymorph have been discussed by a few authors (Threlfall, 2000; Lin et al., 2007;

Bohlin et al., 2009). These are based on interacting with thermodynamics and crystallization kinetics of polymorphs to identify regions (design space) where spontaneous nucleation of the targeted form is guaranteed. Experimental characterization of design space has been reported in the case of stavudine (Lu and Rohani, 2009), famotidine (Lu et al., 2007) and stearic acid (Sato and Boistelle, 1984).

Essentially, to determine a design space for obtaining a specific polymorph, the following basic information must be gathered.

1. Selection of the desired form
2. Solubility curves of polymorphs
3. Metastable zone width
4. Polymorph transformation kinetics

5.2.1. *Selection of the Desired Form*

Once a comprehensive screening for all possible polymorphs has been performed, the desired one should be selected based on careful characterization including the stability and formulation properties. The ideal solid form should be thermodynamically stable, have robust chemical and physical stability, appropriate solubility and suitable drug substance and drug product processability (Ticehurst and Docherty, 2006). According to Miller et al. (2005), the thermodynamically most stable form is almost always considered the most desired crystal form because it has the lowest propensity to phase transformation. However, metastable forms are sometimes deliberately chosen usually for better solubility and thus enhanced bioavailability (Singhal and Curatolo, 2004).

5.2.2. *Solubility Data of Polymorphs*

Accurate solubility data is a crucial part of the design, development and operation of crystallization process. As solubility defines the crystallization boundary, it is important in assessing process yield, level of supersaturation and polymorph stability. A typical experimental procedure for solubility measurement involves agitation of a solution that contains excess solids at a constant temperature for sufficient time (4–24 hours) to allow for equilibration followed by sampling the solution and analyze to determine the solute concentration (Mullin, 1993). There are various techniques available for solution concentration analysis which includes gravimetry or using analytical instruments such as HPLC, UV-Vis spectroscopy etc (Rohani et al., 2005).

A more modern solubility measurement method uses online PAT tools for monitoring the concentration changes in the solution. Such a real time, inline monitoring allows the user to optimize the equilibration time, thus preventing any solid phase changes which may occur when metastable polymorphs are involved. Apart from solubility measurements, reliable in situ monitoring of solute concentration is a prerequisite for the control of supersaturation which is a key parameter in crystallization process control.

There are a wide variety of PATs available for this purpose. The feasibility of Attenuated Total Reflectance-Fourier Transfer Infrared Spectroscopy (ATR-FTIR) for the in situ measurement of solute concentration in dense liquid slurries has been demonstrated (Dunuwila et al., 1994; Dunuwila and Berglund, 1997). Currently, it is the most widely used PAT in crystallization and a number of applications have been reported where ATR-FTIR has been utilized for process monitoring and control (Lewiner et al.,

2001; Togkalidou et al., 2001; Fujiwara et al., 2002; Doki et al., 2004; Liotta and Sabesan, 2004; Pollanen et al., 2005; Scholl et al., 2006; Cornel et al., 2008; Borissova et al., 2009; Kee et al., 2009a). Conductometric probes (Amathieu and Boistelle, 1988; Garcia et al., 2002), density meters (Gutwald and Mersmann, 1990), NIR spectroscopy (Zhou et al., 2006) and ATR UV-Vis spectroscopy (Howard et al., 2009) have also been applied for in-line concentration measurement.

5.2.3. *Metastable Zone Width Measurements*

MZW measurements reflect the nucleation kinetics of a crystallizing system and they have long been used to estimate primary nucleation kinetics (Nyvlt, 1968; Nyvlt et al., 1985; Kim and Mersmann, 2001). In a polymorphic system, nucleation kinetics of different polymorphs can be experimentally determined by measuring MZW corresponding to each polymorph (Teychene and Biscans, 2008). Unlike solubility, MZW is a kinetic property typically influenced by a variety of operating parameters including saturation temperature, rate of supersaturation generation, impurity level, mixing and solution history (Ulrich and Strege, 2002). It is therefore important to characterize MZW under a specific set of operating conditions.

For a given solute-solvent system, MZW can be measured either by *isothermal* or *polythermal* method (Garside et al., 2002). In the isothermal method, induction time (i.e., the time elapsed between creation of supersaturation and the formation of crystals) is measured. This is achieved by the rapid cooling of a saturated solution to a predefined temperature and isothermally kept until the nucleation is detected. In a polythermal method, a saturated solution is cooled at a fixed cooling rate until nucleation occurs. MZW can be calculated as the difference between the nucleation and saturation

temperatures. However, when dealing with polymorphic compounds, in addition to measuring induction time/nucleation temperature, the solid crystallized should also be characterized.

For MZW measurements, a wide variety of techniques have been applied to detect the onset of nucleation. Kubota (2008) classified them into two categories; first category includes those techniques which detect changes related to the amount of grown nuclei. *Methods using naked eye* (Sohnel and Mullin, 1988), *a particle counter* (Barrett and Glennon, 2002; Fujiwara et al., 2002) and *turbidity meter* (Gerson et al., 1991) come under this category. The second category includes those which detect changes in solution concentration. *ATR-FTIR* (Fujiwara et al., 2002), *ultrasound sensor* (Titiz-Sargut and Ulrich, 2003; Chaleepa et al., 2010), *densitometer* (Marciniak, 2002) and *electrical conductivity* (Lyczko et al., 2002) fall into this category. Since these techniques cannot distinguish the solid forms, the crystals are usually separated and subjected to analysis to detect the type of polymorph nucleated.

Teychene and Biscans, (2008) measured the nucleation rates of eflucimibe polymorphs by measuring the induction time using naked eye followed by solid phase analysis using PXRD. Similar studies can be found in the literature (Anuar et al., 2009; Svard et al., 2009). However, this approach may lead to erroneous conclusions as it involves the risk of polymorphic transformation while handling the solid phase. Recently, Raman spectroscopy has been shown as a method for monitoring the onset of nucleation which detects the associated change in solution opacity at the time of nucleation with an additional advantage that it allows for the in situ detection of the type of polymorph nucleated (Hu et al., 2005; Owen et al., 2005; Wu et al., 2009).

5.2.4. *Polymorph Transformation Kinetics*

Knowledge of possible phase transformations, their kinetics and rate controlling mechanism in a polymorphic system is essential when designing a process to isolate the desired form. This information is useful for determining crystallization operating parameters e.g. temperature, batch time etc. to enhance/prevent the desired/undesired transformations. Early work on SMPT characterization involved sampling of suspension at different time intervals to separate the solid and liquid phases and analyze to measure the solute concentration and polymorphic composition (Davey et al., 1985; Davey and Richards, 1985; Kitamura, 1989; Kitamura, 1993; Maruyama et al., 1999). Offline methods such as PXRD, DSC, microscopy and particle size analyzer etc. for polymorphic content and UV-Vis, HPLC, etc. for solute concentration measurements have been used, respectively. However, due to the dynamic nature of polymorphic transformation and the instability of certain polymorphs, offline-analysis is largely affected by sampling errors (Yu et al., 2004). Consequently, in line, real time measurements such as PATs would be more advantageous. Moreover, real time, in line detection of polymorphs and their transformation during crystallization is an asset for process control. Application of PATs for in situ monitoring of solute concentration has been discussed before (refer to section 5.2.2). The same methods can be employed for SMPT characterization. The following discussion emphasizes on PATs for in situ monitoring of polymorphs.

In the past two decades, a wide variety of PATs have been applied for polymorph monitoring (Mangin et al., 2009). Among the many, near-infrared (NIR) and Raman spectroscopy are the most prominent because of their distinct advantage of operating in a remote manner using fiber-optic waveguides and transflectance probes (Stephenson et al.,

2001). The potential of fiber optic NIR spectroscopy to quantitatively monitor polymorphic composition of a solid-state API during an industrial crystallization process has been demonstrated (Fevotte et al., 2004). Recently, Raman spectroscopy has become more popular in pharmaceutical research and is the most widely applied technique in SMPT studies. Its use for polymorph monitoring in suspensions was first demonstrated by Wang et al., (2000) with progesterone as a model system. Similarly, Starbuck et al. (2002) used Raman spectroscopy to determine the rate of polymorphic transformation of a complex multipolymorphic API, referred to as MK-A. The study of SMPT of pseudo polymorphs of citric acid and carbamazepine was also performed using Raman (Caillet et al., 2006; Qu et al., 2006).

As polymorphic changes are often accompanied by a change in morphology, alternative techniques such as *focused beam reflectance measurement* (FBRM) and inline *video microscopy* have been used to monitor polymorphic transformations. FBRM is a probe-based particle counter which utilizes laser backscattering technology to measure, in real time, a chord length distribution (CLD) which is proportional to particle size distribution (O'Sullivan et al., 2003; Yu et al., 2007). In situ video probes such as process vision and measurement (PVM) provide in situ high resolution imaging of particles within the process environment. Relying on the distinct morphological difference between δ and β polymorphs, O'Sullivan and Glennon (2005) successfully monitored the polymorphic transformation of D-Mannitol in aqueous solution using FBRM. Similar studies can be found in the literature (Barthe et al., 2008; Dang et al., 2009; Liu et al., 2009). However, these techniques rely on indirect measurements on polymorphs and

therefore, the information obtained remains qualitative and often the interpretation is difficult.

5.3. PAT in the Present Work

The PAT framework used in the present work mainly consists of two process analyzers, ATR-FTIR and Raman spectroscopy. They were coupled with chemometric techniques and automated for in situ monitoring of crystallization operations. Before going into experimental details, the following text introduces the working mechanism of these instruments and the coupled chemometric methods.

5.3.1. *ATR-FTIR*

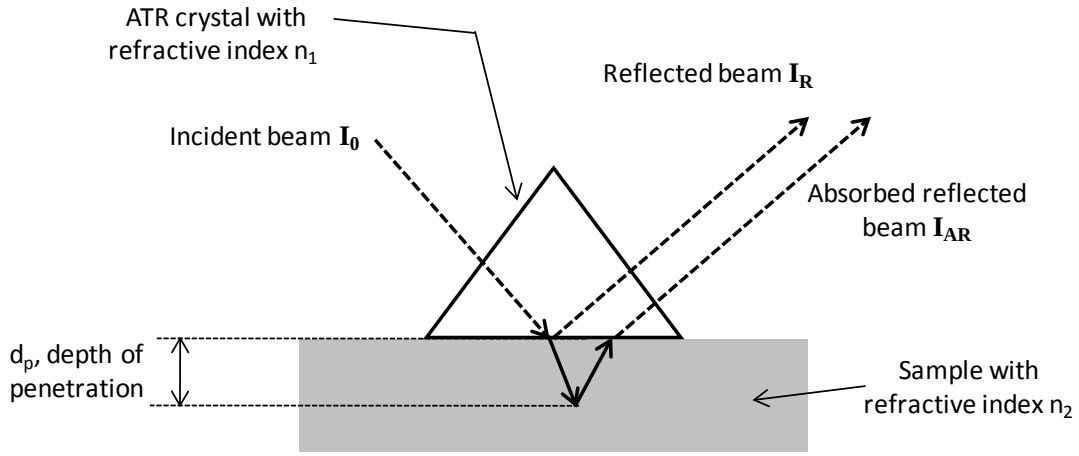

Figure 5.1 Working principle of ATR-FTIR (Lewiner et al., 2001).

The working principle of ATR-FTIR is shown in Fig. 5.1 (For theory, refer to section 2.5.2). A laser beam generated from the FTIR spectrophotometer is directed by optics to the prismatic ATR crystal located at the tip of the probe which is in contact with the slurry. Part of the beam is reflected at the ATR crystal/liquid interface. Another part propagates into the liquid phase where absorption takes place. After being reflected back into the probe it is directed to the detector.

The penetration depth d_p can be calculated by Eq. 5.1:

$$d_p = \frac{\lambda}{2\pi n_1[sin^2\theta - (n_2/n_1)^2]^{1/2}} \quad 5.1$$

The refractive index of ZnSe crystal used in this study is, $n_1 = 2.4$ and $n_2 = 1.5$ for water. With $\theta = 45°$ the penetration depth at $\lambda = 1000$ cm^{-1} is 2 µm. Such a depth is shorter than the boundary layer of laminar flow surrounding the ATR crystal. Therefore the absorbance recorded in the absorbed reflected beam is from the liquid phase in immediate contact with ATR crystal only, with minimum interference from the solid phase. On occasion, the nucleation process can be observed if the nuclei are smaller than a few micrometers, but often the IR absorbance of the particles is weak compared to that of the dissolved species. A significant advantage of using ATR-FTIR compared to NIR is its measuring range which is mid-IR (400–4000 cm^{-1}) where fundamental vibrations are active. Therefore, spectra are less complicated with well-resolved peaks compared to NIR.

5.3.2. *Chemometrics for ATR-FTIR*

The most commonly used chemometric methods with ATR-FTIR for relating the IR spectra to the solute concentration are partial least squares (PLS) and principal component regression (PCR). These methods are based on linear projection of the high dimensional spectral data (**X**) onto the low dimensional latent variable space which contains most of the important information. Those underlying features of new data are used for regression on to a known solute concentration vector (**y**) to develop quantitative models.

However, one important issue with online measurements using IR spectra as well as any other multivariate data is the presence of **y**- unrelated variation in **X** due to

external effects such as temperature, sample characteristics, light scattering, instrumental drift etc. For example, when ATR-FTIR is used in cooling crystallization, temperature varies over a large range which can affect the IR band shapes and such variation is unrelated to solute concentration (Wulfert et al., 2000). Similarly, anti-solvent interference in anti-solvent crystallization, presence of impurities etc. can vary the IR spectrum independent of solute concentration. Such variation is a non-linear phenomenon which complicates the linear multivariate techniques like PLS and PCR. Consequently, the model is forced to use more regression factors than is to be expected by the chemical rank (number of components in the sample). This non-ideal modelling can have adverse effects on model interpretability and robustness (Zeaiter et al., 2005). In order to promote ATR-FTIR as well as any other spectroscopic technique to real-life industrial applications one must consider these issues (Feundale et al., 2002).

It is a common practice to pre-process $\mathbf{X}$ to remove the $\boldsymbol{y}$- unrelated variation before it is subjected to regression modelling. Zeaiter et al., (2005) theoretically proved that pre-processing can significantly enhance the model performance and robustness. The most commonly used methods are *geometrical spectral pre-processing* (standard normal variate (SNV) transformation, multiplicative scatter correction (MSC), smoothing and differentiation) and o*rthogonal projection*. The main drawback of geometrical methods is that they are empirical in nature and thus they have the risk of removing the information which is relevant to model prediction. Orthogonal projection methods are more logical in that they remove only that part from spectra which is linearly unrelated i.e. mathematically orthogonal to $\boldsymbol{y}$. Therefore, there is little scope for losing relevant information. Wold et al. (1998) first introduced this idea by developing orthogonal signal

correction (OSC) filters. They also investigated the applicability of OSC to calibration transfer to different instruments (Sjoblom et al., 1998). Pollanen et al. (2005) has applied OSC to pre-process ATR-FTIR data to develop a stable calibration model for monitoring solute concentration in crystallization operations. They found that OSC filtering has simplified the model and also enhanced the robustness.

Subsequently, several authors have presented different OSC algorithms (Andersson, 1999; Fearn, 2000; Hoskuldsson, 2001; Westerhuis et al., 2001; Feudale et al., 2002; Trygg and Wold, 2002). Svensson et al. (2002) provided a comparison of various OSC algorithms and their effectiveness in improving model interpretability and performance. Among the many OSC algorithms, orthogonal projection to latent structures (OPLS) developed by Trygg and Wold (2002) is unique since it combines the features of PLS with orthogonal projection. This hybridization addresses some of the issues associate with OSC filters (Wold et al., 1998) which often lead to overfitting and degradation of calibration models. In OPLS, OSC filter is built in such a way that it removes only variation in $\mathbf{X}$ explained in each PLS component that is not correlated to $\boldsymbol{y}$. One important property of OPLS is that, for single $\boldsymbol{y}$- variable cases, it will always reduce down to a single regression factor, thereby ensures good model interpretability and robustness. In the same reference in which OPLS is reported (Trygg and Wold, 2002), an extension referred to as OPLS (PCA) which uses principal component analysis (PCA) to remove orthogonal information was also presented. In the present work, OPLS (PCA) algorithm has been coupled with ATR-FTIR and applied for in situ monitoring of solute concentration.

5.3.3. *Raman Spectroscopy*

Raman spectroscopy has emerged in recent years as 'one of the fastest, most reliable and most suitable technique to identify crystal forms and can be easily exploited routinely for monitoring phase changes' (Auer et al., 2003). Samples for Raman analysis may be solids, liquids, or gases, or any forms in between and in combination such as slurries, gels etc. Since crystallization is a multiphase phenomenon, Raman spectra will be a combination of Raman scattering from both the solids and the solution, with the solids dominating due to the greater scattering cross-section. Like ATR-FTIR, Raman also operates in mid-IR range, thus greater chemical selectivity with well-resolved peaks.

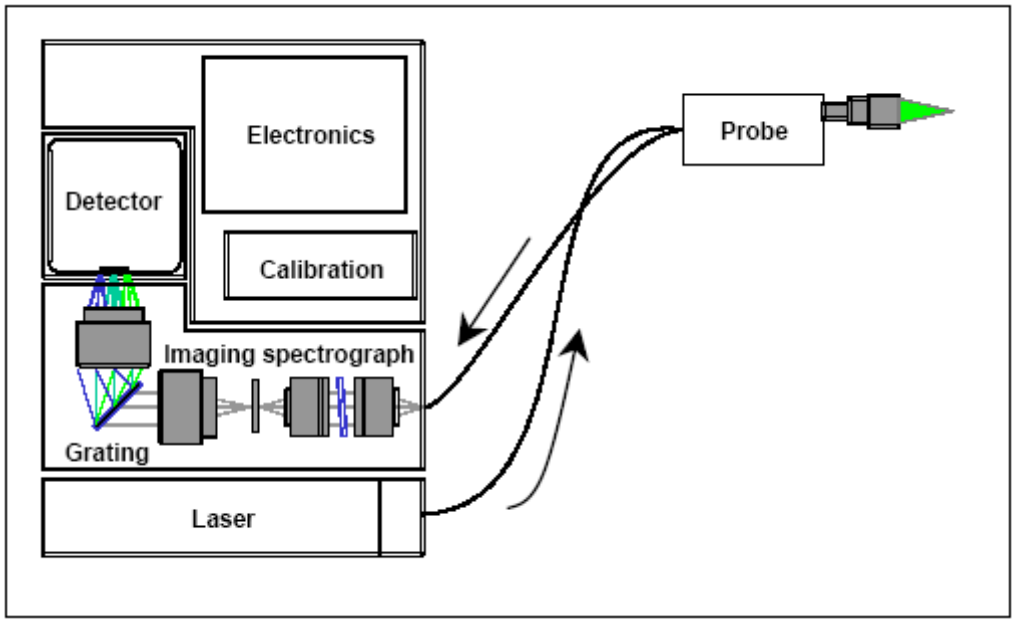

Figure 5.2 Working principle of Raman Spectroscopy (adapted from *Kaiser Optical Systems*).

The working mechanism of Raman spectroscopy is described below (For theory, refer to section 2.5.2). A typical Raman spectrometer is made up of three basic parts: the *laser*, *probe*, and the *spectrograph* (see Fig. 5.2). A laser beam generated in Raman spectrophotometer is directed by optics via a fiber to the probe tip which is in contact

with the slurry to excite Raman spectra. The probe collects the scattered photons via another fiber, filters out the Rayleigh scatter and any background signal from the fiber optic cables, and sends the Raman scatter to the spectrograph. In the spectrograph, Raman scattered photons pass through a transmission grating to separate them by wavelength and passed to a detector, which records the intensity of the Raman signal at each wavelength. This data is plotted as the Raman spectrum.

5.3.4. *Raman with Multivariate Statistical Process Monitoring*

The most commonly used chemometric method with Raman for relating the Raman spectra to the polymorphic composition is the PLS method. There are several studies which reported on quantitative monitoring of polymorphic composition during crystallization using PLS modelling (Starbuck et al., 2002; Scholl et al., 2006; Caillet et al., 2007; Cornel et al., 2008). Despite the success, there are several issues which remained to be addressed. Raman calibration is a time-consuming effort which involves preparing standards at different proportions of polymorphs and dispersing in solution to collect Raman spectra. If one wants to correct for the temperature effect, the whole procedure has to be repeated at different temperatures which is practically less desirable. The other issue is the presence of unrelated variation in Raman data which can complicate PLS models. Raman intensities are observed to be sensitive to external effects such as particle size, suspension density etc. which can vary during the crystallization operations. Some improvements have been reported by using pre-processing (Hu et al., 2006), explicit calibration i.e. modelling the external effects by preparing an extensive set of calibration samples (Cornel et al., 2008) and advanced calibration methods (Chen et al., 2008). In the present work, multivariate statistical process monitoring (MSPM) has

been applied with Raman for polymorph monitoring. An advantage of MSPM is that it is completely data-based, therefore, no sophisticated calibration is required to apply these techniques. The following text provides more details on MSPM.

MSPM using latent variable methods, PCA in particular, has been proven very useful for on line monitoring, analysis and control of industrial chemical processes (Nomikos and Macgregor, 1995; Kourti, 2005). The basis of this approach is to build an empirical PCA model of a historical set of on-line batch process data obtained under normal operating conditions. New batches are then monitored by collecting samples and projecting onto the model to check how good they fit the model. There are several model statistics available to evaluate the goodness of fit. In out of control situation, PCA also offers a means for a proper investigation for the root cause to the process abnormalities.

However, use of spectroscopy in MSPM applications is quite rare. The main challenge is obtaining a reliable reference data for building a model which is valid over a period of time (Gurden et al., 2002). In comparison to engineering data such as temperature, pressure, flowrate etc. spectroscopic data are generally more sensitive to changes in process conditions such as variation in the background medium, temperature fluctuations etc. Recently, Pollanen et al. (2006) has introduced the concept of dynamic PCA based MSPM and applied it for monitoring the onset of crystallization process using ATR-FTIR. In this approach, a PCA reference model was dynamically built using the spectra collected in the undersaturated stage which is called the *training period*. Subsequent spectra were projected on to this model to detect the nucleation event. This is called the *prediction period*. In this way, the uncertainties associated with predefined off-line reference models were eliminated and MSPM with spectroscopy was achieved. In

the present work, we adopted this idea and implemented it with Raman spectroscopy for monitoring polymorphs as well as for the detection of the nucleation event.

5.4. Experimental Section

5.4.1. *Materials*

TB (≥ 98 % purity) was purchased from Junda Pharmaceutical Co.Ltd. (Jiangsu, PR China). The PXRD confirms that it belongs to Form $\mathbf{I^L}$ and used as such without further purification. The solvents (ethanol and deionized water) used were of analytical reagent grade. A mixed solvent ethanol/water (60:40 w/w) was prepared and used for all the experiments. To prepare Form **II**, Form $\mathbf{I^L}$ crystals were suspended in excess in solution at 30 °C and stirred for 4–5 hours to allow polymorphic transformation. The obtained Form **II** crystals were filtered and dried in vacuum oven at RT. Polymorphic purity was verified using PXRD.

5.4.2. *Experimental Setup and Instrumentation*

A schematic diagram of the experimental setup is shown in Fig. 5.3. All the experiments were performed in a 1-liter flat-bottomed glass crystallizer with an inner diameter of 100 mm. It was fitted with four glass baffles on the inner wall to enhance the mixing properties. A marine-type impeller made of stainless steel with a diameter of 42 mm driven by a variable speed overhead stirrer motor was used to provide agitation. An agitation speed of 250 rpm was used which is sufficient to keep the crystals in suspension. The temperature in the crystallizer was controlled by a heating and refrigerated circulator (Julabo FP50-HL) and measured every 2 s using a Pt100 thermocouple.

IR absorbance spectra were collected with a resolution of 4 cm^{-1} on a Nicolet 4700 spectrophotometer (Nicolet Instrument Co.) equipped with a Dipper-210 ATR-FTIR immersion probe (Axiom Analytical Inc.). A conical ZnSe crystal is sealed to one of its end with two ATR reflections. Every spectrum was the average of 64 scans in the range of 600–4000 cm^{-1}. Spectra of ethanol/water (60:40 w/w) solvent at 22 ºC were used as background. The FTIR was purged continuously by purge gas supplied by a FTIR purge gas generator (Parker Balston, model 75-52-12VDC).

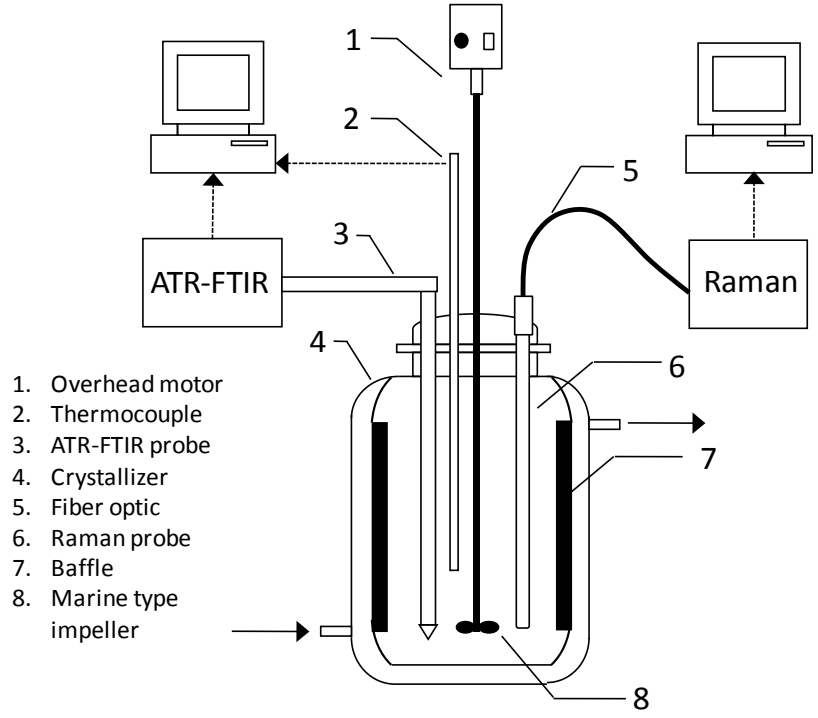

Figure 5.3 Experimental setup for crystallization experiments.

In situ Raman spectra were collected using a Raman Rxn4 analyzer from Kaiser Optical System Inc. (Ann Arbor, MI) equipped with an Invictus NIR external cavity stabilized diode laser operating at 785.714 nm and 450 mW. The system was equipped with single grating f/1.8 holographic imaging spectrograph with a holographic notch filter and Holoplex transmission grating. The detector was a multichannel CCD array detector.

Backscattered radiation was collected from the sample via a $^1/_4$ - in. immersion probe sealed with a sapphire window coupled with the spectrometer fiber-optic cable. Raman spectra were acquired continuously after an exposure time of 5 s and the average of 5 accumulations unless otherwise stated.

In one of the MZW experiments, for a comparison, FBRM probe (Lasentec, model D600L) was also inserted along with Raman probe. FBRM chord length distributions of the TB crystals were obtained in situ with 10 sec measurement duration using the Control Interface Software, version 6.0b16. Data acquired were analyzed using the Data Review Software, version 6.0b16, which displays CLD and the corresponding statistics. In few experiments, Lasentec PVM probe was inserted to collect in situ images of slurry for visual inspection.

For off-line polymorphic verification, the slurry was sampled, filtered and dried overnight in vacuum oven at RT. PXRD measurements of dried crystals were conducted in Bragg-Brentano geometry with a Bruker D8 Advance (Bruker AXS GmbH, Germany) X-ray powder diffractometer equipped with Cu-Kα source (λ = 1.5406 Å), a Nickel-filter, 0.3° divergence slit, a linear position sensitive detector (Vantec-1). Data were collected at RT over a 2θ range of 5 – 50° with an equivalent step size of 2θ = 0.018° at a scan rate of 0.02° sec^{-1}. All samples were rotated to improve the counting statistics.

Solid-state Raman spectra of Forms $\mathbf{I^L}$, **II** and **III** were acquired using a Raman microscope (Invia Reflex, Renishaw) equipped with near infrared enhanced deep-depleted thermoelectrically peltier cooled CCD array detector (576×384) pixels and a high grade Leica microscope. The Raman scattering was excited with a 50-mW NIR diode laser operating at 785 nm. Scans were performed in a spectral window ranging

from 100–2000 cm^{-1} with a sample exposure time of 10 sec and 4 accumulations. 20× objective lens was used to examine the sample.

For ATR-FTIR calibration modeling, OPLS (PCA) algorithm is implemented into PLS toolbox 4.0 (Eigenvector Research, Manson, WA) working under Matlab 7.9 (Mathworks, Natick, MA). ATR-FTIR calibration and measurement of solute concentration were automated using a Visual Basic .NET program that communicates with ATR-FTIR and chemometrics. For polymorph monitoring, dynamic PCA based MSPM was built in Matlab and automated using Raman/Matlab interface.

5.4.3. *Mathematical Methods*

In the following text, matrices are denoted by bold uppercase letters. Vectors are assumed to be column vectors unless indicated by a transposition, for example $\mathbf{x}^{\mathbf{T}}$, and denoted by bold lowercase letters. Scalars are denoted by regular lowercase letters.

For a set of mean centered spectral data matrix $\mathbf{X}(n \times m)$ with n samples and m variables (intensities at wavenumber) and the corresponding concentration vector $\boldsymbol{y}(n \times 1)$, the latent variable models are given by Eqs. (5.2) and (5.3).

$$\mathbf{X} = \mathbf{t_1 p_1^T} + \mathbf{t_2 p_2^T} + \cdots + \mathbf{t_K p_K^T} + \mathbf{E} = \mathbf{T P^T} + \mathbf{E} \tag{5.2}$$

$$\mathbf{y} = q_1 \mathbf{t_1} + q_2 \mathbf{t_2} + \cdots + q_K \mathbf{t_K} + \mathbf{f} = \mathbf{T q^T} + \mathbf{f} \tag{5.3}$$

K is the number of latent variables (LVs). **E** and **f** are the residual matrices, $\mathbf{T}(n \times \mathrm{K})$ is the matrix of **X** scores, and $\mathbf{P}(m \times \mathrm{K})$ and $\mathbf{q}(1 \times \mathrm{K})$ are the loading matrices of **X** and **y**, respectively. $\mathbf{t_i}$ and $\mathbf{p_i}$ are the column vectors of **T** and **P** and q_i is a scalar coefficient, corresponding to i^{th} latent variable, respectively. Typically, the dimension K is quite small compared to the dimension of the original data ($\mathrm{K} \ll m$) which is normally determined by cross-validation or variance analysis. The loading vectors express how the original

variables are weighed together in a corresponding LV and the score vectors contain a score value for each spectrum and signify how each sample is related to other in a particular LV. Three latent variable methods were employed in this work whose mathematical details are described below.

Principal Component Analysis (PCA). PCA models only single space **X** by finding the latent variables called principal components (PCs) that explain the maximum variance in **X**. Mathematically, PCA relies upon the eigenvector decomposition of the covariance matrix ($\mathbf{X^T X}$) to extract PCs. The loading vectors ($\mathbf{p_i}$) are the eigenvectors of the covariance matrix and the corresponding eigenvalues (λ_i's) signify the amount of variance captured by a given PC. To derive an optimum PCA model, a good rule of thumb is to include PCs until the subsequent PC captures <2% variation in λ_i's. The corresponding scores vector $\mathbf{t_i}$ is then generated by the linear projection of **X** on to the PC space using the loading vector ($\mathbf{t_i = Xp_i}$). The unmodeled variation in **X** is considered noise and consolidated into the residual matrix **E**.

There are several PCA statistics including the scores itself can be used for MSPM. For MSPM, score values for any new sample $\mathbf{x}^T$ can be obtained by projecting the sample on to directions defined by loadings ($t_i = \mathbf{x^T p_i}$). Two commonly used PCA statistics are T^2 and Q statistics. T^2 measures the distance of the new sample from the model centre within the model space. This determines whether the projected sample has any systematic deviation from the steady-state region. Q statistic is complementary to T^2 and measures the orthogonal distance of the sample from the model space. It is useful in monitoring the nonsystematic variations which are not explained by the model. Fig. 5.4 shows the geometric interpretation of these statistics for a two-component PCA model.

T^2 and Q statistics can be calculated by Eqs. (5.4) and (5.5).

$$T^2 = \sum_{i=1}^{K} \frac{t_i^2}{\lambda_i} \tag{5.4}$$

$$Q = \sum_{j=1}^{j=m} (x_j - \hat{x}_j)^2 \tag{5.5}$$

t_i is the sample score on i^{th} PC. m is the number of variables and x_j and $\hat{x}_j$ are the measured and predicted spectral values of a new sample corresponding to j^{th} variable.

Along with statistics, PCA also allows to extract variable contribution plots which show the contribution from individual variables to the calculated statistic. Such a plot is highly useful in assessing the process conditions and possible causes.

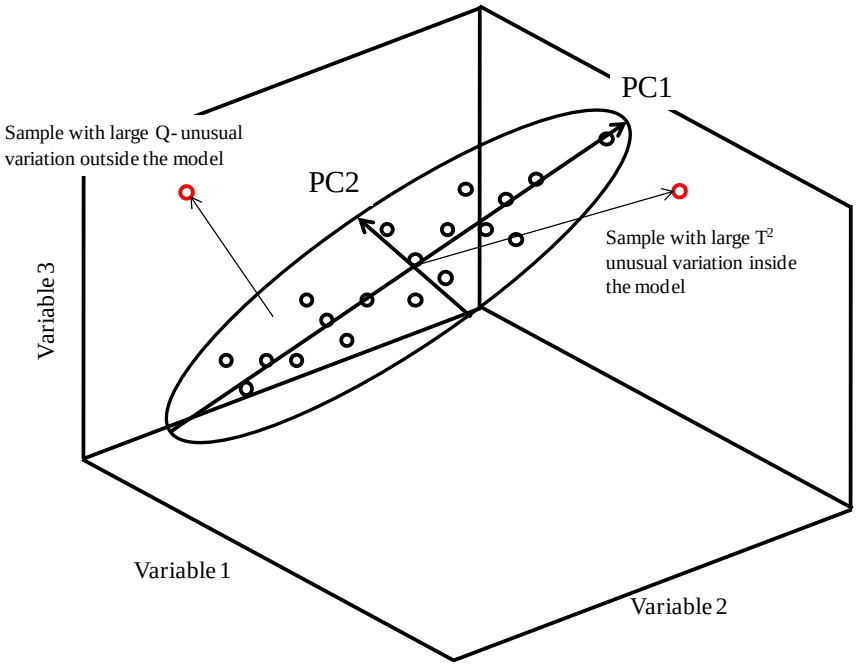

Figure 5.4. Geometrical representation of T^2 and Q statistics.

Contributions to Q statistic:

The difference $(x_j - \hat{x}_j)$ is called the *variable residual* and used for monitoring the contributions to Q statistic.

Contributions to T^2 statistic:

For any given new sample, the variable contribution to T^2 value is given by

$$c_j = \sum_{i=1}^{i=\mathrm{K}} \frac{t_i p_{ji}}{\lambda_i^{1/2}} \tag{5.6}$$

c_j is the T^2contribution of j^{th} variable, t_i is the score value on i^{th} PC, $p_{ji}$is the loading on i^{th} PC corresponding to j^{th} variable, λ_i is the eigenvalue corresponding to i^{th} PC, respectively.

Partial Least Squares (PLS). PLS is a popular latent variable method which can model both **X** and **y** data. The objective of PLS is to find LVs that explain both the maximum variation in **X** and correlates with the variation in $\boldsymbol{y}$. A commonly used PLS NIPALS algorithm (see Table 5.1) operates sequentially to extract each LV and the corresponding model parameters ($\mathbf{w_i}$, $\mathbf{t_i}$, $\mathbf{p_i}$, q_i). In this algorithm, a loading weight vector $\mathbf{w_1}$ is computed in such a way that it maximizes the covariance between $\mathbf{t_1}$ and **y** (step 2). Using standard linear algebra, it can be shown that

$$\mathbf{w_1} = \frac{\mathbf{X^T y}}{\|\mathbf{X^T y}\|} \tag{5.7}$$

$\|\ \ \|$ is the eucledian norm. The corresponding scores and loading vectors $\mathbf{t_1}$, $\mathbf{p_1}$ and a scalar coefficient q_1 are then generated (steps 3–5). $\mathbf{w_2}$ is calculated in the same way with the deflated forms of **X** and **y**, and so on and so forth.

Mathematically, PLS extracts the eigenvectors of the covariance matrix $\mathbf{X^T y y^T X}$ as the loading weight vectors $\mathbf{w_i}$. As the true rank of covariance matrix is only one, ideally PLS should extract only one $\mathbf{w_i}$. However, the presence of $\boldsymbol{y}$- unrelated variation in **X** can disturb the extraction and as a result, PLS extracts additional LVs to satisfy the model requirements. This increase in model complexity can negatively affect the model

robustness and interpretation. To address these issues, the PLS algorithm has been modified to build simpler and robust PLS models.

Table 5.1 Comparison of PLS and OPLS (PCA) algorithms.

Step	PLS	OPLS (PCA)
1	Center and scale	Center and scale
2	$\mathbf{w} = \frac{\mathbf{X^T y}}{\|\mathbf{X^T y}\|}$	$\mathbf{w} = \frac{\mathbf{X^T y}}{\|\mathbf{X^T y}\|}$
3	$\mathbf{t} = \mathbf{Xw}$	$\mathbf{t} = \mathbf{Xw}$
4	$q = \mathbf{y^T t}/(\mathbf{t^T t})$	$q = \mathbf{y^T t}/\mathbf{t^T t}$
5	$\mathbf{p} = \mathbf{X^T t}/(\mathbf{t^T t})$	$\mathbf{p} = \mathbf{X^T t}/\mathbf{t^T t}$
6		$\mathbf{w_{ortho}} = \mathbf{p} - \left[\frac{\mathbf{w^T p}}{\mathbf{w^T w}}\right]\mathbf{w}$
7		$\mathbf{t_{ortho}} = \mathbf{X w_{ortho}}$
8		$\mathbf{p_{ortho}} = \mathbf{X^T t_{ortho}}/\mathbf{t_{ortho}^T t_{ortho}}$
9		$\mathbf{X_{OPLS}} = \mathbf{X} - \mathbf{t_{ortho} p_{ortho}^T}$ For additional orthogonal components, return to step 3 and set $\mathbf{X} = \mathbf{X_{OPLS}}$, otherwise go to step 10
10		$\mathbf{X_{ortho}} = \mathbf{T_{ortho} P_{ortho}}^{\mathbf{T}}$
11		Run PCA on $\mathbf{X_{ortho}}$ $\mathbf{X_{ortho}} = \mathbf{T_{ortho(pca)} P_{ortho(pca)}}^{\mathbf{T}} + \mathbf{E_{ortho(pca)}}$
12		$\mathbf{X_{filt}} = \mathbf{X_{OPLS}} + \mathbf{E_{ortho(pca)}}$, now $\mathbf{X_{filt}}$ is the filtered data matrix
13	$\mathbf{E} = \mathbf{X} - \mathbf{t p^T}$, $\mathbf{f} = \mathbf{y} - \mathbf{t} q^{\mathbf{T}}$ For additional latent variables, return to step 2 and set $\mathbf{X} = \mathbf{E}$ and $\mathbf{y} = \mathbf{f}$	Run PLS using $\mathbf{X_{filt}}$

Orthogonal Partial Least Squares (OPLS) (PCA). OPLS (PCA) is an extension of PLS based on NIPALS algorithm with few additional orthogonalization steps included (see Table 5.1).

In OPLS (PCA), **X** is decomposed into three distinct parts, *correlated,* **y-** *unrelated* and *residual* parts. The model can be written as

$$\mathbf{X} = \mathbf{t_1 p_1^T} + \mathbf{t_2 p_2^T} + \cdots + \mathbf{t_K p_K^T} + \mathbf{t_{ortho1} p_{ortho1}^T} + \mathbf{t_{ortho2} p_{ortho2}^T} + \cdots + \mathbf{t_{orthoR} p_{orthoR}^T} + \mathbf{E}$$

$$= \mathbf{T P^T} + \mathbf{T_{ortho} P_{ortho}^T} + \mathbf{E} \quad (5.8)$$

$$\mathbf{y} = \mathbf{T q^T} + \mathbf{f} \quad (5.9)$$

R is the number of orthogonal components (OCs). $\mathbf{T_{ortho}}$ and $\mathbf{P_{ortho}}$ are the corresponding $\boldsymbol{y}$- orthogonal scores and loading matrices. $\mathbf{t_{orthoi}}$ and $\mathbf{p_{orthoi}}$ are the column vectors of $\mathbf{T_{ortho}}$ and $\mathbf{P_{ortho}}$ corresponding to i^{th} OC.

OPLS (PCA) NIPALS algorithm first computes one ordinary PLS component (steps 1–5). The obtained **w** and **p** are then used to compute a new weight vector $\mathbf{w_{ortho}}$ which is part of **p** that remains orthogonal to **w** (step 6). Using standard linear algebra, Trygg and Wold (2002) showed that this is equal to

$$\mathbf{w_{ortho}} = \mathbf{p} - \left[\frac{\mathbf{w^T p}}{\mathbf{w^T w}}\right] \mathbf{w} \tag{5.10}$$

Using $\mathbf{w_{ortho}}$, the corresponding scores, loadings vectors $\mathbf{t_{ortho}}$ and $\mathbf{p_{ortho}}$ are then generated (steps 7 and 8). In step 9, the orthogonal component is removed from **X**. If further OCs have to be removed, the whole algorithm (steps 3–9) is repeated, including the first PLS step but with new **X**. Otherwise, the orthogonal variation removed from **X** is collected into $\mathbf{X_{ortho}}$ and decomposed using PCA to remove the residual part and added back into the new **X** which forms the new filtered matrix $\mathbf{X_{filt}}$ (steps 10–12). Finally, an ordinary PLS algorithm is run on $\mathbf{X_{filt}}$ to extract the PLS model parameters (step 13). This OPLS (PCA) pretreated PLS model is then used for predictions of new samples. It is important to note that the new samples have to be corrected for orthogonal variation using OPLS (PCA) model parameters before PLS model prediction (For more details, refer to Trygg and Wold, 2002).

Determination of Number of Latent Variables. Choosing the correct number of LVs into the model is critical. Too few LVs mean not all of the variation within **X** explaining $\boldsymbol{y}$ has been included in the model and predictions of new samples are compromised. Too many components in the model mean that irrelevant variation that does not predict $\boldsymbol{y}$ (noise) is

included in the model, which can result in overfitting problems. Such models can be unstable, and although calibration samples fit very well to the model, the predictions for new samples are not accurate. Cross-validation is the common method used to determine the optimal number of LVs.

During cross-validation, parts of the calibration set (test set) are left out of calculations and the model is built using a certain number of LVs and applied to estimate the test set. This procedure is repeated several times for different test sets and the root-mean-square error of cross-validation (RMSECV) between predicted and known values is calculated using Eq. 5.11 to select the number of LVs.

$$\mathrm{RMSECV_K} = \sqrt{\frac{\sum_{i=1}^{\mathrm{K}}(y_i - \hat{y}_i)^2}{n}} \tag{5.11}$$

K is the number of chosen LVs, $\hat{y}_i$ is the predicted value of sample i using a model that was built using a set of samples that does not include sample i. y_i is the known value of sample i. n is the number of calibration samples. The optimal number of LVs is found where RMSECV as a function of the number of LVs reaches a minimum.

There are various cross-validation methods that differ in how the samples are left out of the calibration set. In the present work, leave-one-out (LOO), in which each single sample in the calibration set is used as a test set, was used. The RMSECV value was examined to estimate the optimal number of LVs.

Determination of Number of Orthogonal Components. For pre-processing based on orthogonal projection methods, the number of OCs to be removed is an important parameter. The correction may not be effective if too few components are removed. In contrast, removal of too many results in erosion of useful signal. The classic way is to

adjust this parameter according to RMSECV. In the present work, for OPLS model, OCs were removed until the number of LVs reduces down to one. In addition, the following statistics were also calculated to assess the model performance. The correlation coefficient (R^2X) is a measure of how much of the variance in (**X**) can be explained by the model. The cross-validated variance (Q^2) explains how much of the variance in **X** can be predicted by the model.

$$R^2X = \frac{SS_{tot} - SS_{res}}{SS_{tot}} \tag{5.11}$$

$$Q^2 = \frac{SS_{tot} - PRESS_K}{SS_{tot}} \quad \text{where} \quad PRESS_K = \sum_{i=1}^{n} (y_i - \hat{y}_i)^2 \tag{5.12}$$

SS_{tot} and SS_{res} are the sum of squares of measured data and model residuals, respectively. $PRESS_K$ is the cumulative predicted residual sum of squares (PRESS) corresponding to K^{th} LV.

5.4.4. *Experimental Procedures*

ATR-FTIR Calibration Experiments. Different solute concentrations of TB in 400 g of solvent (Table 5.2) were placed in the crystallizer and heated until all of the crystals dissolved. The solution was cooled at 0.5 °C/ min, while the IR spectra were collected at 30 sec interval. The measurements were stopped once crystals started to appear by observing with naked eye.

ATR-FTIR Calibration Modeling. The calibration experiments resulted in a data set of 234 IR spectra collected from various TB concentrations. The IR spectra in the range 1000–1650 cm^{-1} were used to construct the calibration model. The higher (2800–3500 cm^{-1}) and lower (650–1000 cm^{-1}) wavenumber regions are excluded because of large frequency shifts with temperature which can make the model unstable. As an example,

the raw IR spectra collected for Cs3 in the selected range are shown in Fig. 5.5(a). A clear temperature effect and base-line variations independent of solute concentration were visible in the spectra.

Table 5.2 ATR-FTIR calibration samples for solute concentration measurements.

Calibration sample	Concentration (mg/g solvent)	Temperature range (deg C)	Number of spectra collected
Cs1	19.8	35 – 14.8	54
Cs2	48.9	40 – 21.1	61
Cs3	100.2	50 – 32.5	36
Cs4	150.4	50 – 38.1	25
Cs5	190.7	60.7 – 45.3	33
Cs6	226.7	60.1 – 48	25

Using the calibration set, PLS and OPLS (PCA) regression were applied and the resulted models were summarized in Table 5.3. The cross validation suggests a 7- LV model for PLS with RMSECV value of 0.23 mg/g. PLS extracts the first LV explaining 93% variation in **X** that correlates with 99% variation in **y** with RMSECV value of 3 mg/g. This low correlation can be attributed to the presence of orthogonal **y**- unrelated variation in IR spectra. As a result, PLS uses another 6 LVs to extract all the **y**- related variation in **X** to improve the correlation. In OPLS (PCA), the data was pre-processed to remove 6 OCs to build a PLS model. The filtered spectra are shown in Fig. 5.5(b) for Cs3. OPLS (PCA) has effectively removed the temperature effect and base-line variations. This has significantly improved the covariance in calibration data and as a result PLS model achieves the optimum correlation with only 1 LV (see Table 5.3).

Fig. 5.6 shows the comparison of regression coefficient vectors of 7- LV PLS model with OPLS (PCA) pretreated PLS model. The similarity of the regression vector of OPLS (PCA) model with the original IR raw spectra clearly suggests that the model is

free from ***y***- unrelated variation. On the other hand, PLS regression vector is significantly changed particularly in 1000–1200 cm^{-1} region. It would be interesting to see which variables are mainly contributing to the disturbing variation in IR spectra.

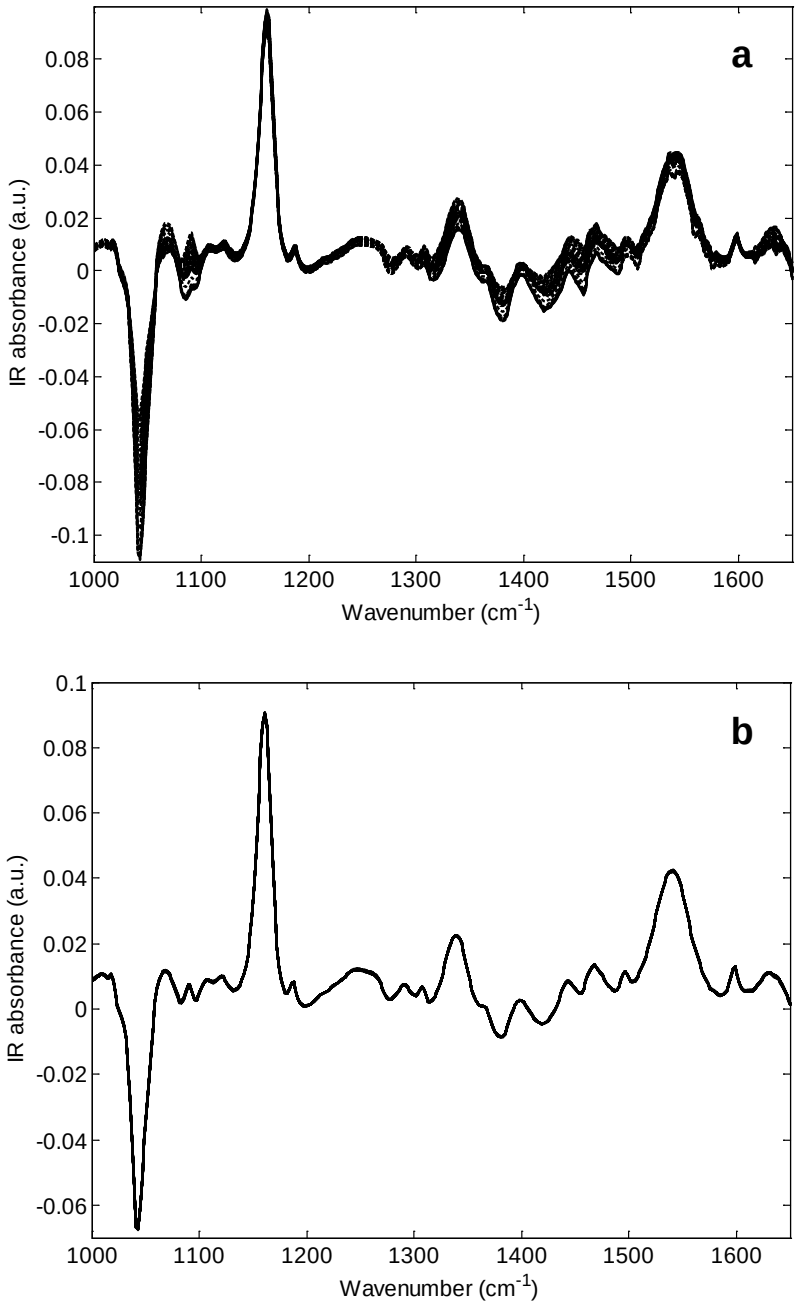

Figure 5.5 ATR-FTIR raw calibration spectra (Cs3) **(a)** without pre-processing **(b)** 6 orthogonal components removed using OPLS (PCA).

Table 5.3 ATR-FTIR calibration model summary for solute concentration measurements.

Ordinary PLS model				Orthogonal PLS (PCA)			
LV	[a]R^2Xcum	[b]Q^2cum	RMSECV (mg/g)	LV	R^2Xcum	Q^2cum	RMSECV (mg/g)
1	93.54	99.83	3.02	1	99.99	100	0.23
2	96.99	99.87	2.66				
3	99.85	99.92	2.04				
4	99.94	99.97	1.35				
5	99.98	99.98	1.15				
6	99.98	99.99	0.53				
7	99.99	100	0.23				

[a] R^2Xcum = cumulative R^2X [b] Q^2cum = cumulative Q^2

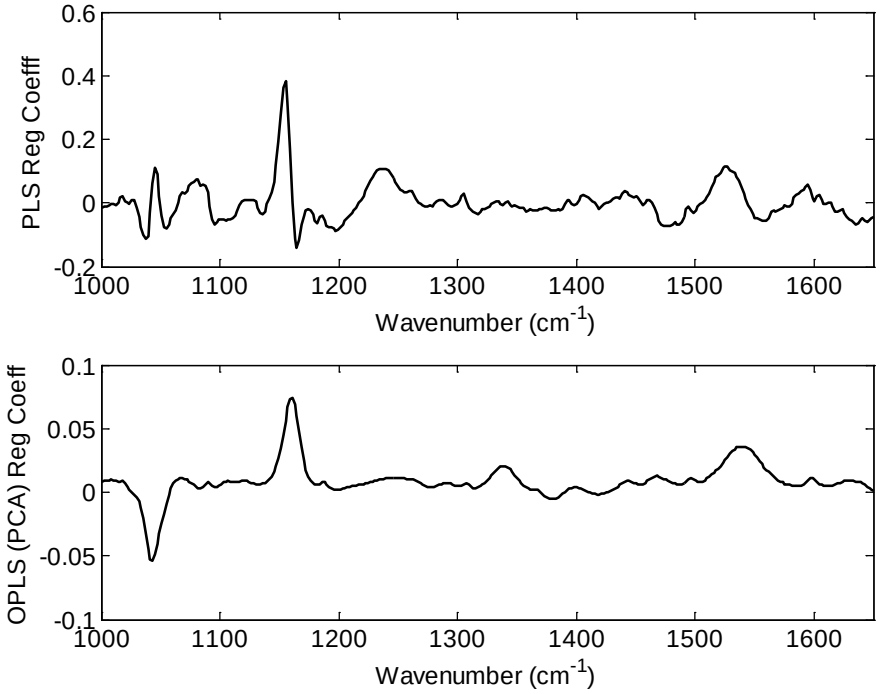

Figure 5.6 Comparison of regression coefficient vectors of PLS model and OPLS (PCA) pretreated PLS model.

Fig. 5.7 shows the principal orthogonal loadings extracted from variation removed from IR spectra. First two loadings explain 97 % of orthogonal variation removed and represent the temperature effect on IR spectra. It should be noted that the major contributions to temperature induced $\boldsymbol{y}$- unrelated variation is from 1020–1110 cm^{-1} and

1145–1185 cm^{-1}. This explains why PLS regression vector significantly changed in 1000–1200 cm^{-1} region. The third loading explains 2% of orthogonal variation removed and represents the baseline variation. Though, OPLS (PCA) removed the $\boldsymbol{y}$- unrelated information in the form of 6 OCs from the spectral data, it does not improve the model predictability since both models gave the same RMSECV value. However, the resulted simple model is expected to be more stable to experimental perturbations.

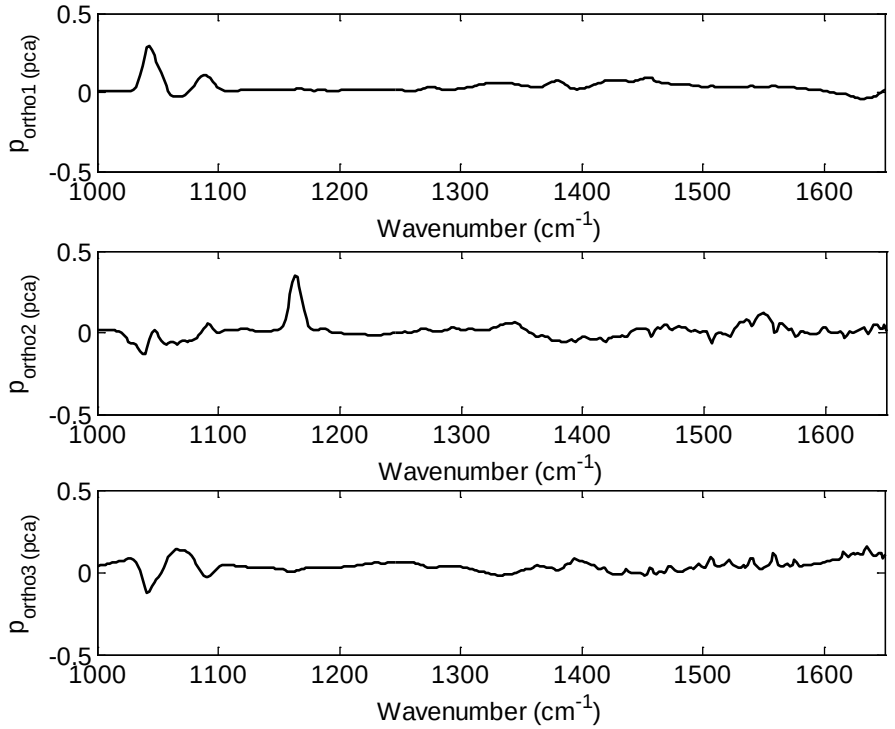

Figure 5.7 Plot of the 3 principal orthogonal loadings ($\mathbf{p_{ortho\ (pca)}}$) removed from IR calibration spectra. The corresponding variation captured is $\mathbf{p_{1ortho1\ (pca)}}$ (93.56%), $\mathbf{p_{ortho2\ (pca)}}$ (3.56%), $\mathbf{p_{3ortho\ (pca)}}$ (1.96%).

Solubility Measurements. Solubilities of TB polymorphs (Forms ($\mathbf{I^L}$, $\mathbf{I^H}$) and **II**) were measured in the chosen solvent by two different methods in the temperature range of 20 – 55 °C. For all measurements, a 400 g of solvent was used. In the first method, an excess amount of corresponding polymorph was added to the solvent which was maintained at a

constant temperature and solute concentration was monitored using ATR-FTIR. As the concentration reaches a plateau, spectral measurement was stopped and the solution was allowed to settle for 1 hour to collect a sample from the supernatant for gravimetric measurements. At the end of each measurement, the suspension was filtered to collect the solid and polymorphic form was verified using PXRD.

In the second method, a saturated suspension of TB was prepared at 20 °C and heated in two segments. Below 30 °C, at a heating rate of 2 °C/h and above 30 °C, at a heating rate of 3 °C/h. The heating rate is chosen such that it is slow enough to keep the suspension in thermodynamic equilibrium and a continuous solubility curve can be measured. Intermittently, crystals were added to the solution to keep it in a suspension state. Solution concentration was monitored using ATR-FTIR. In the case of Form (**I**^{L}, **I**^{H}) the measurement was disturbed by polymorphic transformation to more stable Form **II**. Therefore, its solubility curve was measured in 2.5 hour intervals. After each interval, the measurement was stopped to drain the vessel contents and vessel was washed thoroughly with the solvent and a fresh batch was started again.

Solution Mediated Polymorphic Transformation Experiment. A saturated solution (36 mg/g solvent) of Form **I**^{L} was prepared at 25 °C with 400 g of solvent. Then, 2.07 g of Form **I**^{L} crystals were suspended in excess which corresponds to 0.5% suspension density. The suspension was stirred at 250 rpm while the solution concentration was measured using ATR-FTIR. To monitor the polymorphic changes, Raman spectroscopy was coupled with MSPM.

Fig. 5.8 shows the Raman spectra of solvent, solute and different TB crystal forms (Forms **I**^{L}, **II** and **III**) in the wavenumber range of 600–1800 cm^{-1}. The major differences

between the three polymorphs were apparent in the aromatic ring deformation (785–825 cm^{-1}) and asymmetric stretching of sulfonyl group (1135–1190 cm^{-1}) regions of TB molecule with strong Raman scattering and no overlap with solvent peaks. Therefore, this wavenumber region is selected for MSPM. To implement MSPM, a PCA-based reference model was built dynamically using the first 30 Raman spectra in the training period. The reference data was assumed to be free from abnormalities and number of spectra was chosen such that it captures enough variation for building a model. In the prediction period, samples were projected on to the model to estimate the corresponding T^2 and Q statistics and their variable contributions to monitor the polymorphic variations.

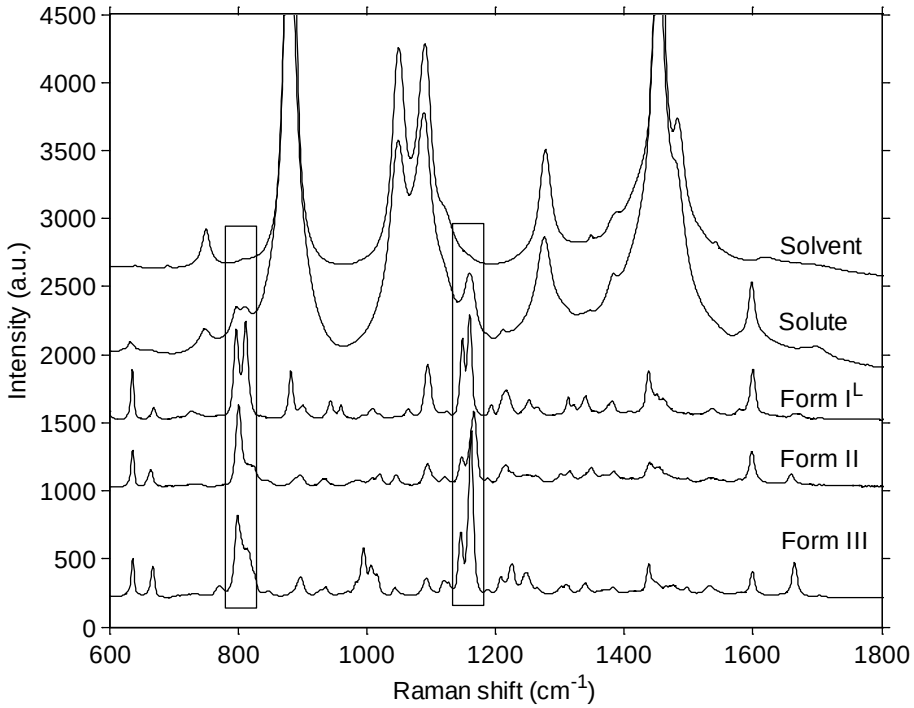

Figure 5.8 Raman spectra of ethanol/water (60:40 w/w), TB solute and crystal forms of TB in the wavenumber range of 600–1800 cm^{-1}.

Metastable Zone Width Measurements. Different saturated solutions corresponding to Form **II** were prepared by dissolving known amounts of TB in 400 g of solvent. To

ensure complete dissolution, the solutions were heated to 5 °C above the saturation temperature and kept constant for 30 min. The solution was then quickly cooled (0.5 °C/min) to the corresponding saturation temperature and held there for another 30 min. Subsequently, the solutions were cooled at different cooling rates (1, 0.5 and 0.1 °C/min) with constant stirring (250 rpm). The Raman spectral acquisition was started immediately after the solution stabilizes at the corresponding saturation temperature.

For MSPM, in the training period, a PCA-based reference model was built dynamically using the first 30 Raman spectra in the wavenumber range of 600-1200 cm^{-1}. In the prediction period, spectra were projected to estimate T^2 and Q statistics and their variable contributions. The temperature corresponding to a sharp dip in T^2 statistic (due to explosive nucleation of crystals) was read as the nucleation temperature. For each measurement, the experiment was repeated twice and the average temperature was noted. Q contribution plots were diagnosed to detect the polymorph nucleated. At the end of each experiment, the solution was filtered and crystals were harvested, dried in vacuum oven at RT and analyzed using PXRD to verify the polymorph nucleated.

Batch Crystallization Experiment. An undersaturated solution of TB at 55 °C was prepared by dissolving a known amount of TB in 400 g solvent corresponding to the solubility of Form **II** at 50 °C. The solution was then cooled at 0.08 °C/min. ATR-FTIR was used to continuously monitor the solute concentration. PVM probe was also inserted to collect the slurry images for visual inspection. The obtained crystalline product was filtered, dried in vacuum oven at RT and subjected to PXRD to verify the polymorphic purity.

CHAPTER 6

Crystallization Process Development for the Isolation of Desired Form of Tolbutamide

In this chapter, using the experimental setup described in chapter 5, a cooling crystallization process was developed for the isolation of the desired form of TB. QbD based strategy described earlier was applied by determining a design space in terms of the metastability of the desired form. A crystallization batch process was successfully operated to achieve the desired polymorph.

6.1. Selection of the Desired Form of TB

For the production of TB, Form **II** is the ideal form to select because it is thermodynamically most stable and has the lowest propensity for polymorphic transformation. However, its innate characteristic of crystallizing in a thin fiber needle shape (refer to Fig. 4.16a) is a major obstacle for its downstream processing such as filtration, drying etc. It has also been observed that Form **II** has the least tendency to nucleate directly from the solution. Therefore, a metastable form is a viable option for this system. In the hierarchy of stability of TB polymorphs, the next stable form is Form ($\mathbf{I^L, I^H}$) which also has good processability characteristics. Therefore, in the present work, this polymorph has been chosen as the desired form for the crystallization of TB.

6.2. Solubility Measurements of TB Polymorphs

The solubility curves of Forms ($\mathbf{I^L, I^H}$) and **II** are shown in Fig. 6.1. The continuous nature of solubility of Form ($\mathbf{I^L, I^H}$) with respect to temperature in the region of 39–41 °C clearly suggests that the equilibrium conditions were prevailed during the measurements. Otherwise, we would have observed a dip in concentration in this region

due to the delay in dissolution caused by the solid-state transformation of Form $\mathbf{I^L} \rightarrow \mathbf{I^H}$ **(**Kawakami, 2007). The concentrations measured using ATR-FTIR showed good agreement with the solubility data obtained using gravimetric method validating the calibration model built using OPLS (PCA). These measurements also suggest that Form **II** is more stable than Form ($\mathbf{I^L}$, $\mathbf{I^H}$) in this temperature range which agrees with our earlier characterization studies (Thirunahari et al., 2010).

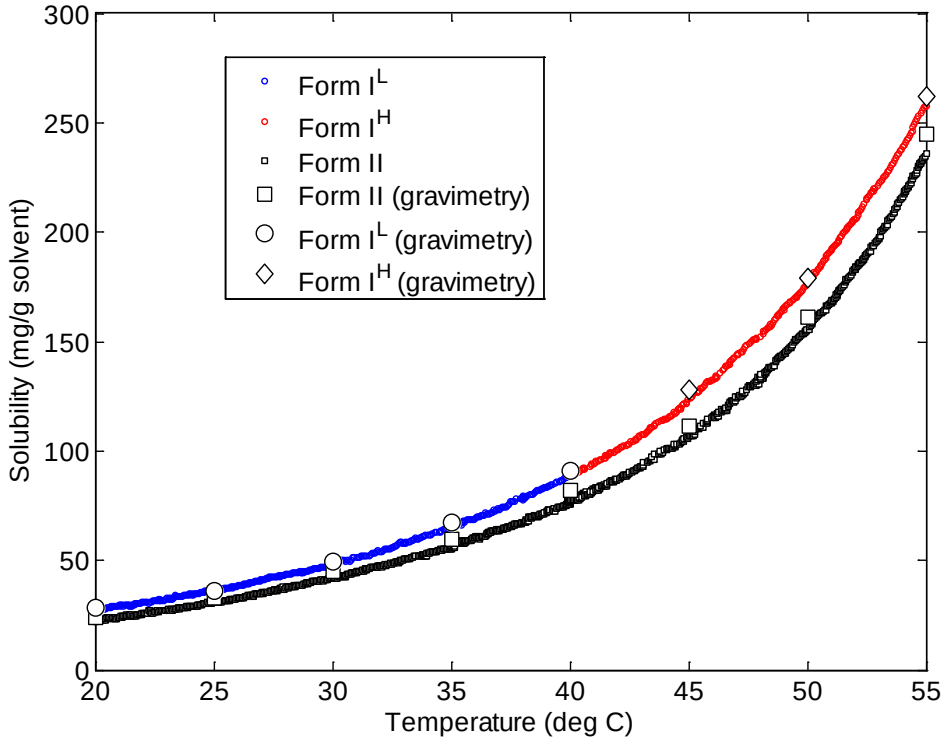

Figure 6.1 Solubility curves of TB Forms ($\mathbf{I^L}$, $\mathbf{I^H}$) and **II** in ethanol/water (60:40 w/w).

6.3. Statistical Monitoring of Polymorphic Transformation

As discussed earlier, SMPT is the main mechanism by which metastable polymorphs undergo transformation during crystallization. Since the desired polymorph of TB is metastable in nature, it may undergo transformation to the more stable Form **II**. Therefore, characterization of transformation kinetics is essential to understand the

fundamental mechanisms governing the process. Such information is useful to determine optimum operating conditions for crystallization to prevent the transformation. To this aim, a seeded polymorphic transformation experiment was performed during which polymorphic content was monitored using Raman spectroscopy and solute concentration was monitored using ATR-FTIR.

Fig. 6.2 displays the time resolved Raman spectra collected in the selected wavenumber range during the seeded transformation experiment. As we can see, as time progressed, in 785–825 cm^{-1} region (Fig. 6.2(a)), the characteristic peaks of Form $\mathbf{I^L}$ at 798 and 812 cm^{-1} decreased in intensity. Towards the end, the peak at 812 cm^{-1} becomes a shoulder peak which is a characteristic of Form **II**. In 1140–1190 cm^{-1} region (Fig. 6.2(b)), the peak at 1161 cm^{-1} gradually shifted to 1164 cm^{-1} which is a characteristic peak of Form **II**. These observations suggest that Raman spectroscopy is capable of detecting the polymorphic changes in TB crystals in suspensions. However, for a mechanistic understanding, the dynamic PCA based MSPM was applied with Raman which is discussed below. The main advantage of MSPM is that it decouples the spectral variations caused by stable and metastable forms, thus making the interpretations much easier.

For dynamic PCA based MSPM with Raman, a reference PCA model was built in the training period which resulted in a two component model with PC1 capturing 89.9% and PC2 capturing 2.2% variation. Subsequent PCs were ignored and added into the model residual space because they capture negligible variation (< 2%). PC1 can be directly related to Form $\mathbf{I^L}$, since the corresponding loadings of PC1 are similar to the spectral features of Form $\mathbf{I^L}$. Physical interpretation of PC2 is difficult, but may be

attributed to the effect of particle size of Form $\mathbf{I^L}$ crystals on Raman scattering. In the prediction period, Raman spectra were projected on to the model and T^2 and Q statistics were estimated.

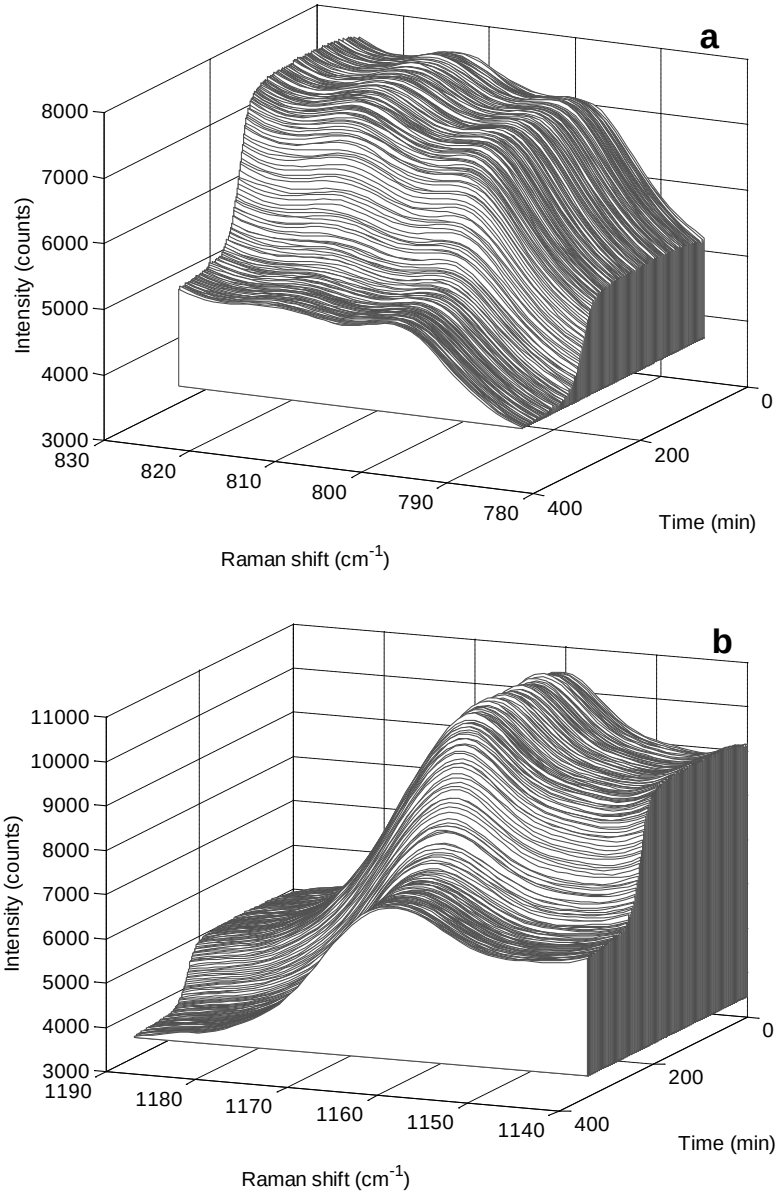

Figure 6.2 Time resolved Raman spectra for a seeded polymorphic transformation of TB Form $\mathbf{I^L}$ to Form **II** at 25 °C in ethanol/water (60:40 w/w) solvent **(a)** 785–825 cm^{-1} **(b)** 1140–1190 cm^{-1}.

6.3.1. *T^2 and Q Plots*

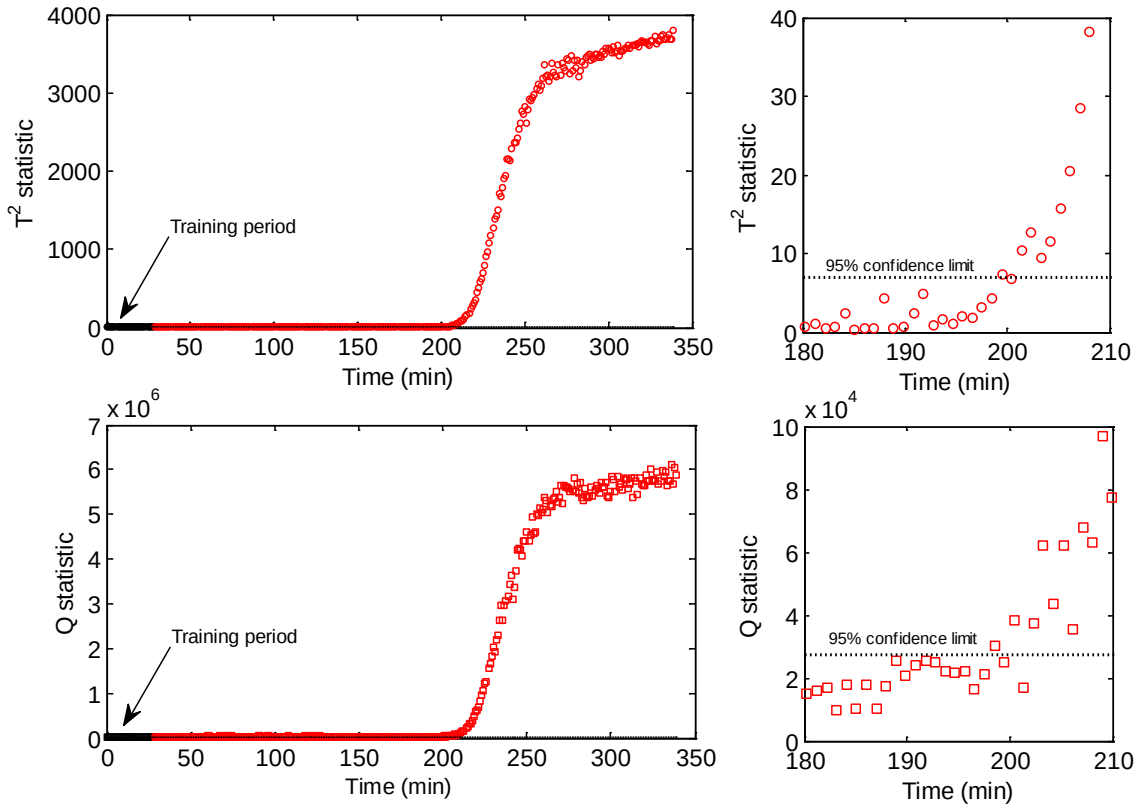

Figure 6.3 T^2 and Q statistic plots for a seeded polymorphic transformation of TB Form $\mathbf{I}^{\mathbf{L}}$ to **II**.

Fig. 6.3 shows the T^2 and Q statistic plots with respect to time. As stated earlier (refer to section 5.4.3), T^2 measures the systematic variation within the model space, therefore it refers to the variations occurring in the metastable form, Form $\mathbf{I}^{\mathbf{L}}$. On the other hand, Q statistic measures the unmodeled variation and therefore it refers to the new variations brought about by the transformation into the process i.e. those variations related to the stable Form **II**. In Fig. 6.3, initially, both statistics were within the 95% confidence limit imposed by the model indicating that no variation in the suspended Form $\mathbf{I}^{\mathbf{L}}$ crystals. After 200 min, both statistics crossed the limit and moved away from the reference. This indicates that the polymorphic transformation of Form $\mathbf{I}^{\mathbf{L}}$ has been

triggered. Towards the end of the experiment i.e. after 300 min or so, both were stabilized at a higher value suggesting the end of transformation.

To verify these interpretations, the variable contribution plots of T^2 and Q were inspected. Fig. 6.4 shows the T^2 and Q contribution plots. Here, the variables are the Raman intensities at different wavenumber. For T^2 contribution calculations, only PC1 was used as it captures the major portion of variation. The arrows shown indicate the direction of the contribution with respect to time.

As we can see, the major contributions to T^2 value during the transformation are from the Raman intensities corresponding to 798 and 810 cm^{-1} in 785–825 cm^{-1} region and 1161 cm^{-1} peak in 1140–1190 cm^{-1} region which are characteristics peaks of Form $\mathbf{I^L}$. The arrows indicate that these contributions are decreasing with respect to time suggesting that Form $\mathbf{I^L}$ crystals are undergoing dissolution. In Q contribution plots, the major contributions to Q value in 785–825 cm^{-1} region are from 798, 811 and 817 cm^{-1}. The arrows indicate that the contributions from 811 and 817 cm^{-1} are decreasing with respect to time. This is consistent with Raman characteristics of Form **II**, for which there is a shoulder peak in this region. On the other hand, a major contribution from 1140–1190 cm^{-1} region is from 1164 cm^{-1} which is a characteristic of Form **II** which increases with time. All these Q contributions clearly suggesting that the jump in Q value is due to the nucleation and growth of Form **II**.

There are a few other contributions, particularly to Q value, which may be due to the unrelated variation gathering in the Raman spectra during the transformation due to change in particle size, suspension density etc. However, contribution plots clearly

provided the evidence that the increase in T^2 and Q values is due to polymorphic transformation.

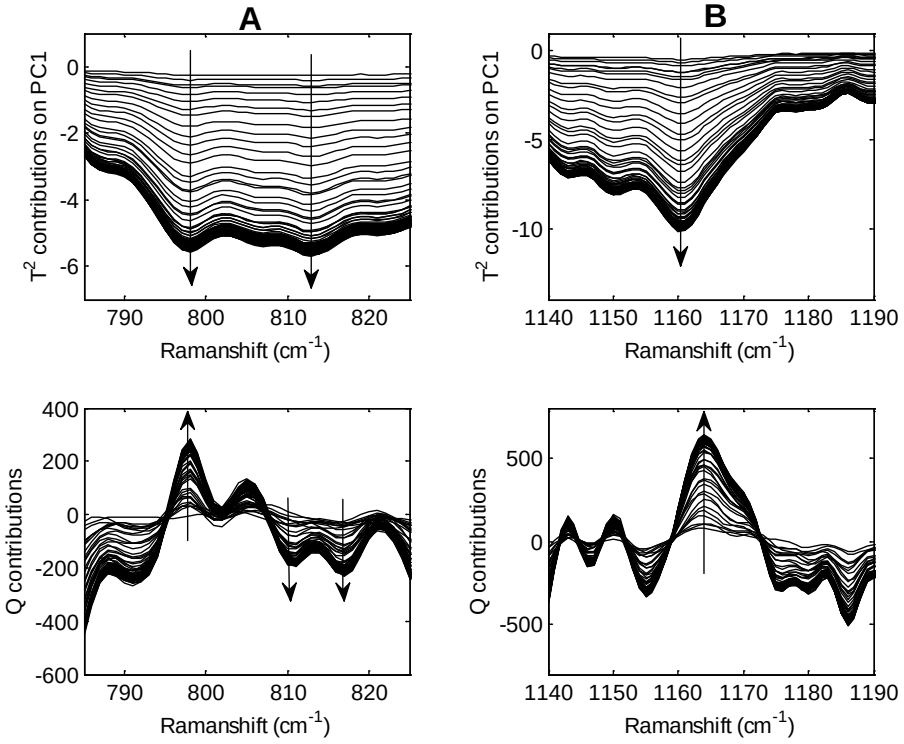

Figure 6.4 Variable contribution plots of T^2 and Q in the selected wavenumber range (**A**) 785–825 cm^{-1} and (**B**) 1140–1190 cm^{-1}.

6.3.2. *Identification of the Rate Controlling Step*

As described earlier in chapter 2, a polymorphic transformation can be controlled by any of the three steps; primary nucleation of the stable form or dissolution of the metastable form or growth of the stable form. This information can be derived by comparing the time profiles of solid and liquid phase composition during the transformation. For this purpose, the time profiles of T^2 and Q were converted into polymorph composition profiles of Form $\mathbf{I}^{\mathbf{L}}$ and Form **II**, respectively. To achieve this, T^2 and Q values were uniformly scaled such that the maximum values of T^2 and Q become

equal to 0% of Form $\mathbf{I}^{\mathbf{L}}$ and 100% of Form **II**, respectively. Fig. 6.5 shows the time profiles of Form $\mathbf{I}^{\mathbf{L}}$ and Form **II** compositions along with the solute concentration profile measured using ATR-FTIR.

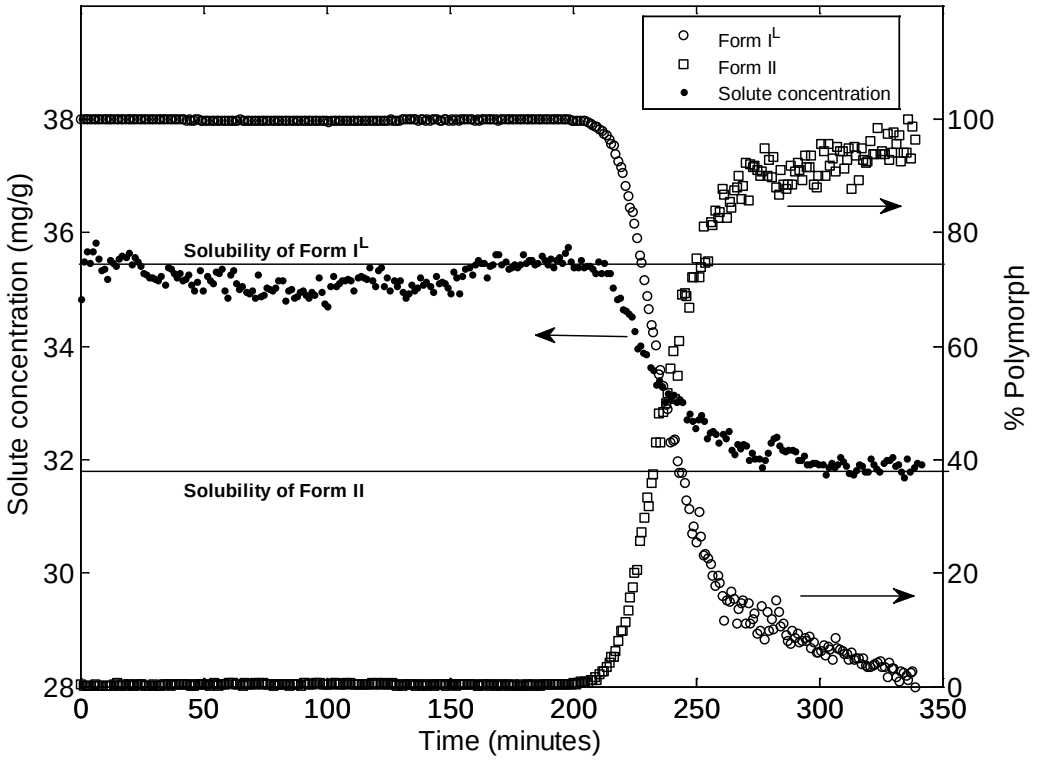

Figure 6.5 Time profiles of solute concentration and polymorph composition of TB during seeded polymorphic transformation at 25 °C in ethanol/water (60:40 w/w) solvent. To get the polymorphic composition, T^2 and Q values were uniformly scaled such that the maximum value equal to 0% Form $\mathbf{I}^{\mathbf{L}}$ and 100% Form **II** respectively.

In Fig. 6.5, during the initial period of 200 min, solute concentration remained at the solubility of Form $\mathbf{I}^{\mathbf{L}}$. This period is the induction time of Form **II** during which solute molecules undergo molecular recognition processes to build Form **II** clusters. Upon reaching the limit, Form **II** nucleates from the solution causing the solute concentration to drop below the solubility of Form $\mathbf{I}^{\mathbf{L}}$. Accordingly, solid composition of Form **II** increases. This simultaneously triggers the dissolution and growth phases of

Form $\mathbf{I}^{\mathbf{L}}$ and **II**, during which solution was supplied with more solute molecules from dissolution of Form $\mathbf{I}^{\mathbf{L}}$, decreasing its solid composition. These molecules are transferred on to the growing Form **II** crystals increasing its solid composition.

During this phase, if the dissolution is faster than growth, solute molecules accumulate and the solute concentration remains closer to the solubility of Form $\mathbf{I}^{\mathbf{L}}$. If the growth is faster than dissolution, solution is depleted out of solute molecules and solute concentration remains closer to the solubility of form **II**. But here neither case happened. The solute concentration continuously decreased after the nucleation of Form **II** indicating that both the dissolution of Form $\mathbf{I}^{\mathbf{L}}$ and growth of Form **II** are equally fast. This phase is continued for another 90 min or so until all the Form $\mathbf{I}^{\mathbf{L}}$ crystals dissolved. By that time, solute concentration has almost reached the solubility of Form **II** and the remaining little supersaturation is quickly consumed by further growth of Form **II** and transformation is ended. This analysis clearly suggests that the rate controlling step for the transformation process is neither the dissolution of Form $\mathbf{I}^{\mathbf{L}}$ nor the growth of Form **II**. It is the primary nucleation of Form **II** which is controlling the transformation.

However, towards the end, the rate of transformation is decreased as evident from the decrease in slope of solid composition profiles. This can be attributed to the morphology of Form **II** crystals which drastically changed the fluid dynamics of the vessel and vessel contents became stagnant towards the end of the transformation. For better evidence, a separate experiment was performed under similar experimental conditions with PVM inserted in the crystallizer to collect slurry images during the polymorphic transformation. Fig. 6.6 shows the PVM images. After 230 min, which corresponds to the initial phase of transformation, the crystals were observed to be freely

floating in the vessel. But, after 270 min i.e. towards the end of transformation, Form **II** crystals filled the entire vessel and vessel contents became stagnant. This could affect the rate of mass transfer and thereby decreasing the rate of transformation.

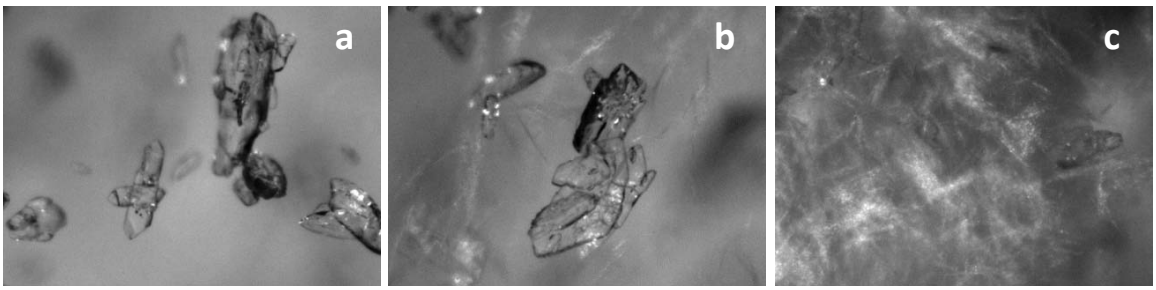

Figure 6.6 PVM images of TB crystals during the seeded polymorphic transformation at 25 °C in ethanol/water (60:40 w/w) solvent (**a**) Seeded Form $\mathbf{I}^{L}$ crystals (**b**) Form **II** nucleated and floating in the crystallizer (**c**) Towards the end of transformation, Form **II** crystals filled the entire vessel and vessel contents became stagnant.

6.4. Metastable Zone Width Measurements.

For MZW measurements, the technique of dynamic PCA based MSPM was combined with Raman to detect the onset of nucleation for a variety of saturated solutions of TB and cooling rates. In these experiments, the exposure time of Raman spectral acquisition was reduced from 5 sec to 2 sec to decrease the sampling period to increase its nucleation detection ability. Moreover, a wider Raman wavenumber range was used spanning 600–1200 cm^{-1} which includes the solvent peaks to account for their sensitivity to nucleation.

6.4.1. *Determination of Nucleation Temperature*

As an illustration, results obtained for an experiment performed at an initial concentration of 109 mg/g solvent corresponding to a saturation temperature of 45 °C and a cooling rate of 0.1 °C/min are shown here. For this experiment, the dynamic PCA

reference model built in the training period resulted in a two component model with PC1 capturing 88.5 % variation and PC2 capturing 2.1 % variation. PC1 can be directly related to the solution phase since the corresponding loadings are similar to the spectral features of solution. Interpretation of PC2 is difficult, possibly another independent variation in the solution phase. In the prediction period, Raman spectra were projected on to the model to estimate T^2 and Q statistics.

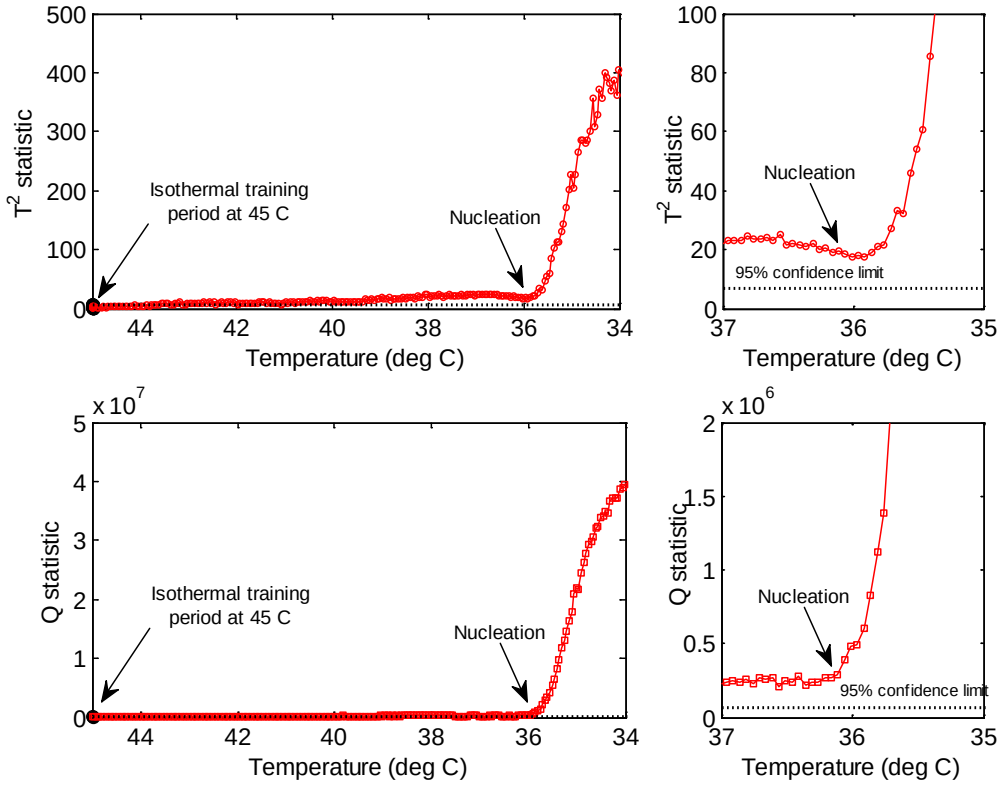

Figure 6.7 T^2 and Q statistic plots of Raman spectra collected in a MZW experiment conducted with an initial concentration of 109 mg/g solvent and 0.1 °C/min cooling rate.

Fig. 6.7 shows the T^2 and Q statistic plot against temperature. Here, T^2 refers to the systematic variation occurring in the solution phase while cooling whereas Q refers to the new variations brought into the process upon generating the supersaturation. Fig. 6.7

suggests that initially, both statistics were within the 95% confidence limit imposed by the model indicating that no variation in the solution. However, T^2 and Q stay only for a short period of time and move out of the limit and keep moving away in a linear fashion. As the nucleation is approached, T^2 sensed the event by a dip in T^2 values followed by a rapid increase. On the other hand, Q statistic senses the event by a higher variation followed by a rapid change.

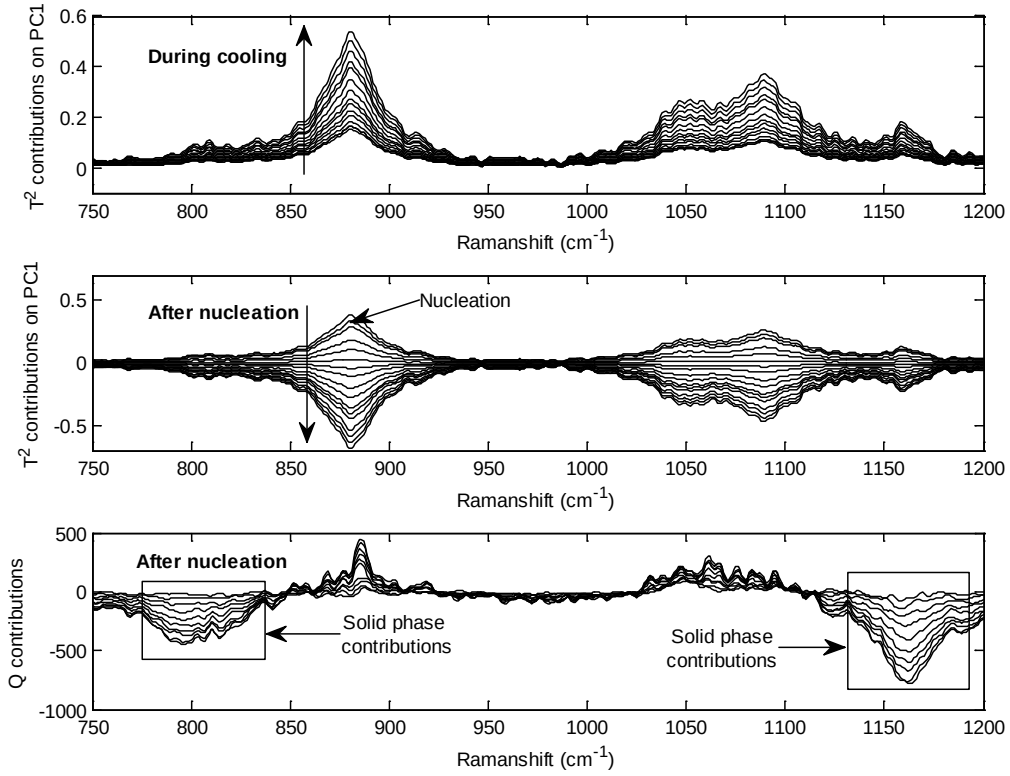

Figure 6.8 T^2 and Q contribution plots of Raman spectra collected in a MZW experiment conducted with an initial concentration of 109 mg/g solvent and 0.1 °C/min cooling rate.

To verify these interpretations related to the sensitivity of T^2 and Q statistics to nucleation phenomena, the T^2 and Q contribution plots are shown in Fig. 6.8. In Fig. 6.8, the major contributions to T^2 value during the cooling are from Raman intensities of solvent peaks (882, 1049 and 1090 cm^{-1}) and solute peak (1161 cm^{-1}) which increased

with time. This explains why T^2 value increased before the nucleation. The increase in Raman intensity can be attributed to the increase in solution density upon cooling due to reduction in volume of the solution (Hu et al., 2005). However, after a while, T^2 contributions suddenly dropped and decreased to zero and then decreased further in the negative region. This variation is reflected in the T^2 value which initially decreased in its value in Fig. 6.7 as the contributions decreased and then increased as the contributions decreased further in the negative region. The sudden decrease in Raman contributions can be attributed to the fact that crystallization tends to reduce Raman intensity because a solution containing crystals is more opaque than the corresponding transparent solution containing molecular clusters prior to formation of crystals. Therefore, it is appropriate to measure the point at which T^2 value showed a dip (this corresponds to the sharp decrease in Raman intensity) as the start of nucleation and the corresponding temperature as the nucleation temperature.

On the other hand, *Q* contributions during cooling are minor and within the noise level, therefore, are not shown here. Possibly, the increase in *Q* value across the limit before the nucleation is due to these minor Raman contributions. However, after the nucleation, Raman contributions were increased as shown in Fig. 6.8. As we can see, the major *Q* contributions are from 785–825 cm^{-1} and 1140–1190 cm^{-1} which are the characteristic regions of TB polymorphs. This explains why *Q* value increased rapidly after nucleation.

Fig. 6.9 provides a comparison of time profiles of a more conventional FBRM measurement during the MZW experiment with Raman based T^2 statistic. FBRM detects the nucleation event by measuring the increase in particle counts. As we can see from

Fig. 6.9, both techniques detected the nucleation event at the same time. However at the point of nucleation, FBRM counts were increased whereas Raman based T^2 statistic decreased due to decrease in Raman scattering because of increase in solution opacity. In detecting the nucleation event, Raman has an additional advantage that it can distinguish the solid nucleated which is discussed in detail in the next section.

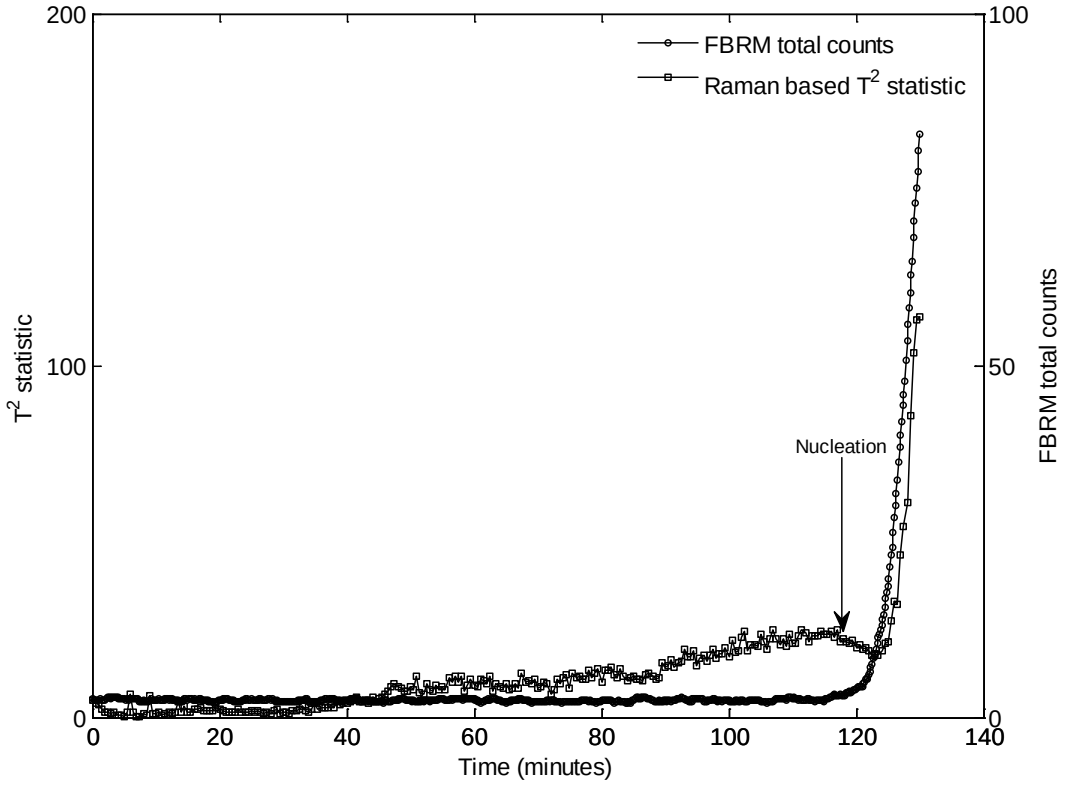

Figure 6.9 Comparison of time profiles of FBRM total counts and Raman based T^2 statistic for detecting the nucleation event in the MZW experiment conducted with initial concentration of 109 mg/g solvent and 0.1 °C/min cooling rate.

6.4.2. *Detection of the Type of Polymorph Nucleated*

To identify the type of polymorph nucleated during the MZW experiments, PXRD measurements were performed. These results suggest that two types of polymorphs of TB (Form $\mathbf{I}^{\mathbf{L}}$ (characteristic PXRD peaks; 12.1° and 13.1°) and Form **III** (characteristic

PXRD peaks; 11.3° and 12.4°)) were crystallized in MZW experiments. Some experiments also resulted in a mixture of these two forms.

However, the polymorphic information can be directly extracted from raw Raman spectra. Moreover, we observed that T^2 and Q contribution plots are more revealing and informative than the corresponding raw Raman spectra as they contain Raman contributions exclusively from the solution and the solid phase. For illustration, three selected MZW experiments (A,B,C) carried out at same initial concentration (109 mg/g solvent) but different cooling rates which resulted in different polymorphic outcome were considered here. The corresponding PXRD patterns were provided in Fig. 6.10. Fig. 6.11 shows a comparison of the raw spectra collected in experiments A, B and C, in the wavenumber range of 1130–1190 cm^{-1}, at the time of nucleation with the corresponding T^2 and Q contribution plots.

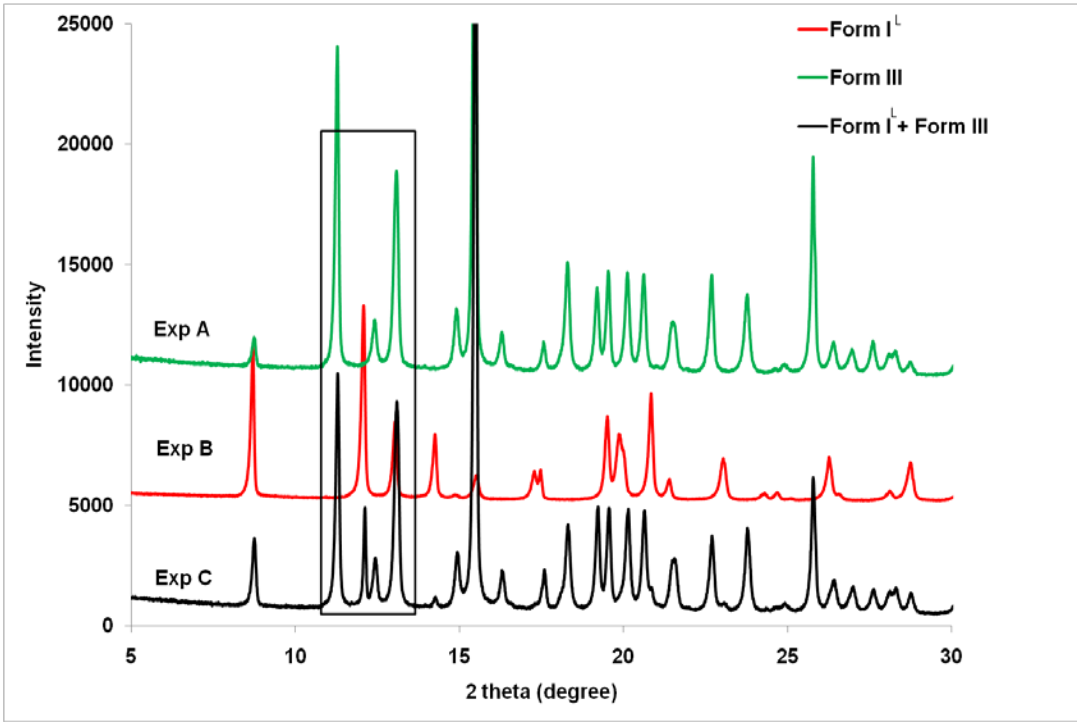

Figure 6.10 Comparison of PXRD patterns obtained for three MZW experiments A, B and C which resulted in different polymorphic outcomes of Form **I^L**, **III** and their mixture, respectively.

Experiment A resulted in the nucleation of Form **III**. In Fig. 6.11, Raman detects the nucleation event by a rapid decrease in intensity at 1161 cm^{-1} which is a characteristic peak of the solute followed by a significant shift in the baseline with two new peaks arising at 1146 and 1163 cm^{-1} which are characteristic of Form **III**. The corresponding T^2 and Q contribution plots clearly decoupled these variations into contributions from solution and Form **III** crystals. A sharp decrease in T^2 contributions from positive to a negative value within a span of one sample interval suggests that the nucleation rate of Form **III** is very high. Contributions to Q value clearly magnified the Raman characteristics of Form **III** which increased as crystals continue to grow facilitating the identification of type of polymorph nucleated.

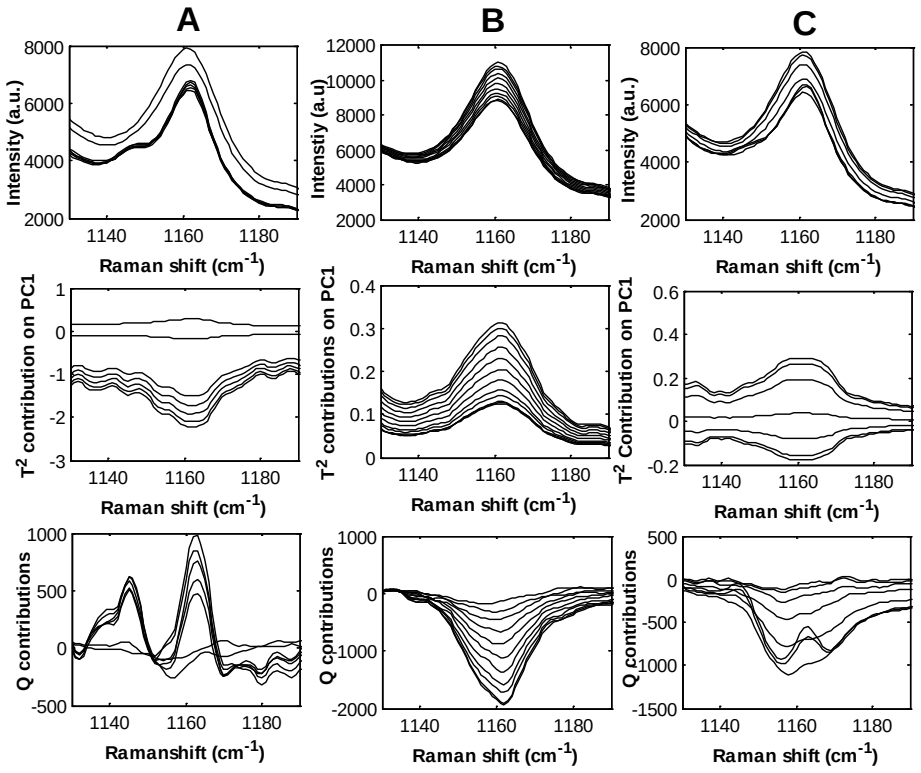

Figure 6.11 Comparison of raw Raman spectra and T^2 and Q contribution plots for three different MZW experiments in which three different polymorphic outcome obtained **(A)** Form **III (B)** Form $\mathbf{I^L}$ **(C)** Form $\mathbf{I^L}$ + Form **III**.

Experiment B resulted in the nucleation of Form $\mathbf{I^L}$. Raman detects the nucleation event by a decrease in intensity at 1161 cm^{-1} which is a characteristic peak of both the solute and Form $\mathbf{I^L}$. Upon nucleation, T^2 contributions were decreased slowly suggesting that the nucleation rate of Form $\mathbf{I^L}$ is low compared to Form **III**. In this case, on the contrary, Q contributions decreased with time suggesting that there are no new contributions to Raman spectra from Form $\mathbf{I^L}$ crystals. Probably, the decrease in Q contributions is due to the continuous shift in baseline as more and more Form $\mathbf{I^L}$ crystals formed which is reflected as a new change in the process upon nucleation. This is typical to Form $\mathbf{I^L}$ and consistently observed whenever Form $\mathbf{I^L}$ nucleated.

Experiment C resulted in the nucleation of a mixture of Form **III** and Form $\mathbf{I^L}$. As we can see, a mixed behavior of experiments A and B was observed in the Raman spectra and the corresponding T^2 and Q contribution plots, suggesting the nucleation of both Forms $\mathbf{I^L}$ and **III**. However, one can clearly see in Q contribution plot, the first nucleated form is Form $\mathbf{I^L}$ followed by the nucleation of Form **III**.

6.4.3. *Crystallization Design Space*

Fig. 6.12 shows the MZW measurements along with the solubility curves measured for TB-ethanol/water system. The corresponding polymorph nucleated was also shown. It should be noted that under the tested experimental conditions, nucleation of Form **II** is not observed. In Fig. 6.12, three domains (D_1, D_2 and D_3) unique to each polymorph can be identified. In domain D_1, sufficiently fast cooling rate and all initial concentrations favored the nucleation of Form **III**. In domain D_2, sufficiently slow cooling rate and all initial concentrations favored the nucleation of Form ($\mathbf{I^L}$, $\mathbf{I^H}$). In

domain D_3, intermediate cooling rates and all initial concentrations favored the nucleation of a mixture of both these forms.

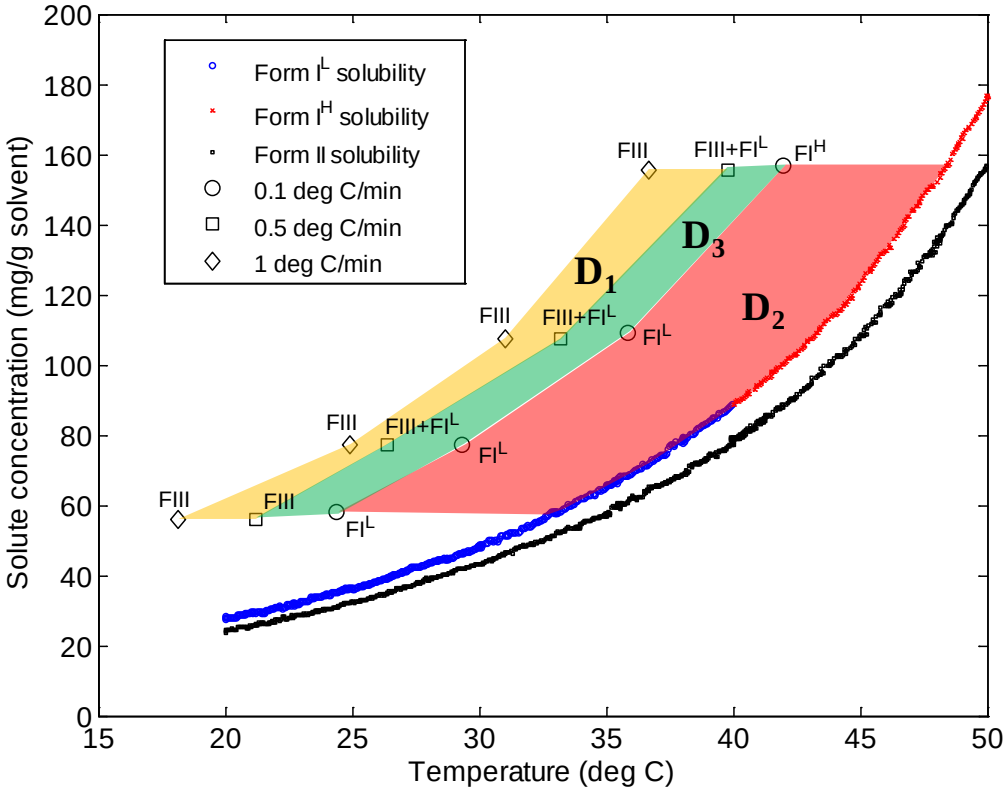

Figure 6.12 Design space for the isolation of Form ($\mathbf{I^L}$, $\mathbf{I^H}$) in terms of its metastability.

Fig. 6.12 suggests that at constant concentration, nucleation energy barrier increases with increase in cooling rate as seen from the increase in MZW. On the other hand, at constant cooling rate, nucleation energy barrier decreases with increase in concentration. CNT suggests that if the energy barrier increases, the nucleation rate (J) increases and vice versa. Therefore, one can expect that the cooling rate and initial concentration have an effect on nucleation kinetics of Forms ($\mathbf{I^L}$, $\mathbf{I^H}$) and **III**. Two important kinetic contributions to nucleation rate are interfacial energy (γ) and preexponential factor (A). Faster cooling rate might have promoted the nucleation of

Form **III** by favoring $J_{III} > J_{I^L}$ with conditions $\gamma_{III} < \gamma_{I^L}$ and $A_{III} > A_{I^L}$. On the other hand, slower cooling rates might have promoted the nucleation of Form (**I**$^{\mathbf{L}}$, **I**$^{\mathbf{H}}$) by favoring $J_{I^L} > J_{III}$ with conditions $\gamma_{I^L} < \gamma_{III}$ and $A_{I^L} > A_{III}$. When intermediate cooling rates were used, the balance of these contributions to nucleation rates of Forms **I**$^{\mathbf{L}}$ and **III** might have favored the condition $J_{I^L} = J_{III}$ and promoted the nucleation of both forms.

Nevertheless, this analysis clearly suggests that the design space for the isolation of desired form of TB is D_2 where primary nucleation of Form (**I**$^{\mathbf{L}}$, **I**$^{\mathbf{H}}$) is guaranteed.

6.5. Design and Operation of Selective Crystallization

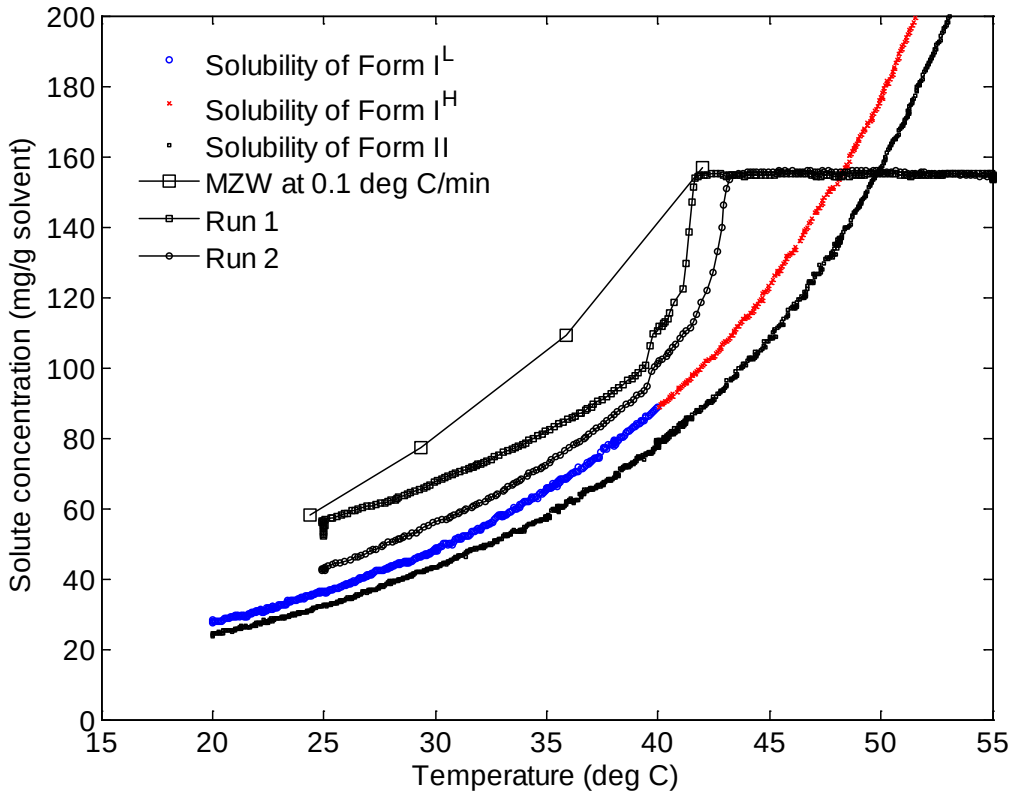

Figure 6.13 Desupersaturation profile measured using ATR-FTIR during batch crystallization while operating in the design space. **Run 1**: 0.08 °C/min cooling rate and 250 rpm stirring rate; **Run 2**: 0.08 °C/min cooling rate and 400 rpm stirring rate.

For selective crystallization, a cooling crystallization process was designed to operate within the design space. However, one possibility which cannot be ignored while operating in the design space is the primary nucleation of more stable Form **II** via SMPT. To prevent any possibility of undesired SMPT to Form **II**, crystallization should be designed such that the total crystallization time (excluding the induction time) should be within the induction period for the nucleation of Form **II** (~200 min). Keeping this in mind, a process was designed with a saturated solution corresponds to a temperature of 50 °C which is cooled at 0.08 °C/min until 25 °C.

Fig. 6.13 shows the desupersaturation profile measured using ATR-FTIR during the crystallization operation for runs 1 and 2. In run 1, a hump in concentration profile in the region of 39–41 °C which is due to the solid state transformation of Form $\mathbf{I^H \rightarrow I^L}$ clearly indicates that the desired form has been achieved. However, as the crystallization proceeds, the stirring rate of 250 rpm was no longer sufficient to keep the growing crystals suspended and the crystals started to settle at the bottom of the crystallizer. Solute concentration would be lower around the crystals as the solute was continually incorporated into the crystals. A concentration gradient thus formed in the crystallizer with the lower concentration at the bottom and higher concentration at the top where the ATR probe was located. Therefore, the desupersaturation profile appeared to steer away from the solubility curve. Run 2 was performed by increasing the stirring rate from 250 to 400 rpm. Now, the drift was suppressed and a desupersaturation profile with decreasing supersaturation was obtained. However, as we can see, increase in stirring rate decreased the MZW. Fig. 6.14 shows the PVM image of crystals obtained. The prismatic morphology typical of Form ($\mathbf{I^L}$, $\mathbf{I^H}$) further confirms that the desired form was achieved.

Hence, a robust crystallization process for the production of the desired form of TB has been successfully demonstrated.

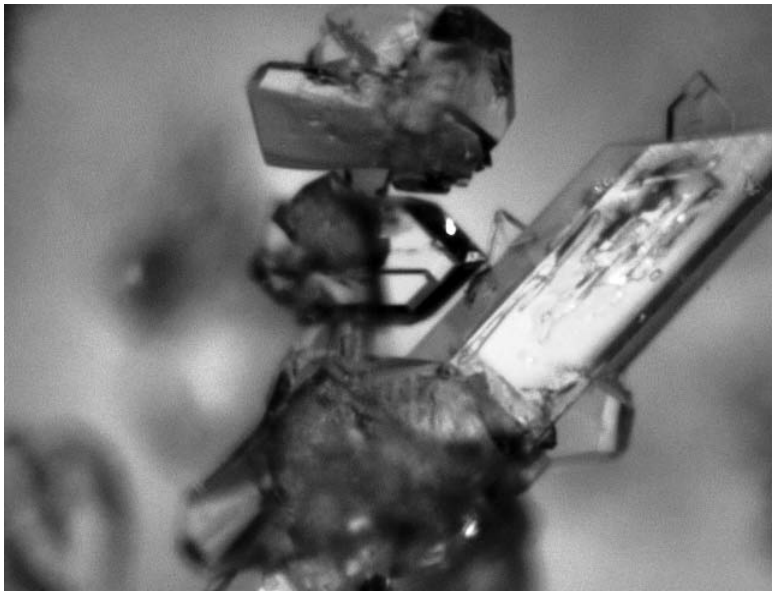

Figure 6.14 PVM image of Form $\mathbf{I^L}$ crystals obtained during batch crystallization operation.

6.6. Summary

A crystallization design space for the isolation of the desired polymorph Form ($\mathbf{I^L}$, $\mathbf{I^H}$) of TB has been determined and a crystallization batch process was operated within the design space to achieve the desired form. QbD based strategy not only assisted in developing a robust process but also provided a good understanding about the crystallization behavior of TB. Characterization of polymorphic transformation of TB polymorphs Form $\mathbf{I^L}\rightarrow$ Form **II** suggests that the primary nucleation of the stable Form **II** is the controlling step for the transformation. MZW measurements indicate that the cooling rate has a strong influence on the nucleation energy barrier and can be used as a manipulator for achieving different TB polymorphs.

This work also demonstrates the application of two PATs, ATR-FTIR combined with OPLS (PCA) and Raman with MSPM in crystallization process characterization and

monitoring. OPLS (PCA) ensures the robustness of the calibration models which is particularly important in industrial environments where process disturbances are not uncommon. MSPM can be combined with Raman and used as a PAT tool for the characterization of polymorphic transformations and nucleation experiments with additional advantage of in situ detection of type of polymorph nucleated. The most appealing part of MSPM is that it is calibration free therefore it can reduce the experimental effort thereby speed up the process development.

CHAPTER 7

CONCLUSIONS AND SCOPE FOR FUTURE WORK

Toward a robust crystallization process development for a specific polymorph, an understanding of the fundamentals of polymorphism and the role of crystallization mechanisms on crystal formation and transformation is essential. With this objective, crystallization of tolbutamide (TB), a polymorphic drug, was investigated in this work. The main findings are briefly reviewed herein.

7.1. Significant Contributions

7.1.1. *Structural Origin of Polymorphism in TB*

The conformational flexibility of the TB molecule and strong hydrogen bonding ability of secondary amide via carbonyl and sulfonyl groups facilitate TB to crystallize into different polymorphic forms (Forms ($\mathbf{I^L}$, $\mathbf{I^H}$) and **II**–**IV**). The rich torsional freedom available for the terminal alkyl chain mainly assists TB molecule to adopt various conformers and crystalline packing arrangements. By elucidating the crystal structures of various polymorphic forms of TB, the present work resolves several discrepancies in the published data on structural features of the polymorphs of this API.

7.1.2. *Stability Aspects of TB Polymorphs*

The relative thermodynamic relationships of TB polymorphic pairs were evaluated and the stability domains were elucidated in the form of a schematic energy-temperature diagram. Form **II** is found to be the thermodynamically stable polymorph from absolute zero to ~353 K and beyond which Form $\mathbf{I^H}$ is the stable polymorph. The discrepancies in the literature related to the relative stability of TB polymorphs at ambient conditions are highlighted and partially resolved.

7.1.3. *Crystallization Process Development for the Isolation of Desired Form of TB*

Using the QbD based strategy, a robust cooling crystallization process was developed for the isolation of desired Form ($\mathbf{I^L}$, $\mathbf{I^H}$) of TB. SMPT study of the desired Form ($\mathbf{I^L}$, $\mathbf{I^H}$) revealed that the primary nucleation of the stable Form **II** is the rate controlling step. MZW measurements indicated that the cooling rate has a significant influence on nucleation energy barrier of TB polymorphs. Using this information, a crystallization design space for the desired polymorph was derived and the process was successfully demonstrated by operating within the design space to achieve the desired polymorph.

7.1.4. *OPLS (PCA) and MSPM in Crystallization Operations*

In the present work, two novel chemometric methods, OPLS (PCA) and MSPM, were applied for crystallization process characterization (solubility, MZW and polymorphic transformation measurements) and monitoring. OPLS (PCA) reduced the model complexity thereby enhanced the model robustness and interpretability which are particularly important when implementing PAT in industrial environments. On the other hand, MSPM is a completely data based and calibration free technique, therefore, significantly reduced the experimental effort and thereby speeding the process development.

7.2. Scope for Future Work

7.2.1. *Raman with MSPM for Polymorph Monitoring and Control during Crystallization*

Present work demonstrates the application of MSPM with Raman spectroscopy for monitoring polymorphic transformations, detection of nucleation and type of polymorph

nucleated during MZW measurements. The same idea can be extended to batch crystallization monitoring and control in which two dynamic PCA models can be separately built, one for undersaturated solution to monitor the polymorph nucleated and one for solid phase to monitor its polymorphic purity and can be integrated with feedback control strategies.

7.2.2. *Quantitative Application of Raman for Polymorph Monitoring using MSPM and OPLS (PCA)*

Quantitative polymorph monitoring using Raman is proved challenging because of the presence of unrelated information in Raman data due to change in particle size, suspension density etc. We believe that MSPM analysis before building quantitative models may facilitate variable selection thereby enhance model performance. For example, in Fig. 6.4 (T^2 and Q contribution plots), choosing Raman wavenumber regions which hold direct relationship with Forms $\mathbf{I}^{\mathbf{L}}$ and **II** i.e. 795–820 and 1160–1175 cm^{-1} may lead to robust models. Furthermore, applying OPLS (PCA) to Raman data lead to simpler models and further improve the model robustness.

7.2.3. *Raman with MSPM – Can be a Powerful Tool for Monitoring Pre-nucleation*

As discussed in chapter 6, Raman based Q contribution plots can monitor variations occurring in supersaturated solutions, therefore, are expected to provide valuable information on pre-nucleation mechanisms. An ultimate control of polymorphic crystallization can be achieved if one can identify these mechanisms and correlate them to predict the polymorph before nucleation. However, a systematic analysis is required before commenting on prediction of polymorphs using Q contribution plots which is part of our future work.

7.2.4. *Fast Track Crystallization Process Development and Scale up*

For any new chemical entity, application of QbD based strategy for crystallization process development requires a thorough screening of process parameters such as solvents, cooling rate etc. and their relationship with polymorphic outcome and transformation is desired. This results in wider design space and gives better regulatory flexibility to industry. To this aim, we believe that the calibration free MSPM can facilitate the process parameter screening and a fast track crystallization process development can be achieved. Furthermore, for process scale up studies, calibration transfer is a significant issue. We believe that OPLS (PCA) can perform better than the conventional PLS models and may facilitate calibration transfer in scale up studies.

References

Accelrys Software Inc. Materials Studio Vesion 4.3. San Diego, CA, USA. (http://accelrys.com/products/datasheets/rplus.pdf).

Aaltonen, J., Alleso, M., Mirza, S., Koradia, V., Gordon, K.C. and Rantanen, J., Solid form screening - a review. *European Journal of Pharmaceutics and Biopharmaceutics* **2009,** 71, (1), 23-37.

Abu Bakar, M.R., Nagy, Z.K. and Rielly, C.D., Seeded batch cooling crystallization with temperature cycling for the control of size uniformity and polymorphic purity of sulfathiazole crystals. *Organic Process Research & Development* **2009,** 13, (6), 1343-1356.

Alleso, M., Van Den Berg, F., Cornett, C., Jorgensen, F.S., Halling-Sorensen, B., De Diego, H.L., Hovgaard, L., Aaltonen, J. and Rantanen, J., Solvent diversity in polymorph screening. *Journal of Pharmaceutical Sciences* **2008,** 97, (6), 2145-2159.

Almarsson, O., Hickey, M.B., Peterson, M.L., Morissette, S.L., Soukasene, S., McNulty, C., Tawa, M., MacPhee, J.M. and Remenar, J.F., High-throughput surveys of crystal form diversity of highly polymorphic pharmaceutical compounds. *Crystal Growth & Design* **2003,** 3, (6), 927-933.

Altomare, A., Giacovazzo, C., Guagliardi, A., Moliterni, A.G.G., Rizzi, R. and Werner, P.E., New techniques for indexing: N-TREOR in EXPO. *Journal of Applied Crystallography* **2000,** 33, 1180-1186.

Altomare, A., Giacovazzo, C., Grazia, A., Moliterni, G. and Rizzi, R., Direct methods optimised for solving crystal structure by powder diffraction data: limits, strategies, and prospects. *Journal of Research of the National Institute of Standards and Technology* **2004,** 109, (1), 125-132.

Alvarez, A.J., Singh, A. and Myerson, A.S., Polymorph screening: comparing a semi-automated approach with a high throughput method. *Crystal Growth & Design* **2009,** 9, (9), 4181-4188.

Amathieu, L. and Boistelle, R., Crystallization kinetics of gypsum from dense suspension of hemihydrate in water. *Journal of Crystal Growth* **1988,** 88, (2), 183-192.

Andersson, C.A., Direct orthogonalization. *Chemometrics and Intelligent Laboratory Systems* **1999,** 47, (1), 51-63.

Anuar, N., Daud, W.R.W., Roberts, K.J., Kamarudin, S.K. and Tasirin, S.M., An examination of the solution chemistry, nucleation kinetics, crystal morphology, and polymorphic behavior of aqueous phase batch crystallized L-isoleucine at the 250 mL scale size. *Crystal Growth & Design* **2009,** 9, (6), 2853-2862.

Anwar, J. and Boateng, P.K., Computer simulation of crystallization from solution. *Journal of the American Chemical Society* **1998,** 120, (37), 9600-9604.

Apperley, D.C., Fletton, R.A., Harris, R.K., Lancaster, R.W., Tavener, S. and Threlfall, T.L., Sulfathiazole polymorphism studied by magic-angle spinning NMR. *Journal of Pharmaceutical Sciences* **1999,** 88, (12), 1275-1280.

Asnani, M., Vyas, K., Bhattacharya, A., Devarakonda, S., Chakraborty, S. and Mukherjee, A.K., Ab initio structure determination of anhydrous sodium alendronate from laboratory powder X-ray diffraction data. *Journal of Pharmaceutical Sciences* **2009,** 98, (6), 2113-2121.

Auer, M.E., Griesser, U.J. and Sawatzki, J., Qualitative and quantitative study of polymorphic forms in drug formulations by near infrared FT-Raman spectroscopy. *Journal of Molecular Structure* **2003,** 661, 307-317.

Barnes, A.F., Hardy, M.J. and Lever, T.J., A review of the applications of thermal methods within the pharmaceutical-industry. *Journal of Thermal Analysis* **1993,** 40, (2), 499-509.

Barrett, M., McNamara, M., Hao, H.X., Barrett, P. and Glennon, B., Supersaturation tracking for the development, optimization and control of crystallization processes. *Chemical Engineering Research & Design* **2010,** 88, (8A), 1108-1119.

Barrett, P. and Glennon, B., Characterizing the metastable zone width and solubility curve using lasentec FBRM and PVM. *Chemical Engineering Research & Design* **2002,** 80, (A7), 799-805.

Barthe, S.C., Grover, M.A. and Rousseau, R.W., Observation of polymorphic change through analysis of FBRM data: Transformation of paracetamol from form II to form I. *Crystal Growth & Design* **2008,** 8, (9), 3316-3322.

Bauer, J., Spanton, S., Henry, R., Quick, J., Dziki, W., Porter, W. and Morris, J., Ritonavir: an extraordinary example of conformational polymorphism. *Pharmaceutical Research* **2001,** 18, (6), 859-866.

Beiny, D.H.M. and Mullin, J.W., Solubilities of higher normal alkanes in m-xylene. *Journal of Chemical and Engineering Data* **1987,** 32, (1), 9-10.

Bennema, P., van Eupen, J., van der Wolf, B.M.A., Los, J.H. and Meekes, H., Solubility of molecular crystals: polymorphism in the light of solubility theory. *International Journal of Pharmaceutics* **2008,** 351, (1-2), 74-91.

Bernstein, J., Davey, R.J. and Henck, J.O., Concomitant polymorphs. *Angewandte Chemie-International Edition* **1999,** 38, (23), 3441-3461.

Bernstein, J., *Polymorphism in Molecular Crystals*. Oxford University Press: New York, 2002.

Bettini, R., Menabeni, R., Tozzi, R., Pranzo, M.B., Pasquali, I., Chierotti, M.R., Gobetto, R. and Pellegrino, L., Didanosine polymorphism in a supercritical antisolvent process. *Journal of Pharmaceutical Sciences* **2009,** 99, (4), 1855-1870.

Bingham, A.L., Hughes, D.S., Hursthouse, M.B., Lancaster, R.W., Tavener, S. and Threlfall, T.L., Over one hundred solvates of sulfathiazole. *Chemical Communications* **2001**, (7), 603-604.

Birch, M., Fussell, S.J., Higginson, P.D., McDowall, N. and Marziano, I., Towards a PAT-based strategy for crystallization development. *Organic Process Research & Development* **2005,** 9, (3), 360-364.

Blagden, N., Davey, R.J., Lieberman, H.F., Williams, L., Payne, R., Roberts, R., Rowe, R. and Docherty, R., Crystal chemistry and solvent effects in polymorphic systems - sulfathiazole. *Journal of the Chemical Society-Faraday Transactions* **1998,** 94, (8), 1035-1044.

Blagden, N. and Davey, R.J., Polymorph selection: challenges for the future? *Crystal Growth & Design* **2003,** 3, (6), 873-885.

Bohlin, M., Jones, H. and Black, S., New developments in scale-up and QbD to ensure control over product quality. *American Pharmaceutical Review* **2009**, (November/December).

Borissova, A., Khan, S., Mahmud, T., Roberts, K.J., Andrews, J., Dallin, P., Chen, Z.P. and Morris, J., In situ measurement of solution concentration during the batch cooling crystallization of L-glutamic acid using ATR-FTIR spectroscopy coupled with chemometrics. *Crystal Growth & Design* **2009,** 9, (2), 692-706.

Borka, L. and Haleblian, J.K., Crystal polymorphism of pharmaceuticals. *Acta Pharmaceutica Jugoslavica* **1990,** 40, (1-2), 71-94.

Borka, L., Review on crystal polymorphism of substances in european pharmacopoeia. *Pharmaceutica Acta Helvetiae* **1991,** 66, 16-22.

Boultif, A. and Louer, D., Indexing of powder diffraction patterns for low-symmetry lattices by the successive dichotomy method. *Journal of Applied Crystallography* **1991,** 24, 987-993.

Bragg, W.L., The diffraction of short electromagnetic waves by a crystal. *Proceedings of the Cambridge Philosophical Society* **1913,** 17, 43-57.

Brittain, H.G., Morris, K.R., Bugay, D.E., Thakur, A.B. and Serajuddin, A.T.M., Solid-state NMR and IR for the analysis of pharmaceutical solids - polymorphs of fosinopril sodium. *Journal of Pharmaceutical and Biomedical Analysis* **1993,** 11, (11-12), 1063-1069.

Brittain, H.G., Spectral methods for the characterization of polymorphs and solvates. *Journal of Pharmaceutical Sciences* **1997,** 86, (4), 405-412.

Brittain, H.G., Methods for the characterization of polymorphs and solvates. In *Polymorphism in Pharmaceutical Solids*, Brittain, H.G., Ed. Marcel Dekker Inc: New York, 1999; pp 227-278.

Brouwer, D.H., Darton, R.J., Morris, R.E. and Levitt, M.H., A solid-state NMR method for solution of zeolite crystal structures. *Journal of the American Chemical Society* **2005,** 127, (29), 10365-10370.

Buerger, M.J., Crystallographic aspects of phase transformations. In *Phase Transformations in Solids*, Smoluchowski, R. et al., Eds. John Wiley & Sons: New York, 1951; pp 183-211.

Bugay, D.E., Solid-state nuclear-magnetic-resonance spectroscopy - theory and pharmaceutical applications. *Pharmaceutical Research* **1993,** 10, (3), 317-327.

Bugay, D.E., Characterization of the solid-state: spectroscopic techniques. *Advanced Drug Delivery Reviews* **2001,** 48, (1), 43-65.

Burger, A., Zur Polymorphie Oraler Antidiabetika. *Scintia Pharmaceutica* **1975**, (43), 161-168.

Burger, A. and Ramberger, R., Polymorphism of Pharmaceuticals and other Molecular-Crystals .1. Theory of Thermodynamic Rules. *Mikrochimica Acta* **1979,** 2, (3-4), 259-271.

Burger, A. and Ramberger, R., Polymorphism of Pharmaceuticals and Other Molecular-Crystals .2. Applicability of Thermodynamic Rules. *Mikrochimica Acta* **1979,** 2, (3-4), 273-316.

Byrn, S.R., Pfeiffer, R.R., Stephenson, G., Grant, D.J.W. and Gleason, W.B., Solid-state pharmaceutical chemistry. *Chemistry of Materials* **1994,** 6, (8), 1148-1158.

Caillet, A., Puel, F. and Fevotte, G., In-line monitoring of partial and overall solid concentration during solvent-mediated phase transition using Raman spectroscopy. *International Journal of Pharmaceutics* **2006,** 307, (2), 201-208.

Caillet, A., Rivoire, A., Galvan, J.M., Puel, F. and Fevotte, G., Crystallization of monohydrate citric acid. 1. In situ monitoring through the joint use of Raman spectroscopy and image analysis. *Crystal Growth & Design* **2007,** 7, 2080-2087.

Canotilho, J., Costa, F.S., Sousa, A.T., Redinha, J.S. and Leitao, M.L.P., Calorimetric study of polymorphic forms of terfenadine. *Thermochimica Acta* **1997,** 299, (1-2), 1-6.

Cardew, P.T. and Davey, R.J., The kinetics of solvent-mediated phase-transformations. *Proceedings of the Royal Society of London Series a-Mathematical Physical and Engineering Sciences* **1985,** 398, (1815), 415-428.

Carteret, C., Dandeu, A., Moussaoui, S., Muhr, H., Humbert, B. and Plasari, E., Polymorphism studied by lattice phonon Raman spectroscopy and statistical mixture analysis method-application to calcium carbonate polymorphs during batch crystallization. *Crystal Growth & Design* **2009,** 9, (2), 807-812.

Chaleepa, K., Szepes, A. and Ulrich, J., Metastable zone determination of lipid systems: Ultrasound velocity versus optical back-reflectance measurements. *European Journal of Lipid Science and Technology* **2010,** 112, (5), 565-573.

Chalmers, J.M. and Dent, G., Vibrational spectroscopic methods in pharmaceutical solid-state characterization. In *Polymorphism in Pharmaceutical Industry*, Hilfiker, R., Ed. Wiley-VCH: Germany, 2006; pp 95-136.

Cheetham, A.K. and Wilkinson, A.P., Structure determination and refinement with synchrotron X-ray-powder diffraction data. *Journal of Physics and Chemistry of Solids* **1991,** 52, (10), 1199-1208.

Chemburkar, S.R., Bauer, J., Deming, K., Spiwek, H., Patel, K., Morris, J., Henry, R., Spanton, S., Dziki, W., Porter, W., Quick, J., Bauer, P., Donaubauer, J., Narayanan, B.A., Soldani, M., Riley, D. and McFarland, K., Dealing with the impact of ritonavir polymorphs on the late stages of bulk drug process development. *Organic Process Research & Development* **2000,** 4, (5), 413-417.

Chen, J., Patience, D.B., Falco, N. and Pachera, R., Using in situ Raman for improved process understanding in development of a crystallization process. *American Pharmaceutical Review* **2009**, (April).

Chen, Z.P., Fevotte, G., Caillet, A., Littlejohn, D. and Morris, J., Advanced calibration strategy for in situ quantitative monitoring of phase transition processes in suspensions using FT-Raman spectroscopy. *Analytical Chemistry* **2008,** 80, (17), 6658-6665.

Clas, S.D., Dalton, C.R. and Hancock, B.C., Differential scanning calorimetry: applications in drug development. *Pharmaceutical Science & Technology Today* **1999,** 2, (8), 311-320.

Colthup, N.B., Daly, L.H. and Wiberley, S.E., *Introduction to Infrared and Raman Spectroscopy*. Academic Press Inc: California, 1990.

Cornel, J., Lindenberg, C. and Mazzotti, M., Quantitative application of in situ ATR-FTIR and Raman spectroscopy in crystallization processes. *Industrial & Engineering Chemistry Research* **2008,** 47, (14), 4870-4882.

Craig, D.Q.M., Characterization of polymorphic systems using thermal analysis. In *Polymorphism in the Pharmaceutical Industry*, Hilfiker, R., Ed. Germany: Wiley-VCH: 2006; pp 43 - 77.

Croker, D. and Hodnett, B.K., Mechanistic features of polymorphic transformations: the role of surfaces. *Crystal Growth & Design* **2010,** 10, (6), 2806-2816.

Cross, W.I., Blagden, N., Davey, R.J., Pritchard, R.G., Neumann, M.A., Roberts, R.J. and Rowe, R.C., A whole output strategy for polymorph screening: combining crystal structure prediction, graph set analysis, and targeted crystallization experiments in the case of diflunisal. *Crystal Growth & Design* **2003,** 3, (2), 151-158.

Cruickshank, D.W.J., The analysis of the anisotropic thermal motion of molecules in crystals. *Acta Crystallographica* **1956,** 9, (8), 754-756.

Cui, Y., A material science perspective of pharmaceutical solids. *International Journal of Pharmaceutics* **2007,** 339, (1-2), 3-18.

Dang, L.P., Yang, H.Y., Black, S. and Wei, H.Y., The effect of temperature and solvent composition on transformation of beta- to alpha-glycine as monitored in situ by FBRM and PVM. *Organic Process Research & Development* **2009,** 13, (6), 1301-1306.

Datta, S. and Grant, D.J.W., Crystal structures of drugs: advances in determination, prediction and engineering. *Nature Reviews Drug Discovery* **2004,** 3, (1), 42-57.

Davey, R. and Garside, J., *From molecules to crystallizers - an introduction to crystallization*. UK: Oxford Science 2000.

Davey, R.J. and Richards, J., A solvent mediated phase-transformation in an aqueous suspension of an azo disperse dye. *Journal of Crystal Growth* **1985,** 71, (3), 597-601.

Davey, R.J., Guy, P.D. and Ruddick, A.J., The IV-III polymorphic phase-transition in aqueous slurries of ammonium-nitrate. *Journal of Colloid and Interface Science* **1985,** 108, (1), 189-192.

Davey, R.J., Cardew, P.T., McEwan, D. and Sadler, D.E., Rate controlling processes in solvent-mediated phase-transformations. *Journal of Crystal Growth* **1986,** 79, (1-3), 648-653.

Davey, R.J., Blagden, N., Potts, G.D. and Docherty, R., Polymorphism in molecular crystals: stabilization of a metastable form by conformational mimicry. *Journal of the American Chemical Society* **1997,** 119, (7), 1767-1772.

Davey, R.J., Pizzas, polymorphs and pills. *Chemical Communications* **2003**, (13), 1463-1467.

Davey, R.J., Dent, G., Mughal, R.K. and Parveen, S., Concerning the relationship between structural and growth synthons in crystal nucleation: Solution and crystal chemistry of carboxylic acids as revealed through IR spectroscopy. *Crystal Growth & Design* **2006,** 6, (8), 1788-1796.

Day, G.M., Trask, A.V., Motherwell, W.D.S. and Jones, W., Investigating the latent polymorphism of maleic acid. *Chemical Communications* **2006**, (1), 54-56.

Desikan, S., Parsons, R.L., Davis, W.P., Ward, J.E., Marshall, W.J. and Toma, P.H., Process development challenges to accommodate a late-appearing stable polymorph: a case study on the polymorphism and crystallization of a fast-track drug development compound. *Organic Process Research & Development* **2005,** 9, (6), 933-942.

Doherty, C. and York, P., Frusemide crystal forms - solid-state and physicochemical analyses. *International Journal of Pharmaceutics* **1988,** 47, (1-3), 141-155.

Doki, N., Seki, H., Takano, K., Asatani, H., Yokota, M. and Kubota, N., Process control of seeded batch cooling crystallization of the metastable alpha-form glycine using an in-situ ATR-FTIR spectrometer and an in-situ FBRM particle counter. *Crystal Growth & Design* **2004,** 4, (5), 949-953.

Dollase, W.A., Correction of intensities for preferred orientation in powder diffractometry - application of the march model. *Journal of Applied Crystallography* **1986,** 19, 267-272.

Donaldson, J.D., Leary, J.R., Ross, S.D., Thomas, M.J.K. and Smith, C.H., The structure of the orthorhombic form of tolbutamide (1-N-Butyl-3-P-Toluenesulfonylurea). *Acta Crystallographica Section B-Structural Science* **1981,** 37, (DEC), 2245-2248.

Dressler, D.H. and Mastai, Y., Controlling polymorphism by crystallization on self-assembled multilayers. *Crystal Growth & Design* **2007,** 7, (5), 847-850.

Dunitz, J.D. and Bernstein, J., Disappearing Polymorphs. *Accounts of Chemical Research* **1995,** 28, (4), 193-200.

Dunitz, J.D., Phase changes and chemical reactions in molecular crystals. *Acta Crystallographica Section B-Structural Science* **1995,** 51, 619-631.

Dunuwila, D.D., Carroll, L.B. and Berglund, K.A., An investigation of the applicability of attenuated total-reflection infrared-spectroscopy for measurement of solubility and supersaturation of aqueous citric-acid solutions. *Journal of Crystal Growth* **1994,** 137, (3-4), 561-568.

Dunuwila, D.D. and Berglund, K.A., ATR-FTIR spectroscopy for in situ measurement of supersaturation. *Journal of Crystal Growth* **1997,** 179, (1-2), 185-193.

Engel, G.E., Wilke, S., Konig, O., Harris, K.D.M. and Leusen, F.J.J., PowderSolve - a complete package for crystal structure solution from powder diffraction patterns. *Journal of Applied Crystallography* **1999,** 32, 1169-1179.

Etter, M.C., Jahn, D.A. and Donahue, B.S., Growth and characterization of small molecule organic-crystals. *Journal of Crystal Growth* **1986,** 76, (3), 645-655.

Etter, M.C. and Baures, P.W., Triphenylphosphine oxide as a crystallization aid. *Journal of the American Chemical Society* **1988,** 110, (2), 639-640.

Etter, M.C., Hydrogen-bonds as design elements in organic-chemistry. *Journal of Physical Chemistry* **1991,** 95, (12), 4601-4610.

Fabbiani, F.P.A., Allan, D.R., David, W.I.F., Davidson, A.J., Lennie, A.R., Parsons, S., Pulham, C.R. and Warren, J.E., High-pressure studies of pharmaceuticals: an exploration of the behavior of piracetam. *Crystal Growth & Design* **2007,** 7, (6), 1115-1124.

Fearn, T., On orthogonal signal correction. *Chemometrics and Intelligent Laboratory Systems* **2000,** 50, (1), 47-52.

Ferrari, E.S., Davey, R.J., Cross, W.I., Gillon, A.L. and Towler, C.S., Crystallization in polymorphic systems: The solution-mediated transformation beta to alpha glycine. *Crystal Growth & Design* **2003,** 3, (1), 53-60.

Feudale, R.N., Tan, H.W. and Brown, S.D., Piecewise orthogonal signal correction. *Chemometrics and Intelligent Laboratory Systems* **2002,** 63, (2), 129-138.

Feundale, R.N., Woody, N.A., Tan, H.W., Myles, A.J., Brown, S.D. and Ferre, J., Transfer of multivariate calibration models: a review. *Chemometrics and Intelligent Laboratory Systems* **2002,** 64, (2), 181-192.

Fevotte, G., Calas, J., Puel, F. and Hoff, C., Applications of NIR spectroscopy to monitoring and analyzing the solid state during industrial crystallization processes. *International Journal of Pharmaceutics* **2004,** 273, (1-2), 159-169.

Fevotte, G., In situ Raman spectroscopy for in-line control of pharmaceutical crystallization and solids elaboration processes: a review. *Chemical Engineering Research & Design* **2007,** 85, (A7), 906-920.

Findlay, W.P. and Bugay, D.E., Utilization of fourier transform Raman spectroscopy for the study of pharmaceutical crystal forms. *Journal of Pharmaceutical and Biomedical Analysis* **1998,** 16, (6), 921-930.

Florence, A.J., Johnston, A., Price, S.L., Nowell, H., Kennedy, A.R. and Shankland, N., An automated parallel crystallisation search for predicted crystal structures and packing motifs of carbamazepine. *Journal of Pharmaceutical Sciences* **2006,** 95, (9), 1918-1930.

Fujiwara, M., Chow, P.S., Ma, D.L. and Braatz, R.D., Paracetamol crystallization using laser backscattering and ATR-FTIR spectroscopy: Metastability, agglomeration, and control. *Crystal Growth & Design* **2002,** 2, (5), 363-370.

Gao, P., Characterization of three crystalline forms (VIII, XI, and XII) and the amorphous form (V) of delavirdine mesylate using C-13 CP/MAS NMR. *Pharmaceutical Research* **1998,** 15, (9), 1425-1433.

Garcia, E., Hoff, C. and Veesler, S., Dissolution and phase transition of pharmaceutical compounds. *Journal of Crystal Growth* **2002,** 237, 2233-2239.

Garside, J., Mersmann, A. and Nyvlt, J., *Measurement of crystal growth and nucleation rates*. Institution of Chemical Engineers Rugby, UK, 2002.

Gavezzotti, A., Quantitative ranking of crystal packing modes by systematic calculations on potential energies and vibrational amplitudes of molecular dimers. *Journal of Chemical Theory and Computation* **2005,** 1, (5), 834-840.

George, S., Nangia, A., Lam, C.K., Mak, T.C.W. and Nicoud, J.F., Crystal engineering of urea a-network via I center dot center dot center dot O2N synthon and design of SHG active crystal N-4-iodopheny-N '-4 '-N '-nitrophenylurea. *Chemical Communications* **2004**, (10), 1202-1203.

Geppi, M., Mollica, G., Borsacchi, S. and Veracini, C.A., Solid-state NMR studies of pharmaceutical systems. *Applied Spectroscopy Reviews* **2008,** 43, (3), 202-302.

Gerson, A.R., Roberts, K.J. and Sherwood, J.N., An instrument for the examination of nucleation from solution and its application to the study of precipitation from diesel fuels and solutions of normal-alkanes. *Powder Technology* **1991,** 65, (1-3), 243-249.

Gibbs, J.W., *Collected works, Vol. I, Thermodynamics*. Yale University Press, New Haven,USA: 1948.

Giron, D., Thermal-analysis and calorimetric methods in the characterization of polymorphs and solvates. *Thermochimica Acta* **1995,** 248, 1-59.

Giron, D., Applications of thermal analysis and coupled techniques in pharmaceutical industry. *Journal of Thermal Analysis and Calorimetry* **2002,** 68, (2), 335-357.

Giron, D., Mutz, M. and Garnier, S., Solid-state of pharmaceutical compounds - impact of the ICH Q6 guideline on industrial development. *Journal of Thermal Analysis and Calorimetry* **2004,** 77, (2), 709-747.

Giron, D., Polymorphism: thermodynamic and kinetic factors to be considered in chemical development - part 1. *American Pharmaceutical Review* **2005**, (July/August).

Glusker, J.P., Lewis, M. and Rossi, M., *Crystal Structure Analysis for Chemists and Biologists*. Wiley-VCH Inc.: 1994.

Grant, D.J.W., Theory and origin of polymorphism. In *Polymorphism in pharmaceutical solids*, Brittain, H.G., Ed. Macel Dekker Inc: New York, 1999; pp 1-33.

Grunenberg, A., Henck, J.O. and Siesler, H.W., Theoretical derivation and practical application of energy temperature diagrams as an instrument in preformulation studies of polymorphic drug substances. *International Journal of Pharmaceutics* **1996,** 129, (1-2), 147-158.

Gu, C.H. and Grant, D.J.W., Estimating the relative stability of polymorphs and hydrates from heats of solution and solubility data. *Journal of Pharmaceutical Sciences* **2001,** 90, (9), 1277-1287.

Gu, C.H., Young, V. and Grant, D.J.W., Polymorph screening: influence of solvents on the rate of solvent-mediated polymorphic transformation. *Journal of Pharmaceutical Sciences* **2001,** 90, (11), 1878-1890.

Gu, C.H., Li, H., Gandhi, R.B. and Raghavan, K., Grouping solvents by statistical analysis of solvent property parameters: implication to polymorph screening. *International Journal of Pharmaceutics* **2004,** 283, (1-2), 117-125.

Guillory, J.K., Generation of polymorphs, hydrates, solvates and amorphous solids. In *Polymorphism in pharmaceutical solids*, Brittain, H.G., Ed. Marcel Dekker, Inc., NY: 1997; pp 183-226.

Gurden, S.P., Westerhuis, J.A. and Smilde, A.K., Monitoring of batch processes using spectroscopy. *Aiche Journal* **2002,** 48, (10), 2283-2297.

Gutwald, T. and Mersmann, A., Batch cooling crystallization at constant supersaturation: technique and experimental results. *Chemical Engineering & Technology* **1990,** 13, 229-237.

Haisa, M., Kashino, S. and Maeda, H., Orthorhombic form of para-hydroxyacetanilide. *Acta Crystallographica Section B-Structural Science* **1974,** B 30, (OCT15), 2510-2512.

Harris, K.D.M., Tremayne, M., Lightfoot, P. and Bruce, P.G., Crystal-structure determination from powder diffraction data by monte-carlo methods. *Journal of the American Chemical Society* **1994,** 116, (8), 3543-3547.

Harris, K.D.M., Tremayne, M. and Kariuki, B.M., Contemporary advances in the use of powder X-ray diffraction for structure determination. *Angewandte Chemie-International Edition* **2001,** 40, (9), 1626-1651.

Harris, K.D.M., Johnston, R.L., Cheung, E.Y., Turner, G.W., Habershon, S., Albesa-Jove, D., Tedesco, E. and Kariuki, B.M., Recent advances in opportunities for solving molecular crystal structures directly from powder diffraction data: new insights in crystal engineering contexts. *Crystengcomm* **2002**, 356-367.

Harris, K.D.M. and Cheung, E.Y., How to determine structures when single crystals cannot be grown: opportunities for structure determination of molecular materials using powder diffraction data. *Chemical Society Reviews* **2004,** 33, (8), 526-538.

Harris, R.K., Yeung, R.R., Lamont, R.B., Lancaster, R.W., Lynn, S.M. and Staniforth, S.E., 'Polymorphism' in a novel anti-viral agent: lamivudine. *Journal of the Chemical Society-Perkin Transactions 2* **1997**, (12), 2653-2659.

Harris, R.K., NMR crystallography: the use of chemical shifts. *Solid State Sciences* **2004,** 6, (10), 1025-1037.

Harris, R.K., NMR studies of organic polymorphs & solvates. *Analyst* **2006,** 131, (3), 351-373.

Hasegawa, G., Komasaka, T., Bando, R., Yoshihashi, Y., Yonemochi, E., Fujii, K., Uekusa, H. and Terada, K., Reevaluation of solubility of tolbutamide and polymorphic transformation from Form I to unknown crystal form. *International Journal of Pharmaceutics* **2009,** 369, (1-2), 12-18.

Hastings, J.B., Thomlinson, W. and Cox, D.E., Synchrotron X-ray-powder diffraction. *Journal of Applied Crystallography* **1984,** 17, (APR), 85-95.

He, X.R., Stowell, J.G., Morris, K.R., Pfeiffer, R.R., Li, H., Stahly, G.P. and Byrn, S.R., Stabilization of a metastable polymorph of 4-methyl-2-nitroacetanilide by isomorphic additives. *Crystal Growth & Design* **2001,** 1, (4), 305-312.

Henck, J.O., Griesser, U.J. and Burger, A., Polymorphism of drug substances - an economic challenge. *Pharmazeutische Industrie* **1997,** 59, (2), 165-169.

Henck, J.O., Bernstein, J., Ellern, A. and Boese, R., Disappearing and reappearing polymorphs. The benzocaine : picric acid system. *Journal of the American Chemical Society* **2001,** 123, (9), 1834-1841.

Higuchi, W.I., Lau, P.K., Higuchi, T. and Shell, J.W., Polymorphism and drug availability - solubility relationships in methylprednisolone system. *Journal of Pharmaceutical Sciences* **1963,** 52, (2), 150-&.

Hilfiker, R., De Paul, S.M. and Szelagiewicz, M., Approaches to polymorphism screening. In *Polymorphism in pharmaceutical industry*, Hilfiker, R., Ed. Wiley-VCH: Germany, 2006; pp 287-308.

Hoskuldsson, A., Variable and subset selection in PLS regression. *Chemometrics and Intelligent Laboratory Systems* **2001,** 55, (1-2), 23-38.

Howard, K.S., Nagy, Z.K., Saha, B., Robertson, A.L. and Steele, G., Combined PAT-solid state analytical approach for the detection and study of sodium benzoate hydrate. *Organic Process Research & Development* **2009,** 13, (3), 590-597.

Howard, K.S., Nagy, Z.K., Saha, B., Robertson, A.L., Steele, G. and Martin, D., A process analytical technology based investigation of the polymorphic transformations during the antisolvent crystallization of sodium benzoate from IPA/Water mixture. *Crystal Growth & Design* **2009,** 9, (9), 3964-3975.

Hu, Y.R., Liang, J.K., Myerson, A.S. and Taylor, L.S., Crystallization monitoring by Raman spectroscopy: simultaneous measurement of desupersaturation profile and polymorphic form in flufenamic acid systems. *Industrial & Engineering Chemistry Research* **2005,** 44, (5), 1233-1240.

Hu, Y.R., Wikstrom, H., Byrn, S.R. and Taylor, L.S., Analysis of the effect of particle size on polymorphic quantitation by Raman spectroscopy. *Applied Spectroscopy* **2006,** 60, (9), 977-984.

Hu, Y.R., Wikstrom, H., Byrn, S.R. and Taylor, L.S., Estimation of the transition temperature for an enantiotropic polymorphic system from the transformation

kinetics monitored using Raman spectroscopy. *Journal of Pharmaceutical and Biomedical Analysis* **2007,** 45, (4), 546-551.

Huang, L.F. and Tong, W.Q., Impact of solid state properties on developability assessment of drug candidates. *Advanced Drug Delivery Reviews* **2004,** 56, (3), 321-334.

Hulme, A.T., Johnston, A., Florence, A.J., Fernandes, P., Shankland, K., Bedford, C.T., Welch, G.W.A., Sadiq, G., Haynes, D.A., Motherwell, W.D.S., Tocher, D.A. and Price, S.L., Search for a predicted hydrogen bonding motif - A multidisciplinary investigation into the polymorphism of 3-azabicyclo[3.3.1]nonane-2,4-dione. *Journal of the American Chemical Society* **2007,** 129, (12), 3649-3657.

Jenkins, R. and Gilfrich, J.V., Figures-of-merit, their philosophy, design and use. *X-Ray Spectrometry* **1992,** 21, (6), 263-269.

Kariuki, B.M., Belmonte, S.A., McMahon, M.I., Johnston, R.L., Harris, K.D.M. and Nelmes, R.J., A new approach for indexing powder diffraction data based on whole-profile fitting and global optimization using a genetic algorithm. *Journal of Synchrotron Radiation* **1999,** 6, 87-92.

Kashchiev, D. and van Rosmalen, G.M., Review: nucleation in solutions revisited. *Crystal Research and Technology* **2003,** 38, (7-8), 555-574.

Kawakami, K., Reversibility of enantiotropically related polymorphic transformations from a practical viewpoint: thermal analysis of kinetically reversible/irreversible polymorphic transformations. *Journal of Pharmaceutical Sciences* **2007,** 96, (5), 982-989.

Kee, N.C.S., Tan, R.B.H. and Braatz, R.D., Selective crystallization of the metastable alpha-form of L-glutamic acid using concentration feedback control. *Crystal Growth & Design* **2009a,** 9, (7), 3044-3051.

Kee, N.C.S., Arendt, P.D., Tan, R.B.H. and Braatz, R.D., Selective crystallization of the metastable anhydrate form in the enantiotropic pseudo-dimorph system of L-phenylalanine using concentration feedback control. *Crystal Growth & Design* **2009b,** 9, (7), 3052-3061.

Kim, B.H., Ahn, M.K. and Hwang, G.T., Hydrogen bonding patterns in sulfonyl ureas: Pattern dependence on the nature of amine substituent. *Bulletin of Korean Chemical Society* **1999,** 20, (3), 273-275.

Kim, K.J. and Mersmann, A., Estimation of metastable zone width in different nucleation processes. *Chemical Engineering Science* **2001,** 56, (7), 2315-2324.

Kimura, K., Hirayama, F. and Uekama, K., Characterization of tolbutamide polymorphs (Burger's forms II and IV) and polymorphic transition behavior. *Journal of Pharmaceutical Sciences* **1999,** 88, (4), 385-391.

Kitamura, M., Polymorphism in the crystallization of L-glutamic acid. *Journal of Crystal Growth* **1989,** 96, (3), 541-546.

Kitamura, M., Crystallization behavior and transformation kinetics of L-histidine polymorphs. *Journal of Chemical Engineering of Japan* **1993,** 26, (3), 303-307.

Kitamura, M., Hara, T. and Takimoto-Kamimura, M., Solvent effect on polymorphism in crystallization of BPT propyl ester. *Crystal Growth & Design* **2006,** 6, (8), 1945-1950.

Klimakow, M., Leiterer, J., Kneipp, J., Rossler, E., Panne, U., Rademann, K. and Emmerling, F., Combined synchrotron XRD/Raman measurements: in situ

identification of polymorphic transitions during crystallization processes. *Langmuir* **2010,** 26, (13), 11233-11237.

Knudsen, K.D., Pattison, P., Fitch, A.N. and Cernik, R.J., Solution of the crystal and molecular structure of complex low-symmetry organic compounds with powder diffraction techniques: fluorescein diacetate. *Angewandte Chemie-International Edition* **1998,** 37, (17), 2340-2343.

Kourti, T., Application of latent variable methods to process control and multivariate statistical process control in industry. *International Journal of Adaptive Control and Signal Processing* **2005,** 19, (4), 213-246.

Kubota, N., A new interpretation of metastable zone widths measured for unseeded solutions. *Journal of Crystal Growth* **2008,** 310, (3), 629-634.

Kuhnert-Brandstatter, M. and Wunsch, S., Polymorphism and mixed crystal formation among sulfonamides and related compounds. *Mikrochimica Acta* **1969**, (6), 1297-&.

Kuhnert-Brandstatter, M., *Thermomicroscopy in the Analysis of Pharmaceuticals*. Pergamon, Oxford: 1971.

Kulkarni, G.U., Kumaradhas, P. and Rao, C.N.R., Charge density study of the polymorphs of p-nitrophenol. *Chemistry of Materials* **1998,** 10, (11), 3498-3505.

Laue, M.V., Eine Quantitative prufung der theorie fur die interferenz-eracheinungen bei rontgenstrahlen. *Sitz.Math.Phys.Klasse Bayer. Akad. Wiss.* **1912**, 363-373.

Leary, J.R., Ross, S.D. and Thomas, M.J.K., On the characterization of the polymorphs of tolbutamide. *Pharmaceutisch Weekblad-Scientific Edition* **1981,** 3, (2), 62-66.

Lewiner, F., Klein, J.P., Puel, F. and Fevotte, G., On-line ATR FTIR measurement of supersaturation during solution crystallization processes. Calibration and applications on three solute/solvent systems. *Chemical Engineering Science* **2001,** 56, (6), 2069-2084.

Lewis, T.C., Tocher, D.A., Day, G.M. and Price, S.L., A computational and experimental search for polymorphs of parabanic acid - a salutary tale leading to the crystal structure of oxo-ureido-acetic acid methyl ester. *Crystengcomm* **2003**, 3-9.

Lin, S.W., Ng, K.M. and Wibowo, C., Integrative approach for polymorphic crystallization process synthesis. *Industrial & Engineering Chemistry Research* **2007,** 46, (2), 518-529.

Liotta, V. and Sabesan, V., Monitoring and feedback control of supersaturation using ATR-FTIR to produce an active pharmaceutical ingredient of a desired crystal size. *Organic Process Research & Development* **2004,** 8, (3), 488-494.

Liu, W.J., Wei, H.Y. and Black, S., An investigation of the transformation of carbamazepine from anhydrate to hydrate using in situ FBRM and PVM. *Organic Process Research & Development* **2009,** 13, (3), 494-500.

Llinas, A. and Goodman, J.M., Polymorph control: past, present and future. *Drug Discovery Today* **2008,** 13, (5-6), 198-210.

Lohani, S. and Grant, D.J.W., Thermodynamics of polymorphs. In *Polymorphism in Pharmaceutical Industry*, Hilfiker, R., Ed. Wiley-VCH, Germany: 2006; pp 21-42.

Lu, J., Wang, X.J., Yang, X. and Ching, C.B., Polymorphism and crystallization of famotidine. *Crystal Growth & Design* **2007,** 7, (9), 1590-1598.

Lu, J. and Rohani, S., Polymorphic crystallization and transformation of the anti-viral/HIV drug stavudine. *Organic Process Research & Development* **2009,** 13, (6), 1262-1268.

Lyczko, N., Espitalier, F., Louisnard, O. and Schwartzentruber, J., Effect of ultrasound on the induction time and the metastable zone widths of potassium sulphate. *Chemical Engineering Journal* **2002,** 86, (3), 233-241.

Mangin, D., Puel, F. and Veesler, S., Polymorphism in processes of crystallization in solution: a practical review. *Organic Process Research & Development* **2009,** 13, (6), 1241-1253.

Marciniak, B., Density and ultrasonic velocity of undersaturated and supersaturated solutions of fluoranthene in trichloroethylene, and study of their metastable zone width. *Journal of Crystal Growth* **2002,** 236, (1-3), 347-356.

Maruyama, S., Ooshima, H. and Kato, J., Crystal structures and solvent-mediated transformation of taltireline polymorphs. *Chemical Engineering Journal* **1999,** 75, (3), 193-200.

Masuda, K., Tabata, S., Kono, H., Sakata, Y., Hayase, T., Yonemochi, E. and Terada, K., Solid-state C-13 NMR study of indomethacin polymorphism. *International Journal of Pharmaceutics* **2006,** 318, (1-2), 146-153.

Materazzi, S. and Curini, R., The coupling of mass spectrometry with thermoanalytical instruments: applications of evolved gas analysis. *Applied Spectroscopy Reviews* **2001,** 36, (2-3), 169-180.

Materazzi, S. and Curini, R., On-line evolved gas analysis by infrared spectroscopy coupled to thermoanalytical instruments. *Applied Spectroscopy Reviews* **2001,** 36, (1), 1-9.

McCabe, J.F., Application of design of experiment (DOE) to polymorph screening and subsequent data analysis. *Crystengcomm* **2010,** 12, (4), 1110-1119.

McCrone, W., *Polymorphism, Physics and Chemistry of Organic Solid State*. Wiley Interscience: New York, 1965; Vol. 2.

McGregor, C. and Bines, E., The use of high-speed differential scanning calorimetry (Hyper-DSC (TM)) in the study of pharmaceutical polymorphs. *International Journal of Pharmaceutics* **2008,** 350, (1-2), 48-52.

McKenzie, P., Kiang, S., Tom, J., Rubin, A.E. and Futran, M., Can pharmaceutical process development become high tech? *Aiche Journal* **2006,** 52, (12), 3990-3994.

Miller, J.M., Collman, B.M., Greene, L.R., Grant, D.J.W. and Blackburn, A.C., Identifying the stable polymorph early in the drug discovery-development process. *Pharmaceutical Development and Technology* **2005,** 10, (2), 291-297.

Mitchell, C.A., Yu, L. and Ward, M.D., Selective nucleation and discovery of organic polymorphs through epitaxy with single crystal substrates. *Journal of the American Chemical Society* **2001,** 123, (44), 10830-10839.

Mitscherlich, E., Sur la relations qui existe entre la forme cristalline et les proportion chimiques. *Annales des Chimie et des Physique* **1820**, (14), 172-190.

Morissette, S.L., Soukasene, S., Levinson, D., Cima, M.J. and Almarsson, O., Elucidation of crystal form diversity of the HIV protease inhibitor ritonavir by high-throughput crystallization. *Proceedings of the National Academy of Sciences of the United States of America* **2003,** 100, (5), 2180-2184.

Morissette, S.L., Almarsson, O., Peterson, M.L., Remenar, J.F., Read, M.J., Lemmo, A.V., Ellis, S., Cima, M.J. and Gardner, C.R., High-throughput crystallization: polymorphs, salts, co-crystals and solvates of pharmaceutical solids. *Advanced Drug Delivery Reviews* **2004,** 56, (3), 275-300.

Muller, M., Meier, U., Wieckhusen, D., Beck, R., Pfeffer-Hennig, S. and Schneeberger, R., Process development strategy to ascertain reproducible API polymorph manufacture. *Crystal Growth & Design* **2006,** 6, (4), 946-954.

Mullin, J.W., *Crystallization*. Butterworth-Heinemann Ltd Oxford, 1993.

Nangia, A., Conformational polymorphism in organic crystals. *Accounts of Chemical Research* **2008,** 41, (5), 595-604.

Nath, N. and Nangia, A., Novel form V of tolbutamide and a high Z' crystal structure of form III. *Crystengcomm* **2011,** 13, 47-51.

Neumann, M.A., X-Cell: a novel indexing algorithm for routine tasks and difficult cases. *Journal of Applied Crystallography* **2003,** 36, 356-365.

Newman, A.W. and Byrn, S.R., Solid-state analysis of the active pharmaceutical ingredient in drug products. *Drug Discovery Today* **2003,** 8, (19), 898-905.

Nirmala, K.A. and Gowda, D.S.S., Structure Determination of Tolbutamide. *Acta Crystallographica Section B-Structural Science* **1981,** 37, (AUG), 1597-1599.

Nomikos, P. and Macgregor, J.F., Multivariate SPC charts for monitoring batch processes. *Technometrics* **1995,** 37, (1), 41-59.

Nyvlt, J., Kinetics of nucleation in solutions. *Journal of Crystal Growth* **1968,** 3, (4), 377-383.

Nyvlt, J., Sohnel, O. and Matuchova, M., *The kinetics of industrial crystallization*. Elsevier, NY: 1985.

O'Sullivan, B., Barrett, P., Hsiao, G., Carr, A. and Glennon, B., In situ monitoring of polymorphic transitions. *Organic Process Research & Development* **2003,** 7, (6), 977-982.

O'Sullivan, B. and Glennon, B., Application of in situ FBRM and ATR-FTIR to the monitoring of the polymorphic transformation of D-mannitol. *Organic Process Research & Development* **2005,** 9, (6), 884-889.

Ono, T., ter Horst, J.H. and Jansens, P.J., Quantitative measurement of the polymorphic transformation of L-glutamic acid using in-situ Raman spectroscopy. *Crystal Growth & Design* **2004,** 4, (3), 465-469.

Ostwald, F.W., Studies on formation and transformation of solid materials. *Zeitschrift fur Physikalische Chemie* **1897,** 22, 289-330.

Owen, H., Welch, M. and Pelletier, M., Raman spectroscopy crystallization analysis method. *United States Patent, US 6,867,858 B2* **2005**.

Oxtoby, D.W., Nucleation of first-order phase transitions. *Accounts of Chemical Research* **1998,** 31, (2), 91-97.

Patlak, M., New weapons to combat an ancient disease: treating diabetes. *Faseb Journal* **2002,** 16, (14).

Payne, R.S., Roberts, R.J., Rowe, R.C. and Docherty, R., Examples of successful crystal structure prediction: polymorphs of primidone and progesterone. *International Journal of Pharmaceutics* **1999,** 177, (2), 231-245.

Pecharsky, V.K. and Zavalij, P.Y., *Fundamentals of Powder Diffraction and Structural Characterization of Materials*. Springer Science: New York, 2003.

Pollanen, K., Hakkinen, A., Reinikainen, S.P., Louhi-Kultanen, M. and Nystrom, L., ATR-FTIR in monitoring of crystallization processes: comparison of indirect and direct OSC methods. *Chemometrics and Intelligent Laboratory Systems* **2005,** 76, (1), 25-35.

Pollanen, K., Hakkinen, A., Reinikainen, S.P., Rantanen, J. and Minkkinen, P., Dynamic PCA-based MSPC charts for nucleation prediction in batch cooling crystallization processes. *Chemometrics and Intelligent Laboratory Systems* **2006,** 84, (1-2), 126-133.

Prashad, M., Sutton, P., Wu, R., Hu, B., Vivelo, J., Carosi, J., Kapa, P. and Liang, J., Process research and development of a MTP inhibitor: another case of disappearing polymorphs upon scale-up. *Organic Process Research & Development* **2010,** 14, (4), 878-882.

Price, S.L., The computational prediction of pharmaceutical crystal structures and polymorphism. *Advanced Drug Delivery Reviews* **2004,** 56, (3), 301-319.

Price, S.L., From crystal structure prediction to polymorph prediction: interpreting the crystal energy landscape. *Physical Chemistry Chemical Physics* **2008,** 10, (15), 1996-2009.

Price, S.L., Computational prediction of organic crystal structures and polymorphism. *International Reviews in Physical Chemistry* **2008,** 27, (3), 541-568.

Prusiner, P. and Sundaralingam, M., Crystal and molecular-structures of 2 polymorphic crystalline forms of virazole (1-beta-D-ribofuranosyl-1,2,4-triazole-3-carboxamide) - new synthetic broad-spectrum antiviral agent. *Acta Crystallographica Section B-Structural Science* **1976,** 32, (FEB15), 419-426.

Qu, H.Y., Louhi-Kultanen, M., Rantanen, J. and Kallas, J., Solvent-mediated phase transformation kinetics of an anhydrate/hydrate system. *Crystal Growth & Design* **2006,** 6, (9), 2053-2060.

Rafilovich, M. and Bernstein, J., Serendipity and four polymorphic structures of benzidine. *Journal of the American Chemical Society* **2006,** 128, (37), 12185-12191.

Raghavan, K., Dwivedi, A., Campbell, G.C., Johnston, E., Levorse, D., McCauley, J. and Hussain, M., A spectroscopic investigation of losartan polymorphs. *Pharmaceutical Research* **1993,** 10, (6), 900-904.

Raghavan, K., Dwivedi, A., Campbell, G.C., Nemeth, G. and Hussain, M.A., A spectroscopic investigation of DUP-747 polymorphs. *Journal of Pharmaceutical and Biomedical Analysis* **1994,** 12, (6), 777-785.

Robertson, J.M. and Ubbelohde, A.R., A new form of resorcinol II. thermodynamic properties in relation to structure. *Proceedings of the Royal Society of London Series a-Mathematical and Physical Sciences* **1938,** 167, (A928), 0136-0147.

Rohani, S., Horne, S. and Murthy, K., Control of product quality in batch crystallization of pharmaceuticals and fine chemicals. Part 1: Design of the crystallization process and the effect of solvent. *Organic Process Research & Development* **2005,** 9, (6), 858-872.

Romero-Torres, S., Huang, J. and Hernadez-Abad, P.E., Practical considerations on PAT analyzer selection - Raman Vs NIR spectroscopy. *American Pharmaceutical Review* **2009**, (November/December).

Rouhi, A., The right stuff. *Chemical and Engineering News* **2003,** 81, (8), 32-35.

Rowe, E.L. and Anderson, B.D., Thermodynamic studies of tolbutamide polymorphs. *Journal of Pharmaceutical Sciences* **1984,** 73, (11), 1673-1675.

Royall, P.G. and Gaisford, S., Application of solution calorimetry in pharmaceutical and biopharmaceutical research. *Current Pharmaceutical Biotechnology* **2005,** 6, (3), 215-222.

Rubin-Preminger, J.M. and Bernstein, J., 3-aminobenzenesulfonic acid: a disappearing polymorph. *Crystal Growth & Design* **2005,** 5, (4), 1343-1349.

Sangwal, K., On the estimation of surface entropy factor, interfacial-tension, dissolution enthalpy and metastable zone-width for substances crystallizing from solution. *Journal of Crystal Growth* **1989,** 97, (2), 393-405.

Saranteas, K., Bakale, R., Hong, Y.P., Luong, H., Foroughi, R. and Wald, S., Process design and scale-up elements for solvent mediated polymorphic controlled tecastemizole crystallization. *Organic Process Research & Development* **2005,** 9, (6), 911-922.

Sato, K. and Boistelle, R., Stability and occurrence of polymorphic modifications of stearic-acid in polar and nonpolar solutions. *Journal of Crystal Growth* **1984,** 66, (2), 441-450.

Sato, K., Polymorphic transformations in crystal-growth. *Journal of Physics D-Applied Physics* **1993,** 26, (8B), B77-B84.

Scholl, J., Bonalumi, D., Vicum, L., Mazzotti, M. and Muller, M., In situ monitoring and modeling of the solvent-mediated polymorphic transformation of L-glutamic acid. *Crystal Growth & Design* **2006,** 6, (4), 881-891.

Schuth, F., Nucleation and crystallization of solids from solution. *Current Opinion in Solid State & Materials Science* **2001,** 5, (5), 389-395.

Simmons, D.L., Ranz, R.J., Gyanchandani, N.D. and Picotte, P., Polymorphism in Pharmaceuticals II - Tolbutamide. *Canadian journal of Pharmaceutical Sciences* **1972**, (7), 121-123 [Form III was prepared by dissolving TB in ethanol at 160 ^{o}C, slowly adding warm water and allowing it to cool to room temperature].

Singhal, D. and Curatolo, W., Drug polymorphism and dosage form design: a practical perspective. *Advanced Drug Delivery Reviews* **2004,** 56, (3), 335-347.

Sjoblom, J., Svensson, O., Josefson, M., Kullberg, H. and Wold, S., An evaluation of orthogonal signal correction applied to calibration transfer of near infrared spectra. *Chemometrics and Intelligent Laboratory Systems* **1998,** 44, (1-2), 229-244.

Sohnel, O. and Mullin, J.W., The role of time in metastable zone width determinations. *Chemical Engineering Research & Design* **1988,** 66, (6), 537-540.

Starbuck, C., Spartalis, A., Wai, L., Wang, J., Fernandez, P., Lindemann, C.M., Zhou, G.X. and Ge, Z.H., Process optimization of a complex pharmaceutical polymorphic system via in situ Raman spectroscopy. *Crystal Growth & Design* **2002,** 2, (6), 515-522.

Stephenson, G.A., Structure determination from conventional powder diffraction data: application to hydrates, hydrochloride salts, and metastable polymorphs. *Journal of Pharmaceutical Sciences* **2000,** 89, (7), 958-966.

Stephenson, G.A., Forbes, R.A. and Reutzel-Edens, S.M., Characterization of the solid state: quantitative issues. *Advanced Drug Delivery Reviews* **2001,** 48, (1), 67-90.

Stephenson, G.A., Anisotropic lattice contraction in pharmaceuticals: the influence of cryo-crystallography on calculated powder diffraction patterns. *Journal of Pharmaceutical Sciences* **2006,** 95, (4), 821-827.

Storey, R., Docherty, R., Higginson, P., Chris, D., Gilmore, C., Barr, G. and Dong, W., Automation of solid form screening procedures in the pharmaceutical industry - how to avoid bottlenecks. *Crystallography Reviews* **2004,** 10, (1), 45-56.

Sun, C.C., Thermal expansion of organic crystals and precision of calculated crystal density: a survey of Cambridge Crystal Database. *Journal of Pharmaceutical Sciences* **2007,** 96, (5), 1043-1052.

Svard, M., Nordstrom, F.L., Jasnobulka, T. and Rasmuson, A.C., Thermodynamics and nucleation kinetics of in-aminobenzoic acid polymorphs. *Crystal Growth & Design* **2009,** 10, (1), 195-204.

Svensson, O., Kourti, T. and MacGregor, J.F., An investigation of orthogonal signal correction algorithms and their characteristics. *Journal of Chemometrics* **2002,** 16, (4), 176-188.

Teychene, S. and Biscans, B., Nucleation kinetics of polymorphs: Induction period and interfacial energy measurements. *Crystal Growth & Design* **2008,** 8, (4), 1133-1139.

Thirunahari, S., Aitipamula, S., Chow, P.S. and Tan, R.B.H., Conformational polymorphism of tolbutamide: a structural, spectroscopic and thermodynamic characterization of Burger's Forms I-IV. *Journal of Pharmaceutical Sciences* **2010,** 99, (7), 2975-2990.

Threlfall, T., Crystallisation of polymorphs: Thermodynamic insight into the role of solvent. *Organic Process Research & Development* **2000,** 4, (5), 384-390.

Threlfall, T., Structural and thermodynamic explanations of Ostwald's rule. *Organic Process Research & Development* **2003,** 7, (6), 1017-1027.

Threlfall, T.L., Analysis of organic polymorphs - a review. *Analyst* **1995,** 120, (10), 2435-2460.

Threlfall, T.L., Turning DSC charts of polymorphs into phase diagrams: a tutorial paper. *Organic Process Research & Development* **2009,** 13, (6), 1224-1230.

Ticehurst, M. and Docherty, R., From molecules to pharmaceutical products - the drug substance/drug product interface. *American Pharmaceutical Review* **2006**, (November/December).

Tishmack, P.A., Bugay, D.E. and Byrn, S.R., Solid-state nuclear magnetic resonance spectroscopy - pharmaceutical applications. *Journal of Pharmaceutical Sciences* **2003,** 92, (3), 441-474.

Titiz-Sargut, S. and Ulrich, J., Application of a protected ultrasound sensor for the determination of the width of the metastable zone. *Chemical Engineering and Processing* **2003,** 42, (11), 841-846.

Togkalidou, T., Fujiwara, M., Patel, S. and Braatz, R.D., Solute concentration prediction using chemometrics and ATR-FTIR spectroscopy. *Journal of Crystal Growth* **2001,** 231, (4), 534-543.

Towler, C.S. and Taylor, L.S., Spectroscopic characterization of intermolecular interactions in solution and their influence on crystallization outcome. *Crystal Growth & Design* **2007,** 7, (4), 633-638.

Trygg, J. and Wold, S., Orthogonal projections to latent structures (O-PLS). *Journal of Chemometrics* **2002,** 16, (3), 119-128.

Ulrich, J. and Strege, C., Some aspects of the importance of metastable zone width and nucleation in industrial crystallizers. *Journal of Crystal Growth* **2002,** 237, 2130-2135.

Vandersluis, P. and Kroon, J., Solvents and X-ray crystallography. *Journal of Crystal Growth* **1989,** 97, (3-4), 645-656.

Vankeirsbilck, T., Vercauteren, A., Baeyens, W., Van der Weken, G., Verpoort, F., Vergote, G. and Remon, J.P., Applications of Raman spectroscopy in pharmaceutical analysis. *Trac-Trends in Analytical Chemistry* **2002,** 21, (12), 869-877.

Variankaval, N., Cote, A.S. and Doherty, M.F., From form to function: crystallization of active pharmaceutical ingredients. *Aiche Journal* **2008,** 54, (7), 1682-1688.

Vekilov, P.G., Dense liquid precursor for the nucleation of ordered solid phases from solution. *Crystal Growth & Design* **2004,** 4, (4), 671-685.

Vishweshwar, P., McMahon, J.A., Oliveira, M., Peterson, M.L. and Zaworotko, M.J., The predictably elusive form II of aspirin. *Journal of the American Chemical Society* **2005,** 127, (48), 16802-16803.

Visser, J.W., A fully automatic program for finding unit cell from powder data. *Journal of Applied Crystallography* **1969,** 2, 89-&.

Volmer, M., *Kinetics Der Phasenbildung*. Steinkopff: Leipzig, 1939.

Wang, F., Wachter, J.A., Antosz, F.J. and Berglund, K.A., An investigation of solvent mediated polymorphic transformation of progesterone using in situ Raman spectroscopy. *Organic Process Research & Development* **2000,** 4, (5), 391-395.

Weissbuch, I., Torbeev, V.Y., Leiserowitz, L. and Lahav, M., Solvent effect on crystal polymorphism: why addition of methanol or ethanol to aqueous solutions induces the precipitation of the least stable beta form of glycine. *Angewandte Chemie-International Edition* **2005,** 44, (21), 3226-3229.

Werner, P.E., Eriksson, L. and Westdahl, M., TREOR - a semi-exhaustive trial-and-error powder indexing program for all symmetries. *Journal of Applied Crystallography* **1985,** 18, (OCT), 367-370.

Westerhuis, J.A., de Jong, S. and Smilde, A.K., Direct orthogonal signal correction. *Chemometrics and Intelligent Laboratory Systems* **2001,** 56, (1), 13-25.

Wold, S., Antti, H., Lindgren, F. and Ohman, J., Orthogonal signal correction of near-infrared spectra. *Chemometrics and Intelligent Laboratory Systems* **1998,** 44, (1-2), 175-185.

Wu, H.Q., Khan, M.A. and Hussain, A.S., Process control perspective for process analytical technology: integration of chemical engineering practice into semiconductor and pharmaceutical industries. *Chemical Engineering Communications* **2007,** 194, (6), 760-779.

Wu, W.J., Mehrman, S.J., Zhou, Y., Pu, S.X., Huang, L., Fermier, A. and Karki, S., The mechanism of the formation of enantiotropic polymorphs of carisbamate in solution crystallization. *Journal of Crystal Growth* **2009,** 311, (13), 3435-3444.

Wulfert, F., Kok, W.T., de Noord, O.E. and Smilde, A.K., Linear techniques to correct for temperature-induced spectral variation in multivariate calibration. *Chemometrics and Intelligent Laboratory Systems* **2000,** 51, (2), 189-200.

Yang, X., Lu, J., Wang, X.J. and Ching, C.B., In situ monitoring of the solution-mediated polymorphic transformation of glycine: characterization of the polymorphs and observation of the transformation rate using Raman spectroscopy and microscopy. *Journal of Raman Spectroscopy* **2008,** 39, (10), 1433-1439.

Young, P.H. and Ando, H.Y., Analysis of known crystals to design polymorph prediction strategies. *Journal of Pharmaceutical Sciences* **2007,** 96, (5), 1203-1236.

Yu, L., Inferring thermodynamic stability relationship of polymorphs from melting data. *Journal of Pharmaceutical Sciences* **1995,** 84, (8), 966-974.

Yu, L., Stephenson, G.A., Mitchell, C.A., Bunnell, C.A., Snorek, S.V., Bowyer, J.J., Borchardt, T.B., Stowell, J.G. and Byrn, S.R., Thermochemistry and conformational polymorphism of a hexamorphic crystal system. *Journal of the American Chemical Society* **2000,** 122, (4), 585-591.

Yu, L.X., Lionberger, R.A., Raw, A.S., D'Costa, R., Wu, H.Q. and Hussain, A.S., Applicatlons of process analytical technology to crystallization processes. *Advanced Drug Delivery Reviews* **2004,** 56, (3), 349-369.

Yu, L.X., Pharmaceutical quality by design: product and process development, understanding, and control. *Pharmaceutical Research* **2008,** 25, (4), 781-791.

Yu, Z.Q., Chew, J.W., Chow, P.S. and Tan, R.B.H., Recent advances in crystallization control - an industrial perspective. *Chemical Engineering Research & Design* **2007,** 85, (A7), 893-905.

Zeaiter, M., Roger, J.M. and Bellon-Maurel, V., Robustness of models developed by multivariate calibration. Part II: The influence of pre-processing methods. *Trac-Trends in Analytical Chemistry* **2005,** 24, (5), 437-445.

Zettlemoyer, A.C., *Nucleation*. Marcel Dekker: New York, 1969.

Zhou, G., Moment, A., Cote, A. and Hu, T., Utilizing spectroscopy for the isolation of desired API crystal form. *American Pharmaceutical Review* **2009**, (July/August).

Zhou, G.X., Crocker, L., Xu, J., Tabora, J. and Ge, Z.H., In-line measurement of a drug substance via near infrared spectroscopy to ensure a robust crystallization process. *Journal of Pharmaceutical Sciences* **2006,** 95, (11), 2337-2347.

List of Publications

International refereed journals:

[1] Thirunahari, S., Aitipamula, S., Chow, P. S. and Tan, R. B. H. **Conformational polymorphism of Tolbutamide: a structural, spectroscopic and thermodynamic characterization of Burger's forms I-IV**. *Journal of Pharmaceutical Sciences* **2010**, 99(7), 2975-2990.

[2] Thirunahari, S., Chow, P.S. and Tan, R. B. H. **Quality by Design (QbD) – based crystallization process development for the polymorphic drug Tolbutamide**. *Crystal Growth and Design* **2011**, 11(7), 3027-3038.

International conference contributions:

[1] Thirunahari, S., Aitipamula, S., Chow, P. S. and Tan, R. B. H. **Conformational polymorphism of Tolbutamide – thermodynamic and structural aspects of Burger's forms I-IV**. Poster presentation at the *American Association of Pharmaceutical Scientists (AAPS) Annual meeting* **2009**, Los Angeles, USA.

[2] Thirunahari, S., Chow, P. S. and Tan, R. B. H. **Crystallization of Tolbutamide – determination of design Space for the isolation of desired polymorph using PAT**. Oral presentation at the *9th International workshop on Crystal Growth of Organic Materials (CGOM)* **2010**, Singapore.

[3] Thirunahari, S., Chow, P. S. and Tan, R. B. H. **Statistical monitoring of solution mediated polymorphic transformation**. Oral presentation at the *Crystal Growth and Crystal Technology (CGCT)-5-Industrial Crystallization symposium, ICMAT* **2011**, Singapore.

[4] Thirunahari, S., Chow, P. S. and Tan, R. B. H. **Application of robust chemometrics for in situ solution concentration measurement using ATR-FTIR**. Poster presentation at the *Crystal Growth and Crystal Technology (CGCT)-5-Industrial Crystallization symposium, ICMAT* **2011**, Singapore.